WOOD AND FIBER SCIENCE

The Sustainable Natural Materials Journal

Volume 54, Number 3_2022 *(ISSN 0735-6161)*

Open Access

JOURNAL OF THE

SWST – International Society of Wood Science and Technology

SOCIETY OF WOOD SCIENCE AND TECHNOLOGY

2022–2023 Officers of the Society

WOOD AND FIBER SCIENCE

Wood and Fiber Science is published quarterly in January, April, July, and October by the Society of Wood Science and Technology, P.O. Box 6155, Monona, WI 53716-6155

There are three classes of membership (electronic only) in the Society: Members – dues $150; Retired Members – dues $75; Student Members – dues $50. We also have membership category for individuals from Emerging Countries where individual members pay $30, individual students pay $10; Emerging Group of 10 pay $290, and Student Groups of 10 pay $90. Institutions and individuals who are not members pay $300 per volume (electronic only). Applications for membership and information about the Society may be obtained from the Executive Director, Society of Wood Science and Technology, P.O. Box 6155, Monona, WI 53716-6155 or found at the website http://wwww.swst.org.

Site licenses are also available with a charge of:
- $300/yr for single online membership, access by password and email
- $500/yr for institutional subscribers with 2–10 IP addresses
- $750/yr for institutional subscribers with 11–50 IP addresses
- $1000/yr for institutional subscribers with 51–100 IP addresses
- $1500/yr for institution subscribers with 101–200 IP addresses
- $2000/yr for institutions subscribers with over 200 IP addresses.

New subscriptions begin with the first issue of a new volume. All subscriptions are to be ordered through the Executive Director, Society of Wood Science and Technology.

The Executive Director, at the Business Office shown below, should be notified 30 days in advance of a change of email address.

Business Office: Society of Wood Science and Technology, P.O. Box 6155, Monona, WI 53716-6155.
Editorial Office: Susan LeVan-Green, sue.levangreen@gmail.com

EFFECT OF TOOL TIP RADIUS ON RING DEBARKER PERFORMANCE OF FROZEN AND UNFROZEN BLACK SPRUCE LOGS

Claudia B. Cáceres
Former Research Associate
E-mail: claudia.caceres@mffp.gouv.qc.ca

*Roger E. Hernández**†*
Professor
Département des Sciences du Bois et de la Forêt
Centre de Recherche sur les Matériaux Renouvelables
Université Laval
2425 Rue de la Terrasse
Quebec G1V 0A6, Canada
E-mail: roger.hernandez@sbf.ulaval.ca

Jedi Rosero-Alvarado
Postdoctoral Fellow
E-mail: jedi.rosero-alvarado@bidgroup.ca

Rentry Augusti Nurbaity
Research Associate
E-mail: rentry.nurbaity@sbf.ulaval.ca

(Received February 2022)

Abstract. The effects of the tool tip radius on debarking quality of unfrozen and frozen black spruce logs were studied. The power, energy consumption, and torque on frozen conditions were also studied. A prototype one-arm ring debarker was used. The experiment consisted of debarking logs using three tool tip radii (40, 180, and 300 μm) for each temperature (−20°C and +20°C). The rotational and feed speeds, tip overlap, and rake angle were kept constants. Debarking quality was evaluated by two criteria: the proportion of bark remaining on log surfaces and the amount of wood in bark residues (WIB). Log characteristics, used as covariates, ie dimensions, eccentricity, bark thickness, knot features, bark/wood shear strength (BWSS), basic densities and moisture contents of sapwood and bark were measured, as well as total removed material after debarking. The results showed that tool tip radius had a significant effect on debarking quality of frozen and unfrozen logs. The proportion of bark on log surfaces increased and the amount of WIB decreased as tip radius increased. At the same applied radial force, a wider tip radius showed a shallower tip penetration leaving bigger regions of bark on the log surfaces. In contrast, a narrower tip radius showed a deeper tip penetration resulting in important wood fiber tear-out. The bark thickness and inner bark MC also affected debarking quality. The mean power, mean torque, and energy consumption increased as the tip radius decreased. However, this effect will depend on the choice of the applied radial force during debarking. Motor performance was also affected by the total removed material, log diameter, and BWSS. Overall, the results highlight the importance of choosing an adequate combination of tool tip radius and applied radial force to obtain the most profitable debarking quality with an efficient energy consumption.

Keywords: Tool tip radius, log temperature, debarking quality, energy consumption, black spruce.

INTRODUCTION

Log debarking is one of the first steps in most of the primary wood manufacturing processes. Several techniques are used for the removal of bark from logs, such as ring, drum, and cradle debarking.

* Corresponding author
† SWST member

In Canada, sawmills producing softwood lumber products mostly use ring debarkers. This debarker is equipped with an array of swing arm knives, mounted on a rotating ring that scrapes down the bark off by a shearing action at the cambium layer as the logs are fed through the ring (Chahal and Ciolkosz 2019). The ring debarker is commonly chosen when superior fiber protection, very clean debarking, and a steady supply of logs into the mill are needed. The main advantages of ring debarkers respect to other techniques are the higher feed speed, reduced maintenance, improved bark removal, and enhanced processing of crooked wood (Bajpai 2016).

The efficiency of debarking is generally assessed by two quality indicators. The first one is the proportion of bark remaining on the log (BRL) surface. This parameter is closely related to the bark particles that will be contained in pulp chips. In Quebec, 71% of the wood raw material supply for the pulp and paper industry already comes in the form of wood chips from sawmills (MFFP—Ministère des Forêts, de la Faune et des Parcs 2018). Bark content in chips is a critical factor that negatively affects the pulping processes, by decreasing pulp brightness, strength, and yield (Erickson 1979). Therefore, an increase in bark content will gradually reduce the value of the chips. The pulp mill tolerances of bark content depend on various factors like the type of pulping process, equipment, and final product (Hartler and Stade 1979). Eastern Canadian pulp mills generally accept up to 1% of bark content, which can increase to 1.5% during winter when logs are frozen (Ding et al 2012). In addition, any BRL prevents an accurate log scanning, which is crucial for maximizing lumber value in sawmills (Bajpai 2016). The second quality indicator is the loss of wood fibers during debarking. In practice, bark removal always generates some wood losses from sapwood. This results in a decrease in log diameter, which will negatively affect chip and lumber recoveries.

The performance of a ring debarker is affected by several factors such as the log environmental and storage conditions, and debarking parameters (Ding et al 2012). Log dimensions, straightness, taper, eccentricity (Kharrat et al 2020a,b), surface roughness (Berlyn 2000), the presence of cracks and knots (Hatton 1987; Kharrat et al 2020a,b), and bark thickness (Wilhelmsson et al 2002; Marshall et al 2006; Ding et al 2012) affect the performance of the ring debarker. The wood species, MC, harvesting season, and log freshness are also related to debarking quality (Baroth 2005) as they directly affect bark/wood shear strength (BWSS) (Fiscus et al 1983; Moore 1987; Belli 1996; Prislan et al 2013; Ugulino et al 2020). This property plays a major role on the efficiency of debarking (Chahal and Ciolkosz 2019; Kharrat et al 2020a,b). Thus, the amount of bark remaining on the surface of logs and the loss of wood fibers are usually higher in winter due to an important increase in BWSS occurring when the log temperature decreases under frozen conditions (Calvert and Garlicki 1974; Laganière 2003; Chow and Obermajer 2004; Laganière and Bédard 2009; Kharrat et al 2020a,b).

Among the parameters of the ring debarker, the feed speed, rotational speed, tool radial force, rake angle, tool tip path overlap, and tool tip radius are the most important affecting the debarking process. In wood machining operations, the shape and condition of the cutting edge is crucial (Denkena and Biermann 2014) as it affects the quality of the machined surface. The shape of the tool tip is usually described by the radius of the tool edge, which is formed by the junction between the rake and clearance faces (Zhao et al 2017). During ring debarking, the strain field in a log produced by the radial force applied is affected by the edge radius of the tips. This would affect the quality of debarking in terms of the two quality indicators cited earlier. Calvert and Garlicki (1972) recommended a tip edge radius between 254 and 1016 μm for debarking both white spruce and balsam fir logs. Laganière and Hernández (2005) used an intermediate tip edge radius of 600 μm for balsam fir. Kharrat et al (2020a) used a freshly sharpened tip edge radius of 78 μm for debarking black spruce. At a same level of radial force, a small edge radius should penetrate more into the bark, pass through the cambium and even remove fibers from sapwood. Conversely, a large edge radius is less powerful, which will prevent adequate penetration of

the tip into the bark, resulting in a greater proportion of BRL surface.

In addition, the applied radial force must be increased during winter given that the BWSS increases. This force can directly increase energy consumption. Knowledge of the effect of wood cutting parameters on energy consumption could increase energy efficiency, reduce operating costs, and increase profitability (Cristóvão et al 2013). Within this context, the aim of this study was to analyze the effects of tool tip radius on the debarking performance of unfrozen and frozen black spruce logs.

MATERIALS AND METHODS

Testing Material

Fifty black spruce (*Picea mariana* [Mill.] B.S.P.) trees were harvested during the winter season (January) from the Montmorency research forest, 72 km North from Quebec City. The stems were cross-cut into two or three logs of 2.4 m long. From these, the best logs were selected. Thus, 90 straight logs of 1.20 m long without any visible decay were obtained. They were separated in two groups of 45 logs each and exposed to two temperature conditions, −20°C and 20°C, respectively. Each group was divided into three subgroups of 15 logs to be assigned to each debarking condition. Small and large end diameters were measured and taper, and log eccentricity were calculated on each log. The eccentricity, defined as the ratio between the smallest and biggest diameter of each end, was calculated as the average of both ends. Log characteristics are described in Table 1. Mean values of these characteristics were examined for each group to keep them as close as possible among groups.

Characterization of the Tool Tip Radius

Three tool tips manufactured by DK-SPEC Inc were used in this study. They had two opposite edges of 50 mm width and a tip edge angle of 32°. Both edges of each tool tip were sharpened until reaching 40 180, and 300 μm of radius. The final step of this sharpening was carried out by manually honing the edges using an abrasive ceramic water stone (Lee Valley Inc.) with 8000 (2 μ) followed by 10,000 (1.2 μ) grit.

The uniformity of the radii obtained for the edges was evaluated on the central 25 mm of the tool

Table 1. Log characteristics and debarking parameters for each debarking treatment.

Log characteristics and debarking parameters	Temperature condition					
	20°C			−20°C		
Log characteristics	—	—	—	—	—	—
Small end diameter (mm)	151 (4)[a]	145 (5)	145 (5)	155 (6)[a]	155 (6)	146 (6)
Large end diameter (mm)	161 (6)	154 (5)	153 (5)	165 (6)	166 (7)	156 (6)
Taper (mm/m)	8 (2)	8 (1)	7 (1)	10 (1)	10 (1)	9 (2)
Eccentricity	0.94 (0.01)	0.944 (0.004)	0.952 (0.009)	0.940 (0.008)	0.939 (0.007)	0.940 (0.009)
Bark thickness (mm)	4.3 (0.2)	4.2 (0.2)	4.3 (0.2)	4.4 (0.2)	4.5 (0.2)	4.0 (0.2)
Number of knots	6 (1)	6 (1)	5 (1)	9 (1)	9 (1)	7 (1)
Mean knot diameter (mm)	13.0 (0.4)	14 (1)	12 (1)	9.4 (0.7)	11.8 (0.6)	10.7 (0.4)
Mean knot area (cm^2)	2.5 (0.3)	5 (1)	4 (1)	3.0 (0.3)	4.5 (0.8)	2.7 (0.6)
Proportion of knot area after debarking (%)	0.23 (0.04)	0.45 (0.05)	0.38 (0.05)	0.20 (0.03)	0.25 (0.05)	0.24 (0.04)
Number of logs	13	14	15	15	12	13
Cutting parameters	—	—	—	—	—	—
Tool tip radius (μm)	40[b]	180	300	40	180	300
Static radial force (N/mm)	16	16	16	16[b]	22	22
Rake angle (°)	80	80	80	80	80	80

[a] Numbers in parentheses are standard errors of the mean.

[b] The static radial force for the 40 μm tool tip radius test at −20°C was reduced to 16 N/mm due to excessive fiber tear-out.

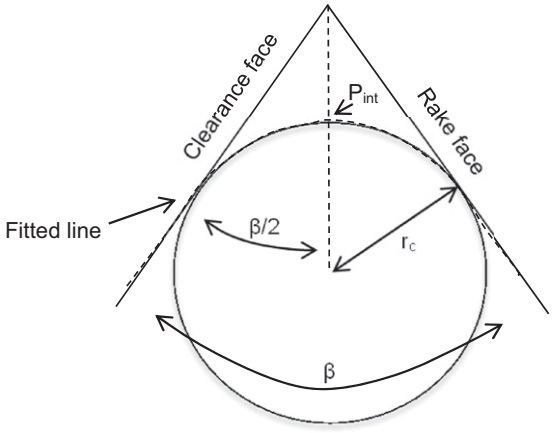

Figure 1. Characterization of a tool tip profile by the gaussian fitted circle method (adapted from Wyen and Wegener 2010).

tip using a ContourGT-I optical profiler (Bruker company, Tucson, AZ). Scan parameters were selected as follows: speed 1×, backscan 0 μm, length 250 μm, thresholding 1%, overlap of 40%, and green illumination. Later, one profile per millimeter was extracted from each surface profile and analyzed with image pro plus V6.2 software.

The tool tip radius was measured following the Gaussian fitted circle method (Wyen and Wegener 2010) (Fig 1). First, a fitted straight line was drawn on each rake face and clearance face of the tip. Second, a dotted straight line was projected from the intersection between the rake and clearance faces. The angle between the fitted lines is β°. A fitted circle was then drawn intersecting the tangents of each fitted straight lines and the point: P_{int}. The radius of the fitted circle (r_c) represents the tool tip radius. Tip radii of the 41, 183, and 308 μm were obtained after honing. 3D and 2D profiles of the tool tips are shown in Fig 2.

Bark/Wood Shear Strength, Basic Density, and MC Measurements

A 200 mm disc was cross-cut from each log to obtain cores for BWSS tests. The discs were wrapped in polyethylene and kept at −20°C to maintain their MC until the beginning of the sample preparation. Three cores of 12.7 mm in diameter and 25 mm in length were obtained from each disc in the radial direction. The core extraction and bark/wood adhesion tests in the transverse direction were performed according to Ugulino et al (2020). Bark thickness, including inner and outer barks, of each core was measured before testing (Table 1). BWSS (MPa) was calculated by dividing the load at failure (N) by the cross-sectional area of the wood/bark interface (mm^2) (Table 2).

Immediately after shearing tests, inner and outer barks were separated using a razor blade. Green mass and volume of sapwood, inner bark, and outer bark samples were then collected. Volume was measured by the water displacement method according to ASTM D2395-17 (2017). Samples were then oven-dried at 103°C for at least 24 h to obtain their oven-dry mass. All-mass measurements were made to the nearest 0.0001 g. Finally, the MC by the oven-drying method (ASTM D4442-16 2016) at the time of

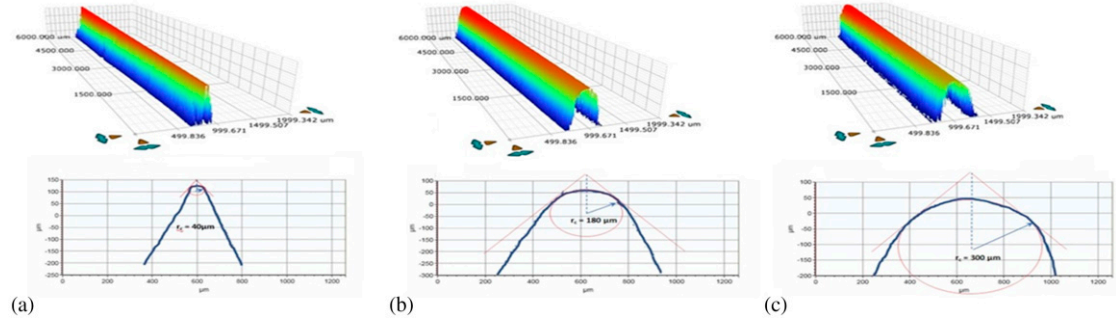

Figure 2. Tool tips 3D and 2D profiles: (a) 40 μm, (b) 180 μm, and (c) 300 μm of radius.

Table 2. Wood properties and total removed material for each debarking condition.

	Temperature condition					
	Unfrozen			Frozen		
	Tool tip radius					
Wood properties	40	180	300	40	180	300
BWSS (MPa)	0.35 (0.02)[a]	0.39 (0.01)	0.35 (0.01)	0.85 (0.06)	1.05 (0.09)	1.05 (0.08)
Sapwood MC (%)	109 (5)	114 (5)	117 (6)	120 (6)	121 (6)	110 (4)
Inner bark MC (%)	150 (5)	146 (5)	152 (5)	136 (5)	139 (6)	134 (8)
Outer bark MC (%)	69 (6)	67 (4)	78 (4)	66 (4)	58 (4)	61 (3)
Sapwood basic density (kg/m^3)	421 (10)	420 (4)	439 (8)	424 (9)	412 (10)	425 (10)
Inner bark basic density (kg/m^3)	412 (13)	401 (6)	410 (5)	417 (13)	418 (6)	414 (18)
Outer bark basic density (kg/m^3)	455 (12)	460 (9)	453 (7)	462 (11)	492 (19)	437 (24)
Total removed material (m^3)	—	—	—	0.0023 (0.0001)	0.0019 (0.0001)	0.0011 (0.0001)

BWSS, Bark/wood shear strength.

[a] Numbers in parentheses are standard errors of the mean.

testing as well as basic densities were calculated. Table 2 shows the mean values of sapwood and bark properties for each debarking condition.

Debarking Experiments and Measurement of Energy Requirements

The debarking operation was performed with a debarker prototype, which is described in detail elsewhere (Kharrat et al 2020a). The debarker was equipped with one tool arm and tips provided by DK-SPEC. The three tool tips described before were used. The feed speed (4.5 m/min) and the rotational speed (100 rpm) were set to have a tool overlap of 10%. The rake angle was fixed at 80° according to the recommendation given by Calvert and Garlicki (1974). Tests were conducted at two log temperatures: 20°C and −20°C. Temperature was measured with an IR thermal camera (Fluke TiX500) just after each debarking test. The static radial force applied for logs at 20°C was 16 N/mm. For logs at −20°C, a radial force of 22 N/mm was applied given that the BWSS increases at temperatures below 0°C (Ugulino et al 2020). However, this force was kept at 16 N/mm when frozen logs were debarked with the 40 μm of tip radius to avoid severe fiber tear-out during testing. Moreover, the radial force at the end of the tip was recorded with the data acquisition system (LabVIEW program) connected to the load cell of the tool arm. Debarking was always done from the small end to the big end of the log. Immediately after debarking, all bark residues were collected, placed in plastic bags, and stored at −20°C for later analysis.

A length of 0.85 m of each log was debarked in 10.7 s. During this time, a data acquisition system connected to the motor drive that rotated the log, was used to record the rotational speed (rpm) and the mean power (W) at a rate of 39 Hz. These values were used to calculate the torque of the motor (N·m) as follows: mean power × 9.549/rotational speed. The energy consumption (W·h), which is the electrical energy supplied for debarking per unit of time, was also calculated. These measurements were performed solely for the frozen condition. The energy measurements considered the energy needed to rotate the log, which depends to its size and mass; plus the debarking energy, which is the energy needed to remove material.

Debarking Quality Indicators

Proportion of BRL. All debarked surfaces were scanned using a Go!Scan Creaform handheld 3D scanner. The proportion of BRL surface

was measured based on the scanned images using a Python program, which was coded to identify and measure all the bark patches remaining on log surfaces. The task of identifying bark regions out of a wood log image was formulated as a semantic segmentation task. The approach used a fully convolutional neural network architecture capable of learning this task on a dataset of log images. Bark patches remaining on the log surfaces were manually tagged to improve the overall accuracy of this program. An overall accuracy of 95% was obtained for the images studied. For a more detailed description, refer to Kharrat et al (2020a). In addition, the number and size (two diameters) of knots bigger than approximately 10 mm were measured on each log. Afterward, the mean knot surface and the proportion of knot surface on the log were calculated (Table 1).

Proportion of WIB. Bark particles were recovered after each debarking test and air-dried indoors to facilitate their separation. Particles were then screened with a classifier in four classes (large, intermediate, small, and fines) following the methods used by Kharrat et al (2020a). All large and intermediate particles were manually separated into their wood and bark components. The size of the small particles makes the separation rather complicated and time consuming. Thus, a Domtar particle separator was used to obtain a representative sample corresponding to one quarter of the small particles. This subsample was also manually separated into wood and bark parts. Results from this subsample were used to define the amount of wood in bark residue for all small particles. The average mass of fine particles represented $<1\%$ of bark residues for unfrozen logs and $<4\%$ for frozen logs. For this reason, fine particles were not taken into account when measuring the amount of wood in bark residue. Finally, the amount of WIB was expressed as a percentage of the total mass of the debarking residue.

The total removed material was estimated as the addition of the bark and fiber volumes that were removed during debarking (Table 2). The former was estimated using the log dimensions, bark thickness, and BRL and the latter was calculated using the mass of fibers removed and the sapwood basic density.

Statistical Analysis

Statistical analysis was performed by means of the SAS package version 9.4 (SAS Institute 2014, Cary, NC). An analysis of covariance (ANCOVA) and multiple comparisons tests were done to evaluate the effect of the tool tip radius on BRL and WIB for each log temperature separately. The mean power, energy consumption, and torque were also evaluated but only for frozen condition. Log characteristics and wood properties were introduced as covariates, keeping only the ones significant for each model. Finally, the normality was verified with Shapiro–Wilk's test, the homogeneity of variance was verified with the graphical analysis of residuals, and statistical significance was tested at 5% and 1% probability levels.

RESULTS AND DISCUSSION

Debarking Quality Parameters

The uniformity of the diameter, taper, and eccentricity of the logs among groups (Table 1) facilitated the study of the effect of the tip radius on the debarking quality indicators. The edge radius of the tip showed a significant effect on BRL and WIB for frozen and unfrozen black spruce logs. BRL significantly increased as tool tip radius increased, regardless of the log temperature (Fig 3). More

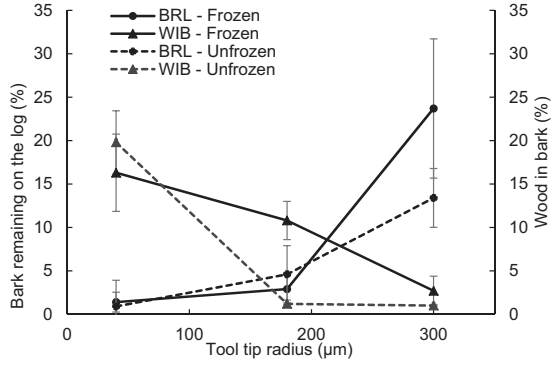

Figure 3. Proportions of bark remaining on the log and wood in bark as a function of the tool tip radius for unfrozen and frozen black spruce logs.

Table 3. Mean values of the proportions of bark remaining on the log and wood in bark for unfrozen and frozen conditions and also mean power, energy consumption, and mean torque for the frozen condition, for three tool tip radius.

Tool tip radius (um)	Unfrozen condition		Frozen condition				
	BRL (%)	WIB (%)	BRL (%)	WIB (%)	Mean power (W)	Energy consumption (W·h)	Torque (N·m)
40	1 (1)[a] A[b]	20 (4) B	1 (1) A	16 (4) B	20584 (753) B	60 (2) B	1966 (74) B
180	5 (3) B	1.2 (0.4) A	3 (2) A	11 (2) B	18351 (896) A	54 (3) A	1787 (88) A
300	13 (3) B	1.0 (0.1) A	24 (8) B	3 (2) A	17255 (612) A	51 (2) A	1679 (60) A

WIB, wood in bark residues; BRL, bark remaining on the log.

[a] Numbers in parentheses are standard errors of the mean.

[b] Means within a column followed by the same uppercase letter are not significantly different at the 5% probability level.

specifically, BRL was statistically similar between 40 and 180 μm but significantly different from 300 μm of tip radius, for both temperature conditions (Table 3). The increase in BRL between 180 and 300 μm of tip radius was more important in frozen conditions (Fig 3). According to Table 3, an increase of 120 μm between the two higher radii (180 and 300 μm) resulted in an increase of 8.8% of BRL for unfrozen logs compared with 20.8% for frozen logs. Therefore, BRL in frozen condition appeared to be more sensitive to a tip radius increase within higher ranges, thus leading to larger regions of bark attached to the log after debarking. The presence of ice in the bark negatively affected the penetration of the tip edge. Below 0°C, a shallow penetration was in fact observed compared with unfrozen condition for the same applied force. In addition, the bark/wood bond becomes stronger below 0°C (Ugulino et al 2020), which will make the debarking action more difficult (Laganière and Hernández 2005; Kharrat et al 2020a,b). As explained earlier, the radial force applied with 40 μm tip radius at frozen condition was maintained at 16 N/mm (same as unfrozen condition) to prevent severe fiber tear-out. Table 3 shows that the BRLs obtained with this tip radius were 0.9% and 1.4% for unfrozen and frozen logs, respectively. Accordingly, a radial force of 16 N/mm adequately removed the bark in frozen logs because of the sharpness of the tip.

The ANCOVA showed that BRL was also affected by the inner bark MC for frozen and unfrozen logs and by the bark thickness for the unfrozen logs (Table 4). A higher MC of the inner bark would facilitate the debarking action, thus reducing the amount of BRL surface for both temperature conditions. Moreover, thicker bark will lead to a higher proportion of BRL in unfrozen condition probably due to a lower penetration of the tip. Thus, an increase in the applied radial force will be required.

WIB decreased significantly as the tool tip radius increased for both log temperatures (Fig 3). The *F*-values showed that effect of the tip radius on

Table 4. F-values obtained from the ANCOVAs of the effect of tool tip radius on the proportions of bark remaining on the log and wood in bark for unfrozen and frozen conditions and also mean power, energy consumption, and mean torque for the frozen condition.

Source of variation	Unfrozen condition		Frozen condition				
	BRL	WIB	BRL	WIB	Mean power	Energy consumption	Torque
Bark thickness	9.6 **[a]	ni	ni	14.5 **	ni	ni	ni
Inner bark MC	13.1 **	ni	6.4 *	5.5 *	ni	ni	ni
Total removed material	ni[b]	ni	ni	ni	7.2 *	6.9 *	7.0 *
Mean log diameter	ni	ni	ni	ni	91.9 **	81.8 **	83.1 **
BWSS	ni	ni	ni	ni	5.0 *	ni	ni
Tool tip radius	10.0 **	89.9 **	19.7 **	21.6 **	9.3 **	6.6 **	6.6 **

WIB, wood in bark residues; BRL, bark remaining on the log; BWSS, bark/wood shear strength.

[a] *,** significant at 5% and 1% probability level respectively.

[b] ni: not included in the ANCOVA.

WIB was stronger for the unfrozen logs than for frozen logs (Table 4). For unfrozen logs, WIB was statistically different between 40 μm and the other two tip radii (180 and 300 μm), which were similar between them (Table 3). For frozen logs, there were no differences in WIB between 40 and 180 μm of tip radius but both were significantly different from 300 μm of tip radius. However, the decrease in WIB between the tip radii of 40 and 180 μm was more abrupt in unfrozen condition (Fig 3). According to Table 3, an increase of 140 μm in the tip radius resulted in a decrease of 18.6% of WIB for unfrozen logs compared with 5.5% for frozen logs. Moreover, a decrease of 18.1% of WIB was found for the latter condition with a much higher increase in tip radius of 260 μm (from 40 to 300 μm). Thus, the use of a tip radius close to 180 μm in unfrozen condition and close to 300 μm in frozen condition would significantly reduce fiber tear-out during debarking. However, this would also result in a noticeable increase in BRL for the latter. In addition, there was no significant difference in WIB between frozen and unfrozen conditions at 40 μm tip radius (Fig 3). Therefore, the fiber tear-out was effectively controlled by keeping the radial force at 16 N/mm for both log temperatures.

On the other hand, none of the studied covariates showed a significant effect on WIB for the unfrozen condition. But, for the frozen condition, WIB was significantly affected by the inner bark MC and by the bark thickness (Table 4). A higher MC in the inner bark and a thinner bark would result in higher fiber tear-out at temperatures below 0°C. The *F*-values showed that the effect of bark thickness on WIB was stronger than that of the inner bark MC. It is important to understand that the proportion of fiber tear-out is the result of a tip penetration (exceeding the cambium layer) at a certain radial force, which is usually higher when debarking frozen logs (Kharrat et al 2020a). Fiber tear-out could, thus, happen more easily and continuously when the bark is thinner. This could be associated to excessive radial force. This result is important because the bark thickness varies within species depending on the site, tree age, individual trees, and along the stem (Smith and Kozak 1971; Laasasenaho et al 2005; Marshall et al 2006).

Debarking quality parameters affect the sawmill productivity in two distinctive ways. The relative importance of each one depends on the particular optimization guidelines of each sawmill. First, the BRLs will affect the proportion of bark in chips, thus affecting their commercialization to pulp mills. However, the degree of its influence on chip quality depends at the same time on the size and shape of the log, as well as the selection of the cutting width, which depends on the cutting pattern chosen for the sawing process. For these reasons, it is quite difficult to estimate a critical amount of BRL as a threshold to keep the required chip quality along the production line. In any case, bark content in chips must not exceed 1% in mass (Ding et al 2012). Second, the amount of wood fibers found in bark residues will affect the global efficiency and sawn lumber yield of a sawmill. Bark residues are usually burn as fuel, including the wood fibers found within them (Isokangas and Leiviskä 2005). In general, sawmills use higher radial forces than the necessary to avoid pulp mills penalties for bark in chips. Although this will assure minimum BRL levels, it would disproportionately increase the amount of WIB at the same time. The selection of an appropriate tool tip radius could be an interesting option to avoid an additional increase of the radial force during debarking. At equal radial force, a narrower tip radius (sharper) will assure a deeper tip edge penetration compared with a wider radius. Therefore, the applied radial force could be regulated to a level that will allow to efficiently remove the bark from the log without tearing-off the wood fibers.

Considering the opposite behavior of the two debarking indicators, the improvement of one indicator goes to the detriment of the other one and vice versa. Thus, the curves between BRL and WIB for unfrozen and frozen log conditions in Fig 3 intersect at a given point. This point should represent a suitable compromise when considering the two debarking quality indicators at an equal degree of importance. The tool tip radii of 158 and 213 μm resulted in 4% and 8.5% for both quality parameters for the unfrozen and frozen logs, respectively

(Fig 3). These tip radii would be the more satisfactory for debarking specifically with the chosen radial forces. Particularly, the lower limit would be more fitted for unfrozen condition and the higher one for the frozen condition (−20°C). However, the same degree of debarking quality could not be reached in both cases with the given radial forces. Figure 3 shows that the radial force applied with a 40 μm tip radius (16 N/mm) was still too high. BRL was 1.2% but WIB was 18.1% (frozen and unfrozen logs pooled). Therefore, it could have been possible to lower the radial force to decrease WIB but without increasing BRL. At 180 μm, BRL (4.6%) was higher than WIB (1.2%) in the unfrozen condition, and, thus, the radial force applied (22 N/mm) could have been slightly increased to reduce BRL but without increasing WIB. But for the frozen condition the same radial force seems to be a little too high, resulting in a WIB of 10.8% and a BRL of 2.9%. At 300 μm, BRL was 18.6% but WIB was 1.8% (frozen and unfrozen logs pooled), thus, a higher radial force could have been used to reduce BRL. However, applying more radial force using a bigger tool tip radius would probably result in an increase in the power consumption, mainly in the frozen condition. Consequently, the best compromise between the BRL and WIB could be obtained with an intermediate tip radius (between 158 and 213 μm) combined with the more appropriate radial force depending on the temperature condition.

Power, Energy Consumption, and Torque Under Frozen Conditions

The ANCOVAs showed that the electrical performance of the motor was significantly affected by the tool tip radius (Table 4). The mean power, energy consumption, and torque decreased as the tip radius increased. These indicators were, thus, significantly higher for 40 μm than for the other two tip radii (180 and 300 μm) even though the applied radial force was lower for the former tool tip (16 N/mm) compared with the other tip radii (22 N/mm) (Table 3).

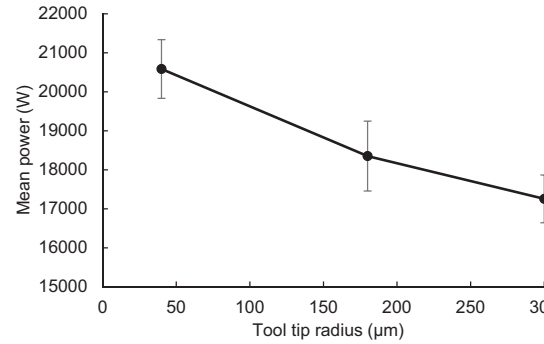

Figure 4. Mean power as a function of the tool tip radius.

Some of the studied covariates showed a significant effect on the motor electrical performance (Table 4). Mean power, energy consumption, and torque were positively affected by the total removed material and by the log diameter. Accordingly, as more material was removed, the debarking forces increased and, therefore, the mean power, energy consumption, and torque also increased. These parameters also increased as log diameter increased. In addition, a higher mean power was needed for debarking as BWSS increased.

The relationship between mean power and tool tip radius is shown in Fig 4. An increase of 140 μm of tool tip radius (from 40 to 180 μm) resulted in a decrease of 11% of mean power; however, a consecutive increase of 120 μm (from 180 to 300 μm) resulted in a decrease of only 6% of mean power. Power is the work performed over a specific amount of time, thus, it could be stated that more work is needed for debarking frozen logs using narrower tool tips. The same behavior was found for the energy consumption. Hence, debarking frozen logs with a tip radius of 40 μm resulted in higher energy consumption compared with using 180 and 300 μm.

The tip of 40 μm radius showed a deeper penetration into the bark compared with wider tips, which occasionally exceeded the cambium layer. The shearing action in that case took place in the sapwood instead of the bark/wood interface. Therefore, the volume of WIB for this condition reached 16.3% (Table 3). Hernández et al (2014) found a shear strength parallel-to-the grain of 9.2 MPa in

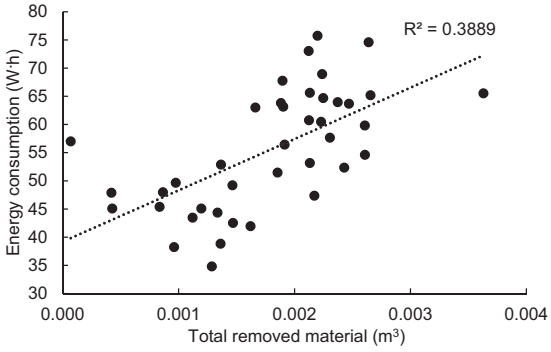

Figure 5. Energy consumption as a function of the total removed material.

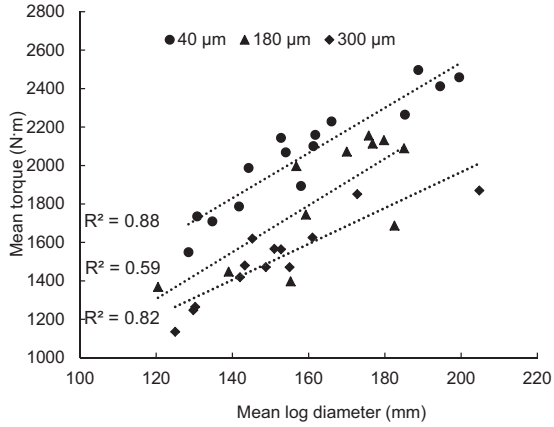

Figure 6. Mean torque as a function of the mean log diameter for each tool tip radius.

black spruce sapwood at −20°C, which could be quite similar in the perpendicular direction. This strength is significantly higher than the BWSS (0.85 MPa for 40 µm, Table 2) needed to remove the bark at the cambium layer. Thus, the energy consumption will increase each time that the shearing action takes place in the sapwood, which could happen more regularly when using narrow tip radius combined with too high radial forces. Therefore, if excessive radial force is applied during debarking with narrow tool tips, the energy consumption would increase even more as it is positively related to the amount of material removed, as previously explained. Hence, Fig 5 shows a significant positive correlation between the energy consumption and the total material removed (R^2: 0.39). From a practical point of view, these results emphasize the importance of choosing an appropriate combination of tool tip radius and applied radial force to sustain an efficient use of energy. Thus, the use of a small tip radius with just enough radial force could be more beneficial to reduce both the energy consumption and mainly the WIB. However, further studies should be done to establish the more adequate combinations of tool tip radius and radial force to confirm this behavior.

The torque of an electric motor is a measure of the driving force that can cause an object to rotate around an axis. Torque was calculated using power, and thus it showed the same behavior in relation to the tool tip radius as shown in Fig 4. Debarking frozen logs with a tip radius of 40 µm needed a greater torque compared with using 180 and 300 µm. As explained earlier, the studied motor performance indicators were significantly affected by the mean log diameter (Table 4). Among them, we choose torque to show this relationship. A strong correlation between the size of the log and the torque needed for debarking is shown in Fig 6. Coefficients of determination (R^2) that ranged from 0.59 to 0.88 were found depending on the tool tip radius. Debarking bigger logs will require greater torque than smaller ones. However, debarking logs of the same diameter will require higher torque when using narrower tool tip radius. This agrees with the results found for mean power and energy consumption.

From an industrial perspective, a direct application between our results and the ring debarking rotor would be difficult. Contrary to the action of the ring debarker, which is a rotating ring provided with tool arms that scrape the bark off the logs as they are fed through the ring; the laboratory debarker pushed the tool arm into the log as it was rotating and moving horizontally (Kharrat et al 2020a). However, at the same applied radial force, a narrow tip radius could penetrate deeper into the bark significantly increasing the amount of fiber tear-out and consequently the energy consumption. On the contrary, a large tip radius could not penetrate enough into the bark leaving larger

regions of bark on the log surface and, thus, lessen the energy consumption. Therefore, it would be more reasonable to recommend an intermediate tip radius (158 and 213 μm depending on log temperature) that will assure a satisfactory debarking quality, for both BRL and WIB, with an efficient use of energy.

CONCLUSIONS

Black spruce ring debarking quality was significantly affected by the tip edge radius and the log temperature. Inner bark MC and bark thickness also affected the debarking action. For frozen and unfrozen conditions, a wider tip radius made a shallower incision in the bark, which left larger patches of bark on the surfaces of debarked log. On the contrary, a narrower tip radius made a deeper incision in the bark increasing the number of torn fibers in the bark residues. Therefore, an acceptable compromise between BRL and WIB could be achieved by using an intermediate tip radius (between 158 and 213 μm) applying sufficient radial force, depending on log temperature.

Mean power, energy consumption, and torque decreased as the tip radius increased. These parameters were also positively affected by the total material removed and the log diameter. Higher power will be needed when the bark/wood adhesion is stronger. A small tip radius will consume more energy if the applied radial force results in a debarking action performed in the sapwood instead of the cambium layer. Also, a large tip radius will require higher radial forces to reach the cambium layer and will, therefore, consume more energy. Therefore, selecting an appropriate combination of tool tip radius and applied radial force to achieve debarking most often at the cambium layer is critical to achieving good quality debarking quality and energy efficiency.

ACKNOWLEDGMENTS

Funding for this project was provided by the Natural Sciences and Engineering Research Council of Canada (NSERC) and DK-SPEC Inc. The authors thank DK-SPEC Quebec, Canada for providing the knife arms and tips. The authors also thank Félix Pedneault, Jean Ouellet, Daniel Bourgault, and Réjean Demers for their valuable assistance.

REFERENCES

ASTM (2016) D4442-16. Standard test methods for direct moisture content measurement of wood and wood-based materials. American Society for Testing and Materials, West Conshohocken.

ASTM (2017) D2395-17. Standard test methods for density and specific gravity (relative density) of wood and wood-based materials. American Society for Testing and Materials, West Conshohocken.

Bajpai P (2016) Energy conservation measures for raw material preparation. Chapter 4, Pages 51-66 *in* Bajpai J, eds. Pulp and Paper Industry, Energy Conservation, Elsevier.

Baroth R (2005) Literature review of the latest development of wood debarking. University of Oulu, Finland.

Belli ML (1996) Wet storage of hickory pulpwood in the southern United States and its impact on bark removal efficiency. Forest Prod J 46(3):75-79.

Berlyn R (2000) Debarking. Tech 2000: Chip & wood quality. Professional development committee, Pulp & Paper Technical Association of Canada, Montreal, Canada, 29 pp.

Calvert WW, Garlicki AM (1972) A study of bark removal at low temperatures by simulated cambium shear methods. Forest Prod J 22(2):37-43.

Calvert WW, Garlicki AM (1974) The use of ring debarkers at low temperatures. Publication No. 1334. Department of the Environment, Canadian Forest Service, Ottawa, ON.

Chahal C, Ciolkosz D (2019) A review of wood-bark adhesion: Methods and mechanics of debarking for woody biomass. Wood Fiber Sci 15(3):1-12.

Chow S, Obermajer A (2004) Wood-to-bark adhesion of subalpine fir (*Abies lasiocarpa*) in extreme temperatures. Wood Sci Technol 38(6):391-403.

Cristóvão L, Ekevad M, Grönlund A (2013) Industrial sawing of *Pinus sylvestris* L.: Power consumption. BioResources 8(4):6044-6053.

Denkena B, Biermann D (2014) Cutting edge geometries. CIRP Ann Manuf Technol 63(2):631-653.

Ding FP, Ibrahim F, Gagné F (2012) MPC based ring debarking process optimization. *in* 25th IEEE Canadian Conference on Electrical and Computer Engineering (CCECE). Montreal, QC.

Erickson JR (1979) Separation of bark from wood. Pages 145-170 *in* Hatton JV ed. Chip quality monograph. Joint Textbook Committee of the Paper Industry, Vancouver, BC.

Fiscus MH, Vaneperen RH, Einspahr DW (1983) Method for obtaining wood bark adhesion measurements on small samples. Wood Fiber Sci 15(3):219-222.

Hatton JV (1987) Debarking of frozen wood. Tappi J 70: 61-66.

Hartler N, Stade Y (1979) Chip specifications for various pulping processes. Pages 273-301 *in* Hatton JV ed, Chip quality monograph. Joint Textbook Committee of the Paper industry, Vancouver, BC.

Hernández RE, Passarini L, Koubaa A (2014) Effects of temperature and moisture content on selected wood mechanical properties involved in the chipping process. Wood Sci Technol 48(6):1281-1301.

Isokangas A, Leiviskä K (2005) Optimisation of wood losses in log debarking drum. Pap Puu-Pap Tim 87(5): 324-328.

Kharrat W, Hernández RE, Cáceres CB, Blais C (2020a) Effects of radial force and log position on the stem on ring debarker efficiency in frozen black spruce logs. Wood Mater Sci Eng 16(3):211-220.

Kharrat W, Hernández RE, Cáceres CB, Blais C (2020b) Ring debarking efficiency of frozen balsam fir logs is affected by the radial force but not by the log position on the stem. Can J Res 50(12):1323-1332.

Laasasenaho J, Melkas T, Aldén S (2005) Modelling bark thickness of *Picea abies* with taper curves. For Ecol Mgmt 206:35-47.

Laganière B (2003) Manual-ring debarking. Special publication SP-525E. Forintek Canada Corp, Québec, QC.

Laganière B, Bédard N (2009) Debarking enhancement of frozen logs. Part I. Effect of temperature on bark/wood bond strength of balsam fir and black spruce logs. Forest Prod J 59(6):19-24.

Laganière B, Hernández RE (2005) Effects of radial force and tip path overlap on the ring debarking efficiency of frozen balsam fir logs. Forest Prod J 55(3):44-49.

Marshall H, Murphy G, Lachenbruch B (2006) Effects of bark thickness estimates on optimal log merchandising. Forest Prod J 56(11):87-92.

MFFP—Ministère des Forêts, de la Faune et des Parcs (2018) Ressources et industries forestières du Québec. Portrait statistique (In French). https://mffp.gouv.qc.ca/wp-content/uploads/PortraitStatistique_2018.pdf (1 December 2020).

Moore GA (1987) The variation of bark/wood bond strength with moisture content of *Pinus radiata* and three eucalypt species during storage. Aust For Res 17: 73-78.

Prislan P, Cufar K, Koch G, Schmitt U, Gricar J (2013) Review of cellular and subcellular changes in the cambium. IAWA J 34:391-407.

SAS Institute (2014) SAS/Stat user's guide. SAS Institute Inc. Version 9.3. Cary, NC.

Smith JH, Kozak A (1971) Thickness, moisture content, and specific gravity of inner and outer bark of some Pacific northwest trees. Forest Prod J 21(2):38-40.

Ugulino B, Cáceres CB, Hernández RE, Blais C (2020) Influence of temperature and moisture content on bark/wood shear strength of black spruce and balsam fir logs. Wood Sci Technol 54:963-979.

Wilhelmsson L, Arlinger J, Spangberg K, Lundqvist S, Grahn T, Hedenberg O, Olsson L (2002) Models for predicting wood properties in stems of *Picea abies* and *Pinus sylvestris* in Sweden. Scand J Fr Res 17(4):330-350.

Wyen CF, Wegener K (2010) Influence of cutting edge radius on cutting forces in machining titanium. CIRP Ann Manuf Technol 59(1):93-96.

Zhao T, Zhou JM, Bushlya V, Ståhl JE (2017) Effect of cutting edge radius on surface roughness and tool wear in hard turning of AISI 52100 steel. Int J Adv Manuf Technol 91:3611-3618.

VARIATION OF CHEMICAL PROPERTIES, CRYSTALLINE STRUCTURE AND CALORIFIC VALUES OF NATIVE MALAYSIAN BAMBOO SPECIES

Syaiful Osman
Sr. Lecturer
E-mail: syaifulosman@uitm.edu.my

Mansur Ahmad
Professor
E-mail: mansur628@uitm.edu.my

Mohd Nazarudin Zakaria
Sr. Lecturer
Faculty of Applied Sciences
School of Industrial Technology
Universiti Teknologi MARA
Shah Alam, Malaysia
E-mail: nazarudin@uitm.edu.my

Balkis Fatomer A. Bakar
Sr. Lecturer
Faculty of Forestry and Environment
Department of Wood and Fiber Industry
Universiti Putra Malaysia
Serdang, Malaysia
E-mail: bfatomer@upm.edu.my

Falah Abu
Sr. Lecturer
E-mail: falah@uitm.edu.my

Siti Hasnah Kamarudin
Sr. Lecturer
E-mail: sitihasnahkam@uitm.edu.my

Shahril Anuar Bahari
Sr. Lecturer
Faculty of Applied Sciences
School of Industrial Technology
Universiti Teknologi MARA
Shah Alam, Malaysia
E-mail: shahril721@uitm.edu.my

* Corresponding author

Wood and Fiber Science, 54(3), 2022, pp. 173-186
https://doi.org/10.22382/wfs-2022-17

*Reza Hosseinpourpia**

Associate Professor
Department of Forestry and Wood Technology
Linnaeus University
Växjö, Sweden
E-mail: reza.hosseinpourpia@lnu.se

(Received February 2022)

Abstract. The chemical properties of four common Malaysian bamboo species locally known as Beting (*Gigantochloa levis*), Semantan (*Gigantochloa scortechinii*), Lemang (*Schizostachyum brachyladum*), and Akar (*Bambusa vulgaris*) were studied. Chemical analysis shows that the alkaline-extractive content of the Malaysian bamboo species ranged from 24.4% to 25.6%, ethanol–toluene extractive content for Malaysian bamboo species ranged from 4.0% to 7.2% and water extractive content ranged from 10.4% to 12.8%. The average value of holocellulose content for Malaysian bamboo was 64.5-70.7%, Klason lignin within 25.3-28.4%, cellulose content was between 28.5% and 33.8%, and α-cellulose content for all bamboo species was within the range of 40.7-47.9%. The crystallinity of bamboo samples was between 42.0% and 44.4%, indicating a semicrystalline structure. Heating value of bamboo ranged between 17.0 MJ/kg and 18.1 MJ/kg with *G. scortechinii* having the highest heating value. The Inductive Couple Plasma Atomic Emission Spectroscopy (ICP-ES) analysis showed that Potassium (K) and Calcium (Ca) were the major elements in the ash of all bamboo samples. This study demonstrates the potential of native bamboo species as an alternative sustainable raw material to wood for a wide range of applications.

Keywords: Bamboo, physicochemical, calorific value, spectroscopic analysis.

INTRODUCTION

Growing population and rapid industrialization contribute significantly to an increasing demand for forest-based materials and energy production. This emphasizes the importance of finding alternatives to the existing materials (Abdulkhani et al 2017). It is estimated that there are around 1400 bamboo species worldwide, whereas in Peninsular Malaysia, there are about 59 bamboo species that consists of 34 indigenous species and 25 species are cultivated (Wong 1995). *Gigantochloa scortechinii* is the most common species in Malaysia, with approximately 70% of the total clump extracted from the bamboo forest (Hisham et al 2005; Mohmod et al 2016). According to Malaysia National Forestry Inventory 4 (NFI4), the total number of clumps of *Gigantochloa scortechinii* and *Gigantochloa levis* in Peninsular Malaysia is 163,000 and 911,956 clumps, respectively with the total area of bamboo in Malaysia is around 0.6 million ha (Kuehl 2015; Anon 2018).

Comparatively, more studies have been conducted to analyze the properties of wood instead of bamboo using the same techniques as in this work (Ghavidel et al 2020, 2021). However, some studies on bamboo behavior are available as a basis for this study. The chemical characteristics of bamboo are one of the critical properties that must be understood to encourage and widen its applications. Liese (1985) claimed that the chemical properties of bamboo vary depending on species, growing conditions, age, and growth site of bamboo culms. Major constituents of bamboo are cellulose (38-50%), hemicelluloses (23-32%), and lignin (15-25%) that make-up to 90% of the total mass (Cao et al 2014).

It was shown previously that top location of bamboo culm shows significantly higher extractive and ash content compared with middle and bottom parts (Kamthai 2003). Bamboo nodes also contain more lignin and ash but less water-soluble extractives than internodes (Kamthai and Puthson 2005). Li (2004) studied the chemical composition of *Phyllostachys pubescens* bamboo at different ages and as a function of culm height. The author claimed that age and height of bamboo culm affect its chemical composition, as the hemicelluloses and α-cellulose content increased from the bottom to the top part of bamboo, but the changes in lignin

and ash content were statistically insignificant. The content of hemicelluloses, α-cellulose, and Klason lignin was higher in outer layer of bamboo than in the epidermis while the epidermis had a higher extractive content compared with the outer layer. The higher content of α-cellulose and Klason lignin is closely related to the fact that the outer layer contributes most to the mechanical strength of culm. Kumar and Chandrashekar (2014) found that Indian bamboo ash had relatively high percentages of silica and potassium and the contents of ash, volatile, and fixed carbon were varied significantly among different bamboo species. Physicochemical characterization of several commercially important Asian bamboo species (*Bambusa nutons*, *Bambusa tulda*, *Bambusa arundinacea*, *Bambusa pallida*, *Bambusa bambus*, *Dendrocalamus strictus,* and *Dendrocalamus strictus teri*) showed the alkali solubility variability between 26.1% and 28.3% in all bamboo species.

Although the decline in wood supply does not apply to all countries (Ekstrom 2022), however, deforestation is still a major problem, as more countries are beginning to make greater efforts to conserve forests. For example, in Sabah, one of the states in Malaysia with a vast area of tropical forest, the timber trade in Sabah has been declining because of various conservation efforts, and this trend is expected to continue for the next 20 yr. Bamboo-based sector and timber industry can complement each other to cater demand from population increase. In addition, there is also a need to promote sustainable materials and to preserve tropical forests (The Malaysian Reserve 2022).

Since there are numerous potentials uses for various bamboo species nationally and worldwide, ranging from pulp and paper to panel manufacturing, chemical and bioenergy industries, it is advisable to understand its chemical properties, which are influenced by culm height. Therefore, the main objective of this study was to comprehensively investigate certain chemical properties of four native Malaysian bamboo species through chemical composition analysis, Fourier Transform IR (FTIR) spectroscopy, elemental analysis, X-ray structure analysis (XRD), and oxygen bomb calorimeter (OBC). This information will contribute to a better understanding of the mentioned native bamboo species to expand their application as an economically viable and alternative renewable material.

MATERIALS AND METHODS

Raw Materials

Four native Malaysian bamboo species; Semantan (*G. scortechinii*), Beting (*G. levis*), Lemang (*S. brachyladum*), and Akar (*B. vulgaris*) with age of 3 yr old were collected from a local source in Peninsular Malaysia, with an approximate height of 180 cm from top to bottom. Samples were air-dried upon arrival and sectionized as shown in Fig 1 indicating the bottom, middle and top part of bamboo. Nodes and internodes sections are also indicatedOuter skin was removed using hand spoke, the bamboo specimens were then cut into smaller pieces and ground using Wiley milling machines (Thomas Scientific, Swedesboro, NJ), and then sieved subsequently screened using a vibrating screening machine. Grounded bamboo particles, 40 mesh in size (Fig 2) were then stored in airtight containers for further analysis. Prior to each analysis, bamboo particles were oven-dried at 70°C for 24 h.

Characterization of Bamboo Species

Specific gravity, acidity, and buffering capacity. Acidity (pH) of bamboo species was determined according to TAPPI-T509 (2006).

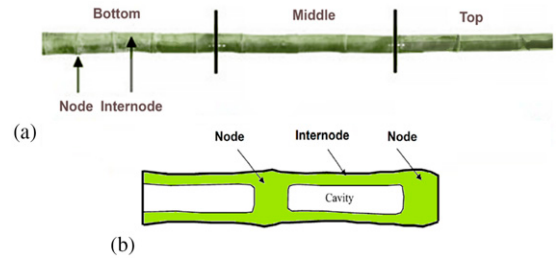

Figure 1. (a) Entire bamboo culm (bottom, middle, and top) with positioning of nodes and internodes; (b) schematic image of longitudinal section of bamboo specimen.

Figure 2. Ground bamboo specimen (40 mesh) used for analysis.

Buffering capacity (β) was calculated as the number of milliequivalents (N × m) required to change the pH to 3.5 as shown in Eq 1.

$$Buffering\ capacity\ (\beta) = \frac{n}{\Delta pH} \qquad (1)$$

Where, n is the number of moles of acid or base added per liter of solution. The Δ pH is calculated by subtracting the initial pH from final pH.

Determination of extractive content. Extractive content of bamboo species was determined using hot water, alkaline, and ethanol–toluene extraction methods. For hot-water extractive content, 2 g of oven-dried particles were placed in a 250 mL Erlenmeyer flask and topped up with 100 mL distilled water. The flask was then placed in a shaking water bath at 95°C for 5 h. The specimens were then removed and filtered by vacuum suction, washed with hot distilled water, and oven-dried at 103 ± 5°C for 24 h. For each bamboo species, the sample size was equivalent to *G. scortechinii* = 25, *G. levis* = 24, *S. brachyladum* = 23, and *B. vulgaris* = 24.

The alkaline-extractive content was determined according to ASTM D1109—84 (2013) using 1% NaOH solution. For each bamboo species, the sample size was equivalent to 25. Ethanol–toluene extractive content was assessed according to standard ASTM D1107—96 (2013) by ethanol–toluene ratio of 2:1 (v/v) through Soxhlet extraction. The extractive content after each extraction method was calculated by following Eq 2:

$$Extractive\ content\ (\%) = [(W1 - W2)/W1] \times 100 \qquad (2)$$

where, $W1$ and $W2$ are weight of oven-dried samples before and after extraction, respectively.

Analysis of cellulose, holocellulose, and α-cellulose content. Measurements of extractive free specimens were performed according to ASTM D1103-60 (1977), ASTM D1104-56 (1978), Li (2004), Pettersen (1984), and Bodirlau et al (2007) and the cellulose/holocellulose and α-cellulose content was calculated by using Eq 3. Each bamboo species was measured six times.

$$cellulose/holo\ cellulose/\alpha\ cellulose\ content\ (\%) = \left[\frac{W2 - W1}{W3}\right] 100 \qquad (3)$$

where, $W1$ is the oven-dried weight of crucible, $W2$ is the oven-dried weight of residue and crucible, $W3$ is the weight of oven-dried extraction-free sample before analysis.

Lignin content determination. Klason lignin content of extraction-free bamboo species was assessed according to ASTM D1106-96 (2001) and using Eq 4. Each bamboo species was measured in sample size as follows; *G. scortechinii* = 26, *G. levis* = 24, *S. brachyladum* = 25, and *B. vulgaris* = 23.

$$\%\ Klason\ lignin = \left[\frac{W1}{W2}\right] \times 100 \qquad (4)$$

where, $W1$ and $W2$ are the respective oven-dried weight of samples after and before measurement.

Ash content analysis and elemental analysis of bamboo. Ash contents were analyzed for lower (bottom section in Fig 1) and upper (combination of middle and top sections in Fig 1) parts along

the bamboo height. Ash content was determined based on the method outlined by ASTM D1102—84 (2013) and each bamboo species were analyzed with the respective sample number of 40 samples for each bamboo species.

The elemental composition of bamboo ash, was evaluated by Inductive Coupled Plasma Optical Emission Spectroscopy (ICP-OES) (Model Optima 5300 DV—Perkin Elmer, Shelton, CT).

Fourier Transform IR (FTIR) spectroscopy. FTIR analysis was performed to determine the functional chemical groups present in the bamboo species using FTIR Spectroscopy (NICOLET 6700 model, Thermo Scientific Inc., Madison, WI) equipped with an attenuated total system (ATR) system and processed with OMNIC software. The oven-dried (60°C for 24 h) bamboo particles were placed in contact with the ATR on the crystal plate. IR spectrum of bamboo specimens was recorded between the wavelengths from 850 cm^{-1} to 3700 cm^{-1} in transmission mode.

X-ray Diffraction (XRD) relative. Crystallinity index of bamboo specimens was analyzed using XRD method on a PANalytical Xpert Pro (X'pert Pro Panalytical, Netherlands) with Cu Kα, 1.54Å radiation source). Measurement was performed at an energy of 45 kV, an electric current of 40 mA in the scan ranges from 10° to 90° at a scan speed of 6°/min. Relative crystallinity of different bamboo fibers was calculated based on Segal method (Segal et al 1959; Yueping et al 2010; Yun et al 2016; Bakar and Kamke 2020) as shown in (Eq 5):

$$CrI = \left[\left(I_{002} - \frac{I_{am}}{I_{002}}\right)\right] \times 100\% \qquad (5)$$

where, Crystallinity index is the relative crystallinity (%), I_{002} is the maximum intensity of the peak between 20° and 25° (crystalline), and I_{am} is the lowest intensity between 15° and 22.7° (amorphous).

Calorific value determination. Calorific values of bamboo species were determined using IKA OBC Model C5000 (Cole-Parmer, Chicago, IL). A crucible containing 0.5 g of the specimen was lit in a combustion chamber. The pressure was set at 30 bars, and specimens were ignited at 298K in oxygen. 1 cm^3 of water was added to the decomposition vessel during analysis. Calorific values of bamboo were expressed in Joule per gram (J/g). Six samples were used for each bamboo species

Statistical analysis. Analysis of two-sample *T*-test was performed to compare sections (nodes and internodes) and locations (lower and upper) of the bamboo culm. One way analysis of variance (ANOVA) followed by Tukey test was used for multiple comparisons when comparing top, middle, and bottom locations of the bamboo culm to compare mean with a 95% confidence interval ($P < 0.05$).

RESULTS AND DISCUSSION

Specific Gravity, pH and Buffering Capacity

Specific gravity (SG) is ratio of density of a material to the density of water (Haygreen and Bowyer 1989). The average SG of all bamboo species ranged from 0.70 to 0.85 (Table 1), which is in the same range as previous studies (Ahmad and Kamke 2005; Kamruzzaman et al 2008; Yu et al 2008; Kaur et al 2016). For each bamboo species, there is statistically significant difference along the culm height for *G. scortechinii* bamboo ($F = 25.19$, $P = 0.00$) and *B. vulgaris* bamboo ($F = 9.35$, $P = 0.002$), at 95% confidence interval. In contrast, no significant differences were found for *G. levis* bamboo ($F = 0.62$, $P = 0.551$) and *S. brachyladum* bamboo ($F = 2.91$, $P = 0.088$). High SG of bamboo becomes a disadvantage when considered it for a specific application such as composite products where the recommended SG range is below 0.5 (Ahmad and Kamke 2005). However, other applications such as energy utilization and high-density feedstock are preferable as they contain more energy per unit volume (Kumar and Chandrashekar 2014).

The pH of the internode section of *G. scortechinii*, *G. levis*, *S. brachyladum*, and *B. vulgaris* were slightly acidic (Table 1). This is similar to other bamboo species such as *Dendrocalamus asper*

Table 1. SG and pH value of bamboo.

	SG*			pH				
Bamboo species	T*	M*	B*	T*	M*	B*	I*	N*
G. scortechinii	0.70^{a**}	0.75^{a**}	0.83^{a**}	4.58^{a**}	4.55^{a**}	4.58^{a**}	4.79^{a**}	4.3^{b**}
	(0.02)	(0.05)	(0.03)	(0.46)	(0.43)	(0.15)	(0.29)	(0.27)
G. levis	0.78^{c**}	0.74^{b**}	0.77^{a**}	5.07^{a**}	5.25^{a**}	4.82^{a**}	5.33^{a**}	4.8^{b**}
	(0.08)	(0.03)	(0.06)	(0.26)	(0.57)	(0.25)	(0.40)	(0.14)
S. brachyladum	0.82^{a**}	0.85^{a**}	0.77^{b**}	5.29^{a**}	5.24^{a**}	5.03^{a**}	5.18^{a**}	5.2^{a**}
	(0.07)	(0.05)	(0.03)	(0.22)	(0.21)	(0.27)	(0.23)	(0.28)
B. vulgaris	0.85^{a**}	0.85^{a**}	0.80^{a**}	4.62^{a**}	4.64^{a**}	4.63^{a**}	4.88^{a**}	4.3^{b**}
	(0.01)	(0.01)	(0.04)	(0.42)	(0.50)	(0.36)	(0.24)	(0.30)

SG, Specific gravity T, Top; M, Middle; B, Bottom; I, Internodes; N, Nodes.

** Results are expressed as mean and standard deviation (in parentheses) based on 71, 24, and 75 measurements for pH analysis, acid buffer capacity, and SG, respectively. Values that do not share a superscript letters (^{a,b}) within the same row are significantly different based on grouping information using Tukey Method, $P < 0.05$. Two-sample *T*-test was conducted to compare internodes and nodes, $P < 0.05$.

and *Dendrocalamus strictus* (Ahmad and Kamke 2003; Malanit et al 2009). pH values of the selected native bamboo species in this study were comparable to common wood species such as *Populous* spp., *Pinus sylvetris*, *Shorea* spp., and *Tsuga canadiensis* with a value of 5.8, 5.1, 4.7, and 5.5, respectively (Wegener 1989).

Buffer capacity varied among species and by internode and node (Fig 3). Compared with other bamboo species, *G. levis* required the greatest amount of acid (mL) to reach pH 3.5. Compared with the nodes, internodes required a higher amount of acid to change the pH of the bamboo species to 3.5. This is especially true for the species *G. levis* and *B. vulgaris*. Buffering capacity of native bamboo in this study ranged from 0.3 to 0.5 milliequivalents, higher than that of Calcutta bamboo (Ahmad and Kamke 2005) and some woody species such as *Populus* spp. (aspen, cottonwood), *Pseudotsuga menziesi* (douglas fir), *Tsuga canadensis* (eastern hemlock), and *Quercus alba* (white oak) (Wegener 1989).

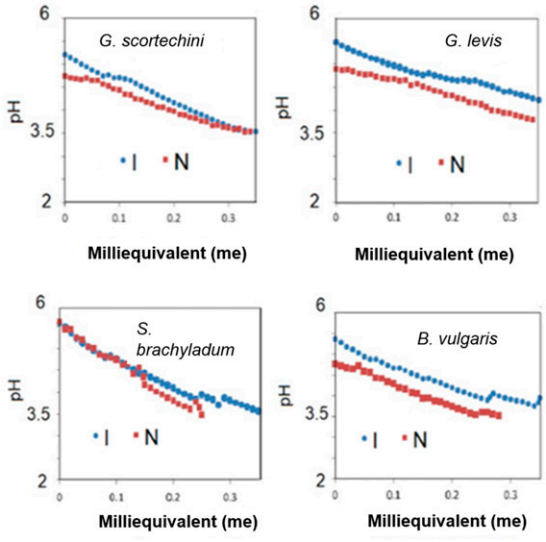

Figure 3. Buffering capacity of various bamboo species at internodes (I) and nodes (N) positions.

Analysis of Chemical Composition

Extractive contents of the studied bamboo species are presented in Fig 4(a). Extractives in bamboo are a minor fraction that consists of nonstructural organic and inorganic components (Qi et al 2013). The respective alkaline soluble content (%) for *G. scortechinii*, *G. levis*, *S. brachyladum,* and *B. vulgaris* bamboo species were 25.6%, 24.4%, 24.9%, and 24.7%, respectively (Fig 4[a]). No statistically significant difference was found along the culm height of *G. scortechinii* bamboo ($F = 0.34$, $P = 0.719$), *G. levis* bamboo ($F = 0.84$, $P = 0.462$), *S. brachyladum* bamboo ($F = 0.63$, $P = 0.549$) and *B. vulgaris* bamboo ($F = 2.25$, $P = 0.152$) (ANOVA, $\alpha = 0.05$). Also, the differences between the nodes and internodes section were statistically insignificant. Kaur et al (2016) reported that alkaline extractives of six Indian

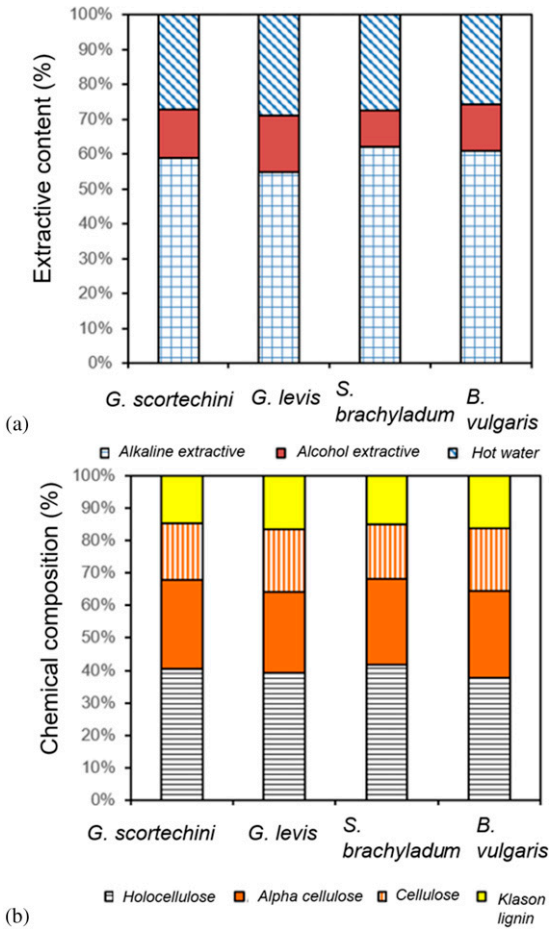

Figure 4. (a) Graphical representation of extractive content, (b) chemical composition for all varieties of bamboo species studied. Number of specimens, n for Alkaline extractive = 96, alcohol extractive = 99, hot-water extractive = 96, holocellulose = 48, α-cellulose = 43, cellulose = 24, Klason lignin = 98, ash = 168, and calorific value = 24.

bamboo species ranged from 26.1% to 28.3%, which is slightly higher than the values obtained in this study (24.7-25.6%). High alkaline-extractive content suggests that the bamboo samples should be properly stored after harvesting to avoid degradation (Kaur et al 2016).

Ethanol–toluene extractive content showed that the respective average values for *G. scortechinii*, *G. levis*, *S. brachyladum*, and *B. vulgaris* were 5.5%, 7.0%, 4.5%, and 3.7% (Fig 4[a]). The values for nodes specimens of *G. scortechinii*, *G. levis*, *S. brachyladum*, and *B. vulgaris* were 4.1%, 4.7%, 3.1%, and 5.4%, respectively. There was no statistically significant difference found between nodes and internodes for all bamboo specimens. Hot-water extractive content indicated that the average values for *G. scortechinii*, *G. levis*, *S. brachyladum*, and *B. vulgaris* were 11.8%, 12.8%, 11.0%, and 10.4%, respectively. The differences between height and types of bamboo species were not statistically significant. This was also true for the nodes and internodes of *S. brachyladum* and *B. vulgaris* samples. However, the differences between hot-water extractive content of internodes and nodes for *G. scortechinii* and *G. levis* bamboo samples were statistically significant (*P*-value equivalent to 0.000 and 0.001, respectively, at 95% confidence interval). The ethanol–toluene content and hot-water extractive content in this study ranged from 4.1% to 7.2% and 10.4% to 12.8%, respectively, which is slightly higher than the values previously reported for bamboo species. Ethanol and hot-water extractive content of bamboo samples from the literature ranged between 3.15% and 5.99% and 5.26% and 12.6% (Li 2004; Kaur et al 2016).

Chemical compositions of native bamboo samples are shown in Fig 4(b). The average holocellulose content ranged from 64.50% to 70.65%. Along bamboo's culm height, only *G. scortechinii* showed a significant difference in the average value. The magnitude of difference between nodes and internodes was not significant in all bamboo species. The average respective values of α-cellulose ranged between 40.73% and 47.86%. These values were higher for internodes than nodes, with the difference being significant in *G. levis* and *B. vulgaris* bamboo. Comparison between all bamboo species indicated a significant difference in terms of α-cellulose ($F = 5.07$, $P = 0.005$) at a 95% confidence interval. In this study, the value of holocellulose was found within 64.49-70.54%, which was lower than the value determined by Kumar and Chandrashekar (2014) for different Indian bamboo species.

Klason lignin content of *G. scortechinii*, *G. levis*, *S. brachyladum,* and *B. vulgaris* was 25.91%, 27.30%, 25.30%, and 28.39%, respectively. No

Table 2. Cellulose to lignin (C/L) ratio of different bamboo species.

Bamboo	C/L ratio
G. scortechinii	1.16
G. levis	1.14
S. brachyladum	1.12
B. vulgaris	1.18

significant differences were found in the culm height of bamboo samples. However, a comparison between internodes and nodes showed a significant difference in *G. levis*, *S. brachyladum*, and *B. vulgaris* samples. The lignin content of selected Malaysian native species consistent with that of Indian native bamboo species previously reported, ranging from 20% to 32.5% (Li 2004; Wahab et al 2013; Kumar and Chandrashekar 2014; Kaur et al 2016). Depending on intended application, high lignin content in bamboo samples might be favorable, eg for biorefinery or energy purposes.

Cellulose to lignin (C/L) ratio ranged from 1.12 to 1.18 (Table 2); lower than the value for most hardwoods (Bodirlau et al 2007). C/L ratio is a significant criterion in biochemical conversion process of biomass and the utilization of biomass for pulping.

FTIR Spectroscopy

FTIR transmittance band assignment and spectra of native bamboo samples are shown in Fig 5 and Table 3. The broad band at around 3300 cm^{-1} may be associated with expanding and contraction vibration of OH, which could be related to the presence of alcoholic and phenolic hydroxyl groups involved in hydrogen bonds (Ghaffar and Fan 2013). The prominent band at around 2890 cm^{-1} is associated with CH can also be observed. Typical assignments of bands at around 1600 cm^{-1}, 1500 cm^{-1}, and 1430 cm^{-1} are related to skeletal vibration of the aromatic ring from lignin, C=C stretching vibration in the aromatic structure of lignin, and CH bending in plane, respectively (Ghaffar and Fan 2013). The vibration at around 1240 cm^{-1} can be attributed to the presence of guaiacyl type lignin in bamboo (Chen et al 2014).

The intensity of FTIR bands was used to evaluate the ratio between aliphatic and aromatic absorption, syringyl/guaiacyl (S/G) ratio, and phenolic OH group and CO group contents, as described previously (Bodirlau et al 2007). Table 4 shows that the absorbance ratio of S/G in Malaysian bamboo is almost similar to each other regardless of species. This ratio is one of the key parameters

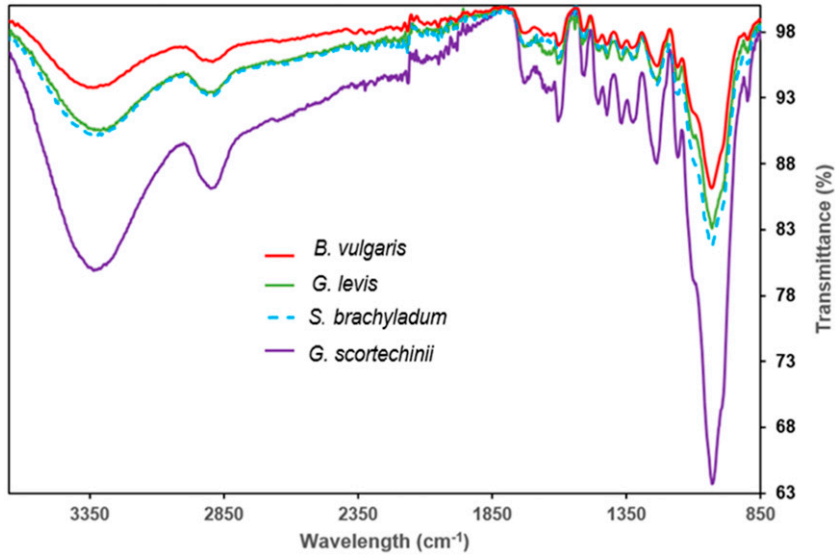

Figure 5. ATR-FTIR spectrum of all different bamboo species.

Table 3. Corresponding chemical bonds to their associated bands.

Wavenumber (cm^{-1})					
G. levis	*G. scortechinii*	*S. brachyladum*	*B. vulgaris*	Corresponding chemical bonds	References
3340.2	3334.5	3333.9	3332.7	O–H, expanding and contracting vibration	Yueping et al 2010; Chen et al 2014; Ghaffar 2016
2893.0	2893.0	2895.0	2893.5	C–H, expanding and contracting vibration	Yueping et al 2010; Chen et al 2014; Ghaffar 2016
1603.4	1603.6	1604.0	1603.1	Skeletal vibration of aromatic ring from lignin	Yueping et al 2010; Ghaffar 2016
1506.5	1506.2	1514.3	1509.1	C=C stretching vibration in aromatic structure of lignin	Chen et al 2014
1423.1	1423.8	1423.1	1421.6	C–H, bending in plane	Yueping et al 2010; Chen et al 2014
1318.1	1318.1	1323.8	1323.5	O–H, bending vibration in plane	Yueping et al 2010
1236.0	1235.0	1238.0	1238.0	Acyl-oxygen CO–OR stretching vibrations in hemicelluloses, C–O of guaiacyl unit stretching vibrations in lignin	Chen et al 2014
1160.0	1152.3	1158.0	1160.0	C–O from *p*-coumaric ester group, typical for H, G and S lignin	Yueping et al 2010; Ghaffar 2016
1030.1	1030.1	1031.6	1027.0	Aromatic C–H in plane deformation, symmetrical C–O stretching	Ghaffar 2016
899.7	894.0	894.0	895.0	C–H deformation in cellulose; C–H stretching out of plane due to β-linkage	Ghaffar 2016

in biomass material as it influences the delignification process and the recalcitrance of sugar release (Yoo et al 2018). Content of phenolic OH groups and aliphatic to aromatic absorbance ratio is also similar for all bamboo species. Phenolic OH groups are important because they enable sulfonation, cleavages of major interunit ether linkages in both acidic and alkaline conditions, and oxidative delignification reaction (Lai and Guo 1991).

Table 4. Ratio of aliphatic to aromatic signals, S/G (syringyl/guaiacyl) ratio, the content of phenolic OH groups, and C–O groups.

	Aliphatic to aromatic absorbance ratio signal (A_{2893}/A_{1506})	S/G ratio (A_{1323}/A_{1506})	Content pf phenolic OH groups (A_{1323}/A_{1502})
G. levis	0.90	1.03	0.96
G. scortechinii	0.96	1.01	0.98
S. brachyladum	0.95	1.02	0.98
B. vulgaris	0.97	1.01	0.98

Crystalline Structure of Native Bamboo Species

Crystalline character of lignocellulosic materials influences their acid/enzymatic hydrolysis behavior (Rambo and Ferreira 2015). The XRD of four Malaysian native bamboo samples are illustrated in Fig 5. The existence of two peaks (16° and 23°) at different diffraction angles indicates the

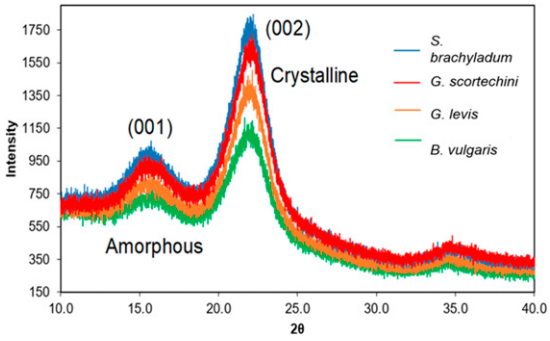

Figure 6. XRD Diffraction of native bamboo species.

semicrystalline structure of bamboo samples. The diffraction peaks at about 16° and 23° can be associated with cellulose I and IV, both exhibiting monoclinic structure (Poletto et al 2014; Mayandi et al 2015).

Crystallinity index of the sample is computed with Eq 5 by removing the intensity approximately at 16°, leaving the crystalline to total material ratio (Fig 6). This technique approximates the crystalline percentage in the sample and neglect other criteria as peak overlap, crystallite size, orientation, and paracrystallinity (French and Santiago Cintrón 2013). Therefore, this method provides relative crystallinity index for comparison purposes within this study.

The crystallinity index of the bamboo species indicated that the crystallinity of different bamboo samples was almost identical, ranging from 42.0% to 44.4% (Table 5). These values are lower than the crystallinity index of *Neosinocalamus affinis* sample (Yueping et al 2010) and higher than Moso bamboo (Yun et al 2016). Generally, the crystallinity of bamboo is significantly lower than flax, banana, sisal, kapok, pineapple leaf and coir (Table 6). This is a favorable characteristic as it indicates low recalcitrance of lignocellulosic biomass to improved sugar access (Chin et al 2017), thus, increasing accessibility to xylans and

Table 5. Crystallinity index (%) of bamboo samples.

Bamboo species	002 Crystal plane angle (2θ)	I_{002}	001 Crystal plane angle (2θ)	I_{am}	Crystallinity index (%)
G. scortechinii	22.1	1724	15.4	958	44.4
G. levis	22.1	1503	15.7	854	43.2
S. brachyladum	22.2	1845	15.7	1070	42.0
B. vulgaris	21.7	1213	15.8	688	43.3

Table 6. Degree of crystallinity (DC) of some other lignocellulosic materials.

Sample type	DC (%)	References
Bamboo (*Neosinocalamus affinis*)	52.5	Yueping et al 2010
Jute	53.8	
Flax	67.4	
Bamboo (*Moso*)	38.3	Yun et al 2016
Banana rachis	80.9	Deepa et al 2015
Sisal	91.3	
Kapok	86.5	
Pineapple leaf	92.3	
Coir	84.5	

DC, Degree of crystallinity.

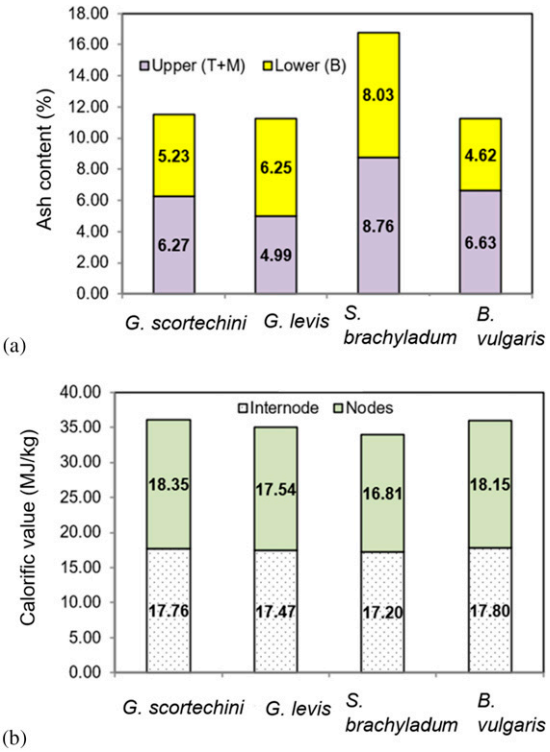

Figure 7. Ash content and calorific value of bamboo species at different culm positions. Number of specimens, *n* for ash = 168 and calorific value = 24.

Table 7. Elemental composition of bamboo ashes.

	Inorganic elements (mg/kg)				
Bamboo species	Al	Ca	Cu	Fe	K
G. scortechinii	12.16[a*]	1022.8[a*]	5.81[a*]	87.42[a*]	1917.2[a*]
	(9.96)	(565.2)	(2.38)	(55.48)	(1213.5)
G. levis	10.21[a*]	1195.5[a*]	2.84[b*]	103.39[a*]	1243.7[a*]
	(8.04)	(320.0)	(1.14)	(49.26)	(1296.0)
S. brachyladum	18.20[a*]	1127.6[a*]	1.92[b*]	110.17[a*]	1077.9[a*]
	(13.94)	(363.2)	(1.20)	(58.53)	(122.2.8)
B. vulgaris	18.26[a*]	1179.8[a*]	5.79[a*]	110.12[a*]	845.9[a*]
	(11.48)	(307.2)	(3.13)	(47.71)	(922.3)
	Mg	Mn	Na	Si	Zn
G. scortechinii	421.6[ab*]	76.69[b*]	98.01[a*]	236.46[a*]	42.27[a*]
	(195.4)	(82.59)	(76.84)	(233.18)	(41.32)
G. levis	465.1[ab*]	95.12[b*]	107.67[a*]	238.27[a*]	78.57[a*]
	(164.1)	(61.48)	(75.14)	(217.97)	(76.34)
S. brachyladum	312.3[b*]	187.05[a*]	206.56[a*]	163.02[a*]	60.10[a*]
	(88.6)	(108.61)	(153.06)	(87.61)	(54.92)
B. vulgaris	648.0[a*]	69.32[b*]	128.59[a*]	400.14[a*]	76.61[a*]
	(312.5)	(58.12)	(70.20)	(339.45)	(110.04)

Means that do not share a superscript letters ([a,b]) within the same column are significantly different based on grouping information using Tukey Method, $P < 0.05$.

* Results are expressed as mean and values in parentheses represent standard deviation based on three measurements for each element.

glucans during enzymatic hydrolysis process, ie during bioethanol production.

Calorific Value and Inorganic Compositions of Native Bamboo Species

Ash content values ranged from 5.43% to 8.50% (Fig 7[a]). Comparison along the culm height of bamboo (upper and lower sections) illustrated that the difference was not significant at 95% confidence interval. However, significant difference was found among the bamboo species ($F = 4.78$, $P = 0.003$). The ash content of current bamboo species ranged from 5.43% to −8.5%, which are higher than the values previously reported from Indian bamboo samples, ie the ash content of Indian native bamboo samples ranged from 0.4% to 3.0% (Kumar and Chandrashekar 2014). Table 7 indicates the ash compositions in Malaysian native bamboo samples. Results indicated that K, Ca, Mg, Si, Na and Fe are the main elements of ash in the bamboo samples. Potassium (K) was the major element among all bamboo species (846 mg/kg-1917.2 mg/kg) and the highest amount was found in *G. scortechinii* bamboo

Mean calorific values of *G. scortechinii*, *G. levis*, *S. brachyladum,* and *B. vulgaris* were 18.06 MJ/kg, 17.50 MJ/kg, 17.00 MJ/kg, and 17.97 MJ/kg, for both internodes and nodes respectively (Fig 7[b]). The differences among bamboo species were statistically significant (ANOVA, $\alpha = 0.05$, $F = 10.70$, $P = 0.000$). Comparison between nodes and internodes suggested that the magnitude of differences was not significant. The low calorific value of *S. brachyladum* could be due to high ash content (8.09%) and low lignin content (25.33%) compared with other bamboo species. These results are consistent with Kumar and Chandrashekar (2014) who reported high ash content and low lignin content may contribute to lower calorific value. High SG of bamboo (0.7-0.85) with calorific value values between 17.06 and 18.06 MJ/kg indicates that the current native Malaysian bamboo species have great energy potential, although relatively high ash content of some species, eg *S. brachyladum*, may negatively affect its heating value.

Traces of mineral ions in lignocellulosic materials may affect their use for future applications.

Inorganic elements in ash do not burn to generate heat, and are, therefore, a hindrance in energy utilization. The content of potassium (K) was the highest in all bamboo species (846-1917.2 mg/kg) and the highest amount was found in *G. scortechinii* bamboo. The second highest element was calcium (Ca), with an average value of 1022-1180 mg/kg. Potassium (K) is among the major alkali element in most lignocellulosic materials (Mlonka-Mędrala et al 2020) with an average concentration of 21-70% in ash composition of bamboo (Kumar and Chandrashekar 2014; Samadhi et al 2018). During combustion process, potassium (K) and sodium (Na) are responsible for lowering the ash melting point. This can cause clinkers problems that can jam the furnace. Slugging and fouling can also occur when ash is vaporized and condensed in the boiler, leading to hard formation on heat transfer surfaces (Clarke and Preto 2011). Alternately, calcium (Ca) and magnesium (Mg) will increase the melting point of ash. Lignocellulosic materials with higher amounts of calcium such as wood are preferred over the material with a higher alkali metal. They pose fewer fouling problems than herbaceous materials such as straws and grass (Miles et al 1996; Kumar and Chandrashekar 2014). Bamboo has similarity with wood biomass materials in terms of desirable fuel characteristics such as low alkali index and low ash content. Although its heating value is considerably lower than some wood species, it is still higher than straws, grasses, and most agricultural residues (Chin et al 2017).

CONCLUSIONS

Experiments were conducted to determine the physicochemical properties of four Malaysian bamboo species. The four bamboo species showed a similar range of values in all the experiments tested, especially in SG, chemical compositions, FTIR spectra, crystallinity, and elemental analysis. However, the node showed greater variability in pH, buffering capacity, α-cellulose, and lignin content. Culm height had only influenced some bamboo species for SG values. In manufacturing, the minimum variability could lead to maximum utilization of raw material. Nodes could be excluded from certain composite products because they exhibited greater variability.

Additionally, the indication of SG showed a value >0.7, indicating that the four bamboo species are suitable for producing composite materials that minimize the increase of SG in the final products such as oriented strand board (OSB), laminated veneer lumber (LVL), plywood and glued-laminated lumber (glulam). Chemical nature of the four bamboo species is critical for the selection of an adhesive system. Acidity values through pH and buffer capacity are among the principal factors was addressed. The four bamboo species are more on acidic conditions and exhibit a high buffer capacity, thus relating it to the certain formulation to maximize the quality of adhesive system. The properties of the four bamboo species studied are comparable to those of other bamboo species. This suggests that the use of bamboo for the production of bioresin production in the wood industry is possible and could solve the problem of supply of certain bamboo species.

REFERENCES

Abdulkhani A, Alizadeh P, Hedjazi S, Hamzeh Y (2017) Potential of soya as a raw material for a whole crop biorefinery. Renew Sustain Energy Rev 75:1269-1280.

Ahmad M, Kamke FA (2003) Analysis of Calcutta bamboo for structural composite materials: Surface characteristics. Wood Sci Technol 37:233-240.

Ahmad M, Kamke FA. (2005) Analysis of Calcutta bamboo for structural composite materials: Physical and mechanical properties. Wood Sci Technol 39:448-459.

Anon. (2018) Rattan and Bamboo. Forestry Department of Peninsular Malaysia. https://www.forestry.gov.my/index.php/en/buluh-dan-rotan

ASTM D1102—84 (2013) Standard test method for ash in wood. http://www.astm.org/cgi-bin/resolver.cgi?D1102-84(2013)

ASTM D1103-60 (1977) Method of test for Alpha-cellulose in wood.

ASTM D1104-56 (1978) Method of test for holocellulose in wood.

ASTM D1106-96 (2001) Standard test method for acid-insoluble lignin in wood.

ASTM D1107—96 (2013) Standard test method for ethanol–toluene solubility of wood. http://www.astm.org/cgi-bin/resolver.cgi?D1107-96(2013)

ASTM D1109—84 (2013) Standard test method for 1% sodium hydroxide solubility of wood. http://www.astm.org/cgi-bin/resolver.cgi?D1109-84(2013)

Bakar BFA, Kamke FA (2020) Comparison of alkali treatments on selected chemical, physical and mechanical properties of grape cane fibers. Cellulose 27(13):7371-7387.

Cao X, Peng X, Sun S, Zhong L, Sun R (2014) Hydrothermal conversion of bamboo: Identification and distribution of the components in solid residue, water-soluble and acetone-soluble fractions. J Agric Food Chem 62: 12360-12365.

Chen C, Luo J, Qin W, Tong Z (2014) Elemental analysis, chemical composition, cellulose crystallinity, and FT-IR spectra of toona sinensis wood. Monatsh Chem 145(1): 175-185.

Chin KL, Ibrahim S, Hakeem KR, San H'ng P, Seng HL, Mohd AML (2017) Bioenergy Production from bamboo: Potential source from Malaysia's perspective. BioResources 12(3):6844-6867.

Clarke S, Preto F (2011) Biomass burn characteristics. http://www.omafra.gov.on.ca/english/engineer/facts/11-033.htm.

Deepa B, Abraham E, Cordeiro N, Mozetic M, Mathew AP, Oksman K, Faria M, Thomas S, Pothan LA (2015) Utilization of various lignocellulosic biomass for the production of nanocellulose: A comparative study. Cellulose 22(2):1075-1090.

Ekstrom H (2022) The large softwood timber surplus in the US south is likely to diminish over the next decade, resulting in regional increases in sawlog prices. https://finance.yahoo.com/news/large-softwood-timber-surplus-us-205100534.html.

French AD, Santiago Cintrón S (2013) Cellulose polymorphy, crystallite size, and the Segal crystallinity index. Cellulose 20(1):583-588.

Ghaffar SH (2016) Aggregated understanding of characteristics of wheat straw node and internode with their interfacial bonding mechanisms. Brunel University London, London, UK.

Ghaffar SH, Fan M (2013) Structural analysis for lignin characteristics in biomass straw. Biomass Bioenerg 57: 264-279.

Ghavidel A, Hosseinpourpia R, Gelbrich J, Bak M, Sandu I (2021) Microstructural and chemical characteristics of archaeological white elm (*Ulmus laevis* p.) and poplar (*Populus* spp.). Applied Sciences (Switzerland) 11(21): 10271.

Ghavidel A, Hosseinpourpia R, Militz H, Vasilache V, Sandu I (2020) Characterization of archaeological European white elm (*Ulmus laevis* spp.) and Black Poplar (*Populus nigra* L.). Forests 11(12):1-13.

Haygreen JG, Bowyer JL (1989) Forest products and wood science: An introduction. 2nd edition. Iowa State University Press, Ames, IW.

Hisham, HN, Othman S, Rokiah H, Mohmod AL, Ani S, Mustafa MT (2005) Characterization of bamboo *Gigantochloa scortechinii* at different ages. J Trop For Sci 18(4):236-242.

Kamruzzaman M, Saha SK, Bose AK, Islam MN (2008) Effects of age and height on physical and mechanical properties of bamboo. J Trop For Sci 20(3):211-217.

Kamthai S (2003) Alkaline sulfite pulping and ECF-bleaching of sweet bamboo (*Dendrocalamus Asper Backer*). Kasetsart University, Bangkok.

Kamthai S, Puthson P (2005) The physical properties, fiber morphology and chemical compositions of sweet bamboo (*Dendrocalamus Asper Backer*). Witthayasan Kasetsat Witthayasat 39(4):581-587.

Kaur, PJ, Kardam V, Pant KK, Naik SN, Satya S (2016) Characterization of commercially important Asian bamboo species. Eur J Wood Wood Prod 74(1):137-139.

Kuehl Y (2015) Resources, yield, and volume of bamboos of Bamboos BT - Bamboo: The Plant and its Uses (W. Liese & M. Köhl (eds.); pp. 91-111). Springer International Publishing, Switzerland

Kumar R, Chandrashekar N (2014) Fuel properties and combustion characteristics of some promising bamboo species in India. J For Res 25(2):471-476.

Lai YZ, Guo XP (1991) Variation of the phenolic hydroxyl group content in wood lignins. Wood Sci Technol 25(6):467-472.

Li X (2004) Physical, chemical, and mechanical properties of bamboo and its utilization potential for fiberboard manufacturing. LSU Master's Theses. 866, Louisiana State University. https://digitalcommons.lsu.edu/gradschool_theses/866.

Malanit P, Barbu MC, Frühwald A (2009) The gluability and bonding quality of an Asian bamboo (*Dendrocalamus Asper*) for the production of composite lumber. J Trop For Sci 21(4):361-368.

Mayandi, K, Rajini N, Pitchipoo P, Sreenivasan V, Jappes JW, Alavudeen A (2015) A comparative study on characterisations of *Cissus quadrangularis* and *Phoenix reclinata* natural fibres. J Reinf Plast Compos 34(4): 269-280.

Miles TR, Baxter LL, Bryers RW, Jenkins BM, Oden LL (1996) Alkali deposits found in biomass power plants, Vol 1. NREL Report, Golden, CO.

Mlonka-Mędrala A, Magdziarz A, Gajek M, Nowińska K, Nowak W (2020) Alkali metals association in biomass and their impact on ash melting behaviour. Fuel 261: 116421.

Mohmod AL, Othman AR, Husain H, Mustafa MT (2016) Bamboo as a commodity: It is a dream or a possibility. *In* Proceedings of ASEAN Bamboo Symposium, 27-29 September 2016, Kuala Lumpur, Malaysia. Published by Forest Research Insititute Malaysia (FRIM), Kepong, Malaysia.

Pettersen RC (1984) The chemical composition of wood. Page 57-126 *in* R Rowell ed. The Chemistry of Solid Wood. Advances in Chemistry Series No. 207. ISBN 0-84120796-8. Washington 1984: American Chemical Society

Poletto M, Ornaghi Júnior HL, Zattera AJ (2014) Native cellulose: Structure, characterization and thermal properties. Materials (Basel) 7(9):6105-6119.

Qi J, Xie J, Hse CY, Shupe TF (2013) Analysis of *phyllostachys pubescens* bamboo residues for liquefaction: Chemical components, infrared spectroscopy, and thermogravimetry. BioResources 8(4):5644-5654.

Rambo MKD, Ferreira MMC (2015) Determination of cellulose crystallinity of banana residues using near infrared spectroscopy and multivariate analysis. J Braz Chem Soc 26(7):1491-1499.

Bodirlau R, Spiridon I, Teaca CA (2007) Chemical investigation of wood tree species in temperate forest in East Northern Romania. BioResources 2(1):41-57.

Samadhi T, Narcia F, Amril H (2018) Preliminary evaluation of potassium extraction from bamboo ash. *in* MATEC Web of Conferences Volume 156, The 24th Regional Symposium on Chemical Engineering (RSCE 2017), 15-16 Nov 2017, Semarang, Indonesia. https://doi.org/10.1051/matecconf/201815603027. Published by EDP Sciences, Les Ulis, France.

Segal L, Creely JJ, Martin AE, Conrad CM (1959) An empirical method for estimating the degree of crystallinity of native cellulose using the X-ray diffractometer. Textile Res J 29(10):786-794.

TAPPI-T509 (2006) Hydrogen Ion Concentration (Ph) of Paper Extracts (Cold Extraction Method).

The Malaysian Reserve (2022) Sabah Timber Trade on a Decline for next 20 Years. https://themalaysianreserve.com/2017/03/31/sabah-timber-trade-on-a-decline-for-next-20-years/ (18 April 2022).

W. Liese, Bamboos-Biology, Silvics, Properties, Utilization. Eschborn: Deutsche Gesellschaft für Technische Zusammenarbeit, 1985.

Wahab R, Mustafa MT, Sudin M, Mohamed A, Rahman S, Samsi HW, Khalid I (2013) Extractives, holocellulose, α-cellulose, lignin and ash contents in cultivated tropical bamboo *Gigantochloa brang*, *G. levis*, *G. scortechinii* and *G. wrayi*. Curr Res J Biol Sci 5(6): 266-272.

Wegener DFG (1989) Wood: Chemistry, ultrastructure, reactions. Walter de Gruyter, Berlin [etc.].

Wong KM (1995) The bamboos of peninsular Malaysia. Forest research institute Malaysia, Published by Forest Research Intitute Malaysia (FRIM) in collaboration with Forest Research Centre, Forestry Department, Sabah, Malaysia.

Yoo CG, Dumitrache A, Muchero W, Natzke J, Akinosho H, Li M, Sykes RW (2018) Significance of lignin S/G ratio in biomass recalcitrance of *Populus trichocarpa* variants for bioethanol production. ACS Sustain Chem Eng 6(2):2162-2168.

Yu HQ, Jiang ZH, Hse CY, Shupe TF (2008) Selected physical and mechanical properties of moso bamboo (*Phyllostachys pubescens*). J Trop For Sci 20(4):258-263.

Yueping W, Ge W, Cheng H, Tian G, Zheng L, Qiao QF, Zhou X, Han X, Gao X (2010) Structures of bamboo fiber for textiles. Textile Res J 80(4):334-343.

Yun H, Li K, Tu D, Hu C (2016) Effect of heat treatment on bamboo fiber morphology crystallinity and mechanical. Wood Res 61(2):227-234.

THE INFLUENCE OF FOAM DISCONTINUITY IN THE SHEAR ZONE OF STRUCTURAL INSULATED PANEL BEAMS

R. Shmulsky†

Department Head and Warren S. Thompson
Professor Department of Sustainable Bioproducts
Mississippi State University
Mississippi State, MS
E-mail: rs26@msstate.edu

*L. Khademibami**

Postdoctoral Associate
Department of Sustainable Bioproducts
Mississippi State University
Mississippi State, MS
E-mail: lk475@mssatte.edu

C. A. Senalik

Research General Engineer
U.S. Forest Service Forest Products Laboratory
United States Department of Agriculture
Wisconsin State, WI
E-mail: christopher.a.senalik@usda.gov

R. D. Seale

Warren S. Thompson Professor
Department of Sustainable Bioproducts
Mississippi State University
Mississippi State, MS
E-mail: dan.seale@msstate.edu

R. J. Ross

Supervisory Research Gen. Engineer
U.S. Forest Service Forest Products Laboratory
United States Department of Agriculture
Wisconsin State, WI
E-mail: robert.j.ross@usda.gov

(Received April 2022)

Abstract. The effect of foam discontinuity in the shear zone of structural insulated panel (SIP) beams was investigated in the current research. Two depths of 15.24 cm and 31.11 cm (6.5 in. and 12.25 in.) SIPs were evaluated in 1/3-point bending. Panels were sawn into beams, each approximately 29.84 cm (11.75 in.) wide, for the mechanical testing. Half of the panels had joints or discontinuities in the foam layer in a location that was subject to shear stress during the bending tests. Half of the panels did not have joints or discontinuities in the foam layer in the locations that were subject to shear stress during the bending tests. The specimens with no foam discontinuity, stressed in shear, were approximately twice as strong as the specimens with a foam discontinuity. This finding has implications for routine testing and evaluation as well as for allowable properties. In the case of routine testing, foam discontinuities should purposefully be located in the zone of maximum shear as these appear to be a limiting factor. In cases where a producer

* Corresponding author
† SWST member

manufactures SIPs with zero discontinuities, it may be prudent to seek premium value as those panels would achieve superior properties.

Keywords: Structural insulated panels, shear stress, bending test, foam, joints, and routine testing.

INTRODUCTION

Structural insulated panels (SIPs) contain an insulating foam core sandwiched between two structural facings, typically oriented strand board (OSB). Other facing materials include plywood, gypsum sheathing, sheet metal, fiber cement siding, magnesium oxide board, fiberglass mat, and composite structural siding panels. The cores of SIPs are composed of foam products, expanded polystyrene (EPS), extruded polystyrene (XPS), and polyurethane (PUR) (Morley 2000; Aldrich et al 2010).

SIPs are well established as a form of residential and light commercial building construction and widely used in both residential and nonresidential construction industries. They are extremely strong, energy-efficient, and cost-effective with excellent thermal resistance (Aldrich et al 2010; Cox and Hamel 2021). SIPs offer excellent energy performance as well as safe and reliable strength, stiffness, and other mechanical properties. Due to their superior thermal performance, decreased construction time and waste, and reducing carbon footprints, SIPs are increasingly becoming popular for commercial and residential construction in the United States and Canada (Morley 2000; Medina et al 2008; Mcintosh and Guthrie 2010). Although most SIPs are used in wall applications, they can also be used as roof or floor panels that are exposed to long-term transverse loading (McDonald et al 2014). With respect to building code compliance, SIPs are recognized by the International Residential Code. One of the properties that remains to be well investigated and modeled is load duration. The study detailed herein, related to static bending properties, is a component of a larger load duration study. Typically, during manufacturing, ridged foam insulation is sandwiched between matching layers of OSB facers. The ridged foam is commonly EPS, polyurethane, or XPS. The OSB facers are often full-length jumbo sheets (up to 7.31 m [24 ft.]) or end jointed (finger jointed or scarf jointed) 1.21 × 2.43 m (4 × 8 ft.) sheets. The foam core is bonded to the OSB facers with adhesives. In some cases, the foam may be the full length of the panel. In other cases, the foam may have end joints. These foam end joints act as discontinuities. These discontinuities have reduced shear capacity as compared with nonend jointed foam. While discontinuities in the foam are not necessarily randomly located, they are considered existent in the design and allowable properties. This consideration is prudent because a designer or engineer won't always know the extent to which a given SIP will have a discontinuity in a shear-critical area or application.

Creep or duration-of-load evaluation of SIPs follows ASTM D6815 (ASTM 2015b). Therein, the dead load values (and associated bending stress values) for the long-term "creep-rupture" or duration of load testing are based on laboratory short-term bending tests: "The specimens selected for these tests shall be tested at a constant stress level, f_b, … as determined in accordance with Eq 1 … where … f_b = 0.55 × (5% PE) where f_b = minimum applied bending stress, and 5% PE = the lower five percent point estimate, as determined from the short-term bending tests … " In the case of the 30-specimen samples herein, the respective 5% parametric point estimates are determined as mean minus the standard deviation times 1.645. Testing is specified per either ASTM (2015a) or ASTM (2013). Each of those methods specifies full-scale flexural testing, ie testing in the structural size(s) in 1/3-point bending at a span: depth ratio ranging from 17:1 to 21:1.

Therefore, the objective of this research is to investigate the influence of foam discontinuities on the flexural performance of SIPs. It is hypothesized that the inclusion of a foam discontinuity in the area of maximum shear stress (locations between reaction supports and load head in a 1/3-point bending test) would significantly influence the flexural performance of the SIP beams.

MATERIALS AND METHODS

The research detailed herein occurred in three phases. Each phase used similarly specified SIP beams. Essentially, the beams had EPS foam cores, specified at a density of approximately 0.016 g/cm^3 (1.0 lb/ft.^{3}). All beams had 1.11-cm (7/16 in.) thick OSB facers. All OSB was the Engineered Wood Association (APA) rated, Exposure 1, 24/16 span rated. Test specimens were constructed with the OSB strength axis oriented parallel with the length of the SIP panel. Specimens were categorized into one of two depth classes, ie, either 15.24 cm and 31.11 cm (6.5 in. or 12.25 in.) deep. All specimens were approximately 29.84 cm (11.75 in.) wide. Specimens were tested in 1/3-point flexure at an approximate 18:1 span to depth ratio. As a target, half of the specimens had EPS foam with at least one discontinuity in the zone of maximum shear, ie between the reaction support and the load head; between zero and 1/3 of the span from the reaction support. Half of the specimens had EPS foam that did not have at least one discontinuity in the zone of maximum shear (Fig 1). Those specimens did have an EPS discontinuity, but it was located within the middle 1/3 of the span, ie the zone with zero shear stress.

As the first step in this evaluation (Study 1), a preliminary study was conducted and reported (McDonald et al 2014). There, 31.11-cm (12.25 in.) deep specimens were tested. The results of the bending tests are presented in McDonald et al (2014). These beams were tested in 1/3-point bending over a 5.48-m (18 ft. = 216 in.) long span (17.6:1 span: depth ratio). Summarized results from the short-term bending tests, with foam flush ends is shown in Table 1.

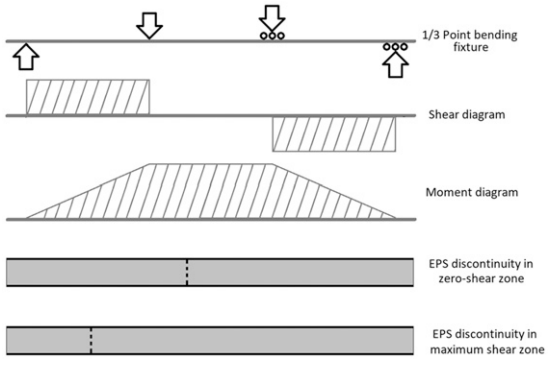

Figure 1. Diagram of 1/3 point flexural bending set up along with shear and moment diagrams, and sketch of expanded polystyrene (EPS) foam discontinuity location(s).

Also, the following information is footnoted to these results in that investigation: "Two failure modes were observed, each with a consistent strength value: Specimen that had adhesion failure failed near 5338 N (1,200 lbf). Specimen that had flange compression failed near 8896 N (2000 lbf)". Also, Figures 12 and 13 in McDonald et al (2014) illustrate the two failure modes: adhesion due to shear at EPS discontinuity and compression failure in the OSB, respectively. This study does not however discern which specimens had an EPS discontinuity in the zone of maximum shear and which do not. Next (Study 2), a full complement (28 specimens of each size) of 15.24 cm and 31.11 cm (6.5 in. deep and 12.25 in.) deep specimens were tested in bending (McDonald et al 2018). This number of specimens was selected because it is the minimum number from which a nonparametric 5th percentile can be computed. The 15.24-cm (6.5 in.) deep specimens were tested over a 300-cm (118.5 in.) long span (18.2 span: depth ratio). Similar to the previous work, the 31.11-cm (12.25 in.) deep specimens were tested over a 5.48-m (18 ft = 216 in.) long span

Table 1. Maximum load values for preliminary tests on 31.11 cm (12.25 in) deep SIPs beams.

Sample ID	P_{Max} (lbf)	P_{Max} (N)
13A	1237	5492.28
22A	1226	5443.44
23A	1264	5612.16
31A	1136	5043.84
38A	1232	5470.08
43A	1233	5474.52
1A	2011	8928.84
16A	2021	8973.24
24A	2109	9363.96
Average	1497	6645
StDev	415	1843
COV (%)	28	28

SIP, structural insulated panel.

(17.6 span: depth ratio). The maximum load values (P_{Max}) for those tests are shown in Table 2.

In general, these specimens each contained a discontinuity within the zone of maximum shear, in the EPS core. Appendix E in McDonald et al (2018) states that "the static bending tests typically failed in shear at the manufactured discontinuities in the EPS web. These discontinuities are points of dramatically decreased shear strength." As a comparison, for P_{Max} of the 31.11 cm (12.25 in.) deep specimens, the coefficients of variation (COV) for Study 1 and Study 2 were 28% and 7%, respectively. Study 1 listed two modes of failure (shear at EPS discontinuity and compression in OSB) whereas Study 2 listed only one mode of failure (shear at EPS discontinuity).

The third study (Study 3) was a generally a replication of Study 2 with the exception that none of the specimens contained an EPS discontinuity in the zone of maximum shear. These specimens were considered to be analogous to the stronger specimens that were noted in Study 1. In Study 3,

Table 2. Static bending (short term) test results for specimens which generally contained an EPS discontinuity within the zone of maximum shear.

15.24 cm (6.5 in) deep specimens			31.11 cm (12.25 in) deep specimens		
Specimen ID	P_{Max} (lbf)	P_{Max} (*N*)	Specimen ID	P_{Max} (lbf)	P_{Max} (*N*)
6-1	1154	5124	12-1	1017	4515
6-2	1179	5235	12-2	907	4027
6-3	1127	5004	12-3	1003	4453
6-4	1127	5004	12-4	873	3876
6-5	1029	4569	12-5	883	3921
6-6	1121	4977	12-6	902	4005
6-7	1137	5048	12-7	1022	4538
6-8	1072	4760	12-8	967	4293
6-9	1117	4959	12-9	941	4178
6-10	1016	4511	12-10	966	4289
6-11	1179	5235	12-11	918	4076
6-12	1054	4680	12-12	994	4413
6-13	1047	4649	12-13	1061	4711
6-14	1079	4791	12-14	1082	4804
6-15	1033	4587	12-15	1039	4613
6-16	997	4427	12-16	1062	4715
6-17	1000	4440	12-17	1079	4791
6-18	1001	4444	12-18	1086	4822
6-19	953	4231	12-19	1068	4742
6-20	955	4240	12-20	1069	4746
6-21	996	4422	12-21	1000	4440
6-22	981	4356	12-22	1081	4800
6-23	934	4147	12-23	1045	4640
6-24	909	4036	12-24	1093	4853
6-25	931	4134	12-25	1034	4591
6-26	911	4045	12-26	1065	4729
6-27	942	4182	12-27	1054	4680
6-28	909	4036	12-28	1069	4746
Average	1032	4581	Average	1014	4500
StDev	85.9	381.4	StDev	68.1	302.5
COV%	8	8	COV%	7	7
Nonparametric 5th percentile	909	4043	Nonparametric 5th percentile	873	3883
Parametric 5th percentile	871	3874	Parametric 5th percentile	886	3941

COV, coefficients of variation; EPS, expanded polystyrene.

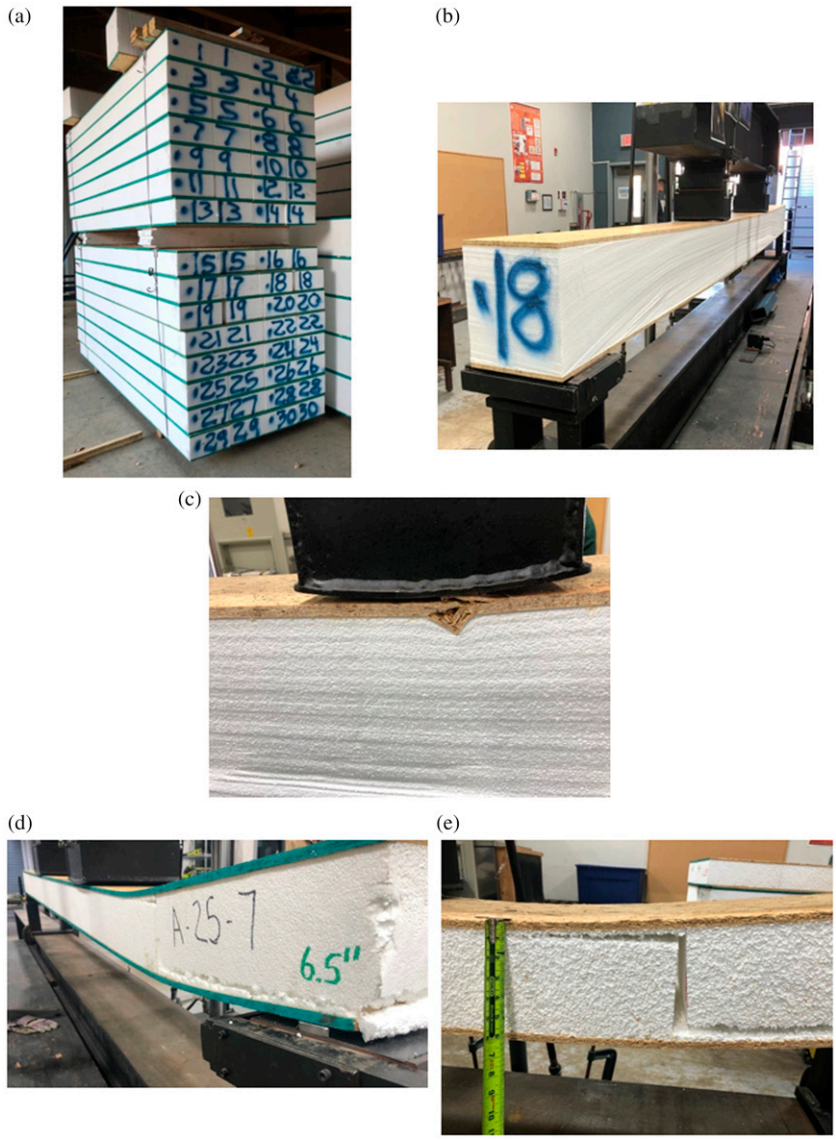

Figure 2. Photos of the specimens before (a and b), during (c), and after testing (d and e).

another full complement (28 specimens of each thickness) of 15.24 cm and 31.11 cm depths (6.5 in. and 12.25 in.) specimens were tested in bending (Fig 2 [a-e]). The 15.24-cm (6.5 in.) deep specimens were tested over a 298.5-cm (117.5 in.) long span (18.2 span: depth ratio). Similar to the previous work (McDonald et al (2018)), the 31.11-cm (12.25 in.) deep specimens were tested over a 548.6-cm (18-ft = 216 in.) long span (17.6 span: depth ratio). The maximum load values (P_{Max}) for those tests are shown in Table 3.

STATISTICAL ANALYSIS

In this study, the experimental design was completely randomized design. Two-tailed *t*-tests, assuming equal variance, were used to compare the P_{Max} values. Additionally, all

Table 3. Static bending (short-term) test results for specimens that did not contain an EPS discontinuity within the zone of maximum shear.

15.24 cm (6.5 in) deep specimens			31.11 cm (12.25 in) deep specimens		
Specimen ID	P_{Max} (lbf)	P_{Max} (N)	Specimen ID	P_{Max} (lbf)	P_{Max} (N)
6-1	2082	9244	12-1	2644	11,739
6-2	2163	9604	12-2	2393	10,625
6-3	2136	9484	12-3	2524	11,207
6-4	2259	10,030	12-4	2584	11,473
6-5	2119	9408	12-5	2554	11,340
6-6	2123	9426	12-6	2578	11,446
6-7	2123	9426	12-7	2562	11,375
6-8	2171	9639	12-8	2641	11,726
6-9	2247	9977	12-9	2665	11,833
6-10	2166	9617	12-10	2362	10,487
6-11	2024	8987	12-11	2726	12,103
6-12	2126	9439	12-12	2289	10,163
6-13	2101	9328	12-13	2477	10,998
6-14	2216	9839	12-14	2511	11,149
6-15	2220	9857	12-15	2512	11,153
6-16	2156	9573	12-16	2442	10,842
6-17	2116	9395	12-18	2217	9843
6-18	2175	9657	12-19	2408	10,692
6-19	2174	9653	12-20	2547	11,309
6-20	2060	9146	12-21	2591	11,504
6-21	2143	9515	12-22	2584	11,473
6-22	2281	10,128	12-23	2800	12,432
6-23	2245	9968	12-24	2417	10,731
6-24	2257	10,021	12-25	2702	11,997
6-25	2096	9306	12-26	2434	10,807
6-26	2248	9981	12-27	2659	11,806
6-27	2196	9750	12-28	2757	12,241
6-28	2312	10,265	12-29	2614	11,606
Average	2169	9631	Average	2543	11,289
StDev	71	316	StDev	139	616
COV%	3	3	COV%	5	5
Nonparametric 5th percentile	2024	9003	Nonparametric 5th percentile	2217	9861
Parametric 5th percentile	2036	9656	Parametric 5th percentile	2283	10,155

COV, coefficients of variation; EPS, expanded polystyrene.

P_{Max} values within the 15.24 cm and 31.11 cm (6.5 in and 12.25 in.) depths sizes from Study 2 (with EPS discontinuity in zone of maximum shear) and Study 3 (without EPS discontinuity in zone of maximum shear) were analyzed by analysis of variance (ANOVA) using the procedure for general linear mixed models (PROC GLIMMIX) of SAS 9.4 (Statistical Analysis System [SAS] Institute 2013). Differences were deemed significant at $p \leq 0.05$.

RESULTS AND DISCUSSIONS

The cumulative frequencies of the 15.24 cm and 31.11 cm (6.5 in. and 12.25 in.) depths, have been illustrated in Figs 3 and 4, respectively. These charts indicate that within each depth, there appears to be a bimodal frequency distribution stemming from the two different failure modes.

Two-tailed *t*-tests were used to compare the P_{Max} values within the 15.24 cm and 31.11 cm (6.5 in and 12.25 in.) depths sizes from Study 2 (with

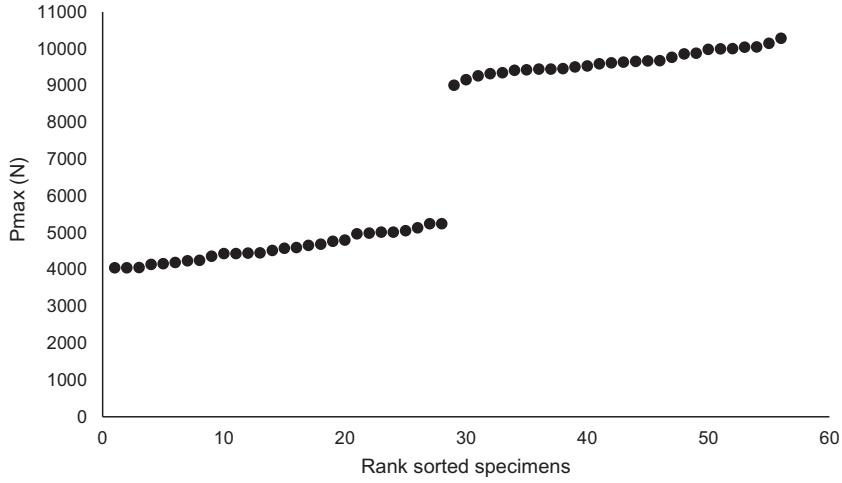

Figure 3. Cumulative frequency distribution chart for the 15.24 cm (6.5 in) deep structural insulated panel (SIP) beams.

EPS discontinuity in zone of maximum shear) and Study 3 (without EPS discontinuity in zone of maximum shear). It was possible to compare P_{Max} values directly because specimen sizes and test-machine set ups were comparable for both Study 2 and Study 3. The summary statistic comparing the flexural strength of beams with and without EPS discontinuities in the zone of maximum shear within each of the two thicknesses, which is shown in Tables 4 and 5 illustrates the summary statistics of the pooled data (from both beams with and without EPS discontinuities in the maximum shear zone) for each of the two thicknesses.

The results of ANOVA analysis have been shown in Tables 6 and 7. According to the results of Tables 6 and 7, there was significant differences between with and without EPS discontinuity and between EPS discontinuity and depth of the specimens.

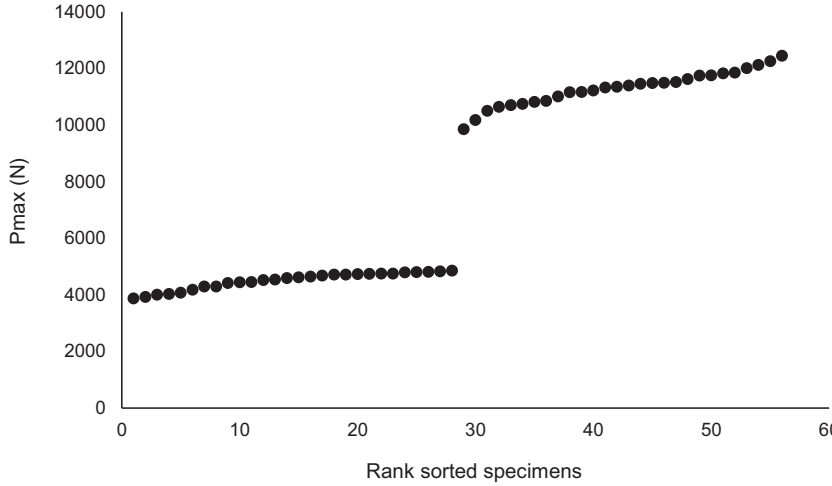

Figure 4. Cumulative frequency distribution chart for the 31.11 cm (12.25 in) deep structural insulated panel (SIP) beams.

Table 4. P_{Max} (*N* and lbf) summary statistics for the specimens either with or without EPS discontinuities in each size. *N* for each group is 28.

Depth cm (in)	EPS discontinuity	Mean *N* (lbf)	Nonparametric 5th percentile *N* (lbf)	Parametric 5th percentile *N* (lbf)	COV%	*p* value from *t*-tests
15.24 (6.5)	With	4590 (1032)	4043 (909)	3874 (871)	8	5.63 × 10-49
15.24 (6.5)	Without	9648 (2169)	9003 (2024)	9056 (2036)	3	
31.11 (12.25)	With	4510 (1014)	3883 (873)	3941 (886)	7	5.04 × 10-31
31.11 (12.25)	Without	11,311 (2543)	9861 (2217)	10,155 (2283)	5	

EPS, expanded polystyrene.

As it was hypothesized, for each thickness 15.24 cm and 31.11 cm (6.5 in. and 12.25 in.), statistically significant differences were detected by the *t*-test between specimens with an EPS discontinuity in the zone of maximum shear vs specimens without an EPS discontinuity. In the case where the EPS discontinuity is considered and specimens are separated, the parametric and nonparametric 5th percentiles are similar. This finding suggests that the data are not skewed in either direction about the mean. In the case where this discontinuity is considered and specimens are thereby separated, their respective COV values for P_{Max} are relatively low and on the order of 5-7%. In the case where this type of discontinuity is not considered and specimens are pooled, their respective COV values are relatively high and on the order of 40%. This finding suggests that these two very different failure modes create a bimodal distribution of strength data with one mode (OSB compression) developing strength levels approximately two times the other mode (shear critical). Figures 3 and 4 support this conclusion. This issue becomes particularly punitive if the parametric 5th percentile were to be used to calculate design strength and moment capacity because the relatively high variability produces a relatively low 5th percentile, which directly leads to a relatively low allowable capacity. This finding suggests that when SIPS are testing in 1/3-point bending, it is prudent to purposefully include at least one discontinuity in the foam in the zone of maximum shear. This finding also suggests that should a manufacturer produce SIPs with no discontinuities in the foam then their product would likely develop superior design values.

CONCLUSIONS

The effect of foam discontinuity in the shear zone of SIP beams was investigated in the current research. The results of EPS discontinuity showed that the specimens with no foam discontinuity had more strength in comparison with the specimens with a foam discontinuity. This finding has implications for routine testing and evaluation as well as for allowable properties. It should be considered that in the case of routine testing, foam discontinuities should purposefully be located in the zone of maximum shear as these appear to be a limiting factor. In cases where a producer manufactures SIPs with zero discontinuities, it may be prudent to seek premium value as those panels

Table 5. P_{Max} (*N* and lbf) summary statistics for the pooled specimens, both with and without EPS discontinuities in each size.

	Mean *N* (lbf)	Nonparametric 5th percentile *N* (lbf)	Parametric 5th percentile *N* (lbf)	COV%
6.5-inch-deep, pooled, both with and without EPS discontinuity	7117 (1600)	4043 (909)	2482 (558)	36
12.25-inch-deep, pooled, both with and without EPS discontinuity	7909 (1778)	3928 (883)	1672 (376)	44

EPS, expanded polystyrene.

Table 6. Mean P_{Max} (N) along with p value levels of significance as well as mean separations. Materials with the same letter were not statistically different from each other at 0.05 level of significance.

	Depth of specimens	
	15.24 cm (6.5 in)	31.11 cm (12.25 in)
EPS discontinuity	P_{Max} (N)	
With	4581[b]	4500[b]
Without	9631[a]	11,289[a]
SEM	93.5	91.7
p value	<0.0001	<0.0001

would achieve superior properties. Also, if producers wish to seek premium or high-grade products, they might also apply adhesive to the foam discontinuities at the time of manufacture, thereby reducing or eliminating the reductions in strength associated therewith.

ACKNOWLEDGMENTS

This publication is a contribution of the Forest and Wildlife Research Center, Mississippi State University. The authors acknowledge the support from USDA Forest Service Forest Products Laboratory (FPL) in Madison, WI, as a major contributor of technical assistance, advice, and guidance to this research.

Table 7. P_{max} (N) values with and without EPS discontinuities in each size along with p value levels of significance as well as mean separations (materials with the same letter were not statistically different from each other at the alpha = 0.05 level of significance).

EPS discontinuity	Depth of specimens	P_{Max} (N)
With	15.24 cm (6.5 in)	4581[c]
Without	15.24 cm (6.5 in)	9631[b]
With	31.11 cm (12.25 in)	4500[c]
Without	31.11 cm (12.25 in)	11,289[a]
Pooled SEM		80.0
p value	EPS discontinuity	<0.0001
	Depth	<0.0001
	EPS discontinuity × Depth	<0.0001

EPS, expanded polystyrene.

REFERENCES

Aldrich RA, Arena L, Zoeller W (2010) Practical residential wall systems: R-30 and beyond *in* Proceedings of Building Enclosure Science & Technology (BEST2) Conference, National Institute of Building Sciences, Washington, DC.

American Society of Testing and Materials (ASTM) (2015a) Standard test methods of static tests of lumber in structural sizes. American Society of Testing and Materials, West Conshohocken, PA. ASTM D198-15.

American Society of Testing and Materials (ASTM) (2013) Standard test methods for mechanical properties of lumber and wood-base structural material. American Society of Testing and Materials. ASTM D4761-13. ASTM, West Conshohocken, PA.

American Society of Testing and Materials (ASTM) (2015b) ASTM, West Conshohocken, PA.

American Society of Testing and Materials (ASTM) (2015b) Standard specification for evaluation of duration of load and creep effects of wood and wood-based products. ASTM D6815-15. ASTM, West Conshohocken, PA.

Cox NI, Hamel SE (2021) Static modeling of plywood–polyurethane structural insulated panels in bending. J Struct Eng 147(2):04020334.

McDonald D, Begal M, Senalik CA, Ross R, Skaggs TD, Yeh B, Williamson T 2014. Creep behavior of structural insulated panels (SIPs): Results from a pilot study. Research Note FPL-RN-0332. U.S. Department of Agriculture, Forest Service, Forest Products Laboratory, Madison, WI. 12 pp.

McDonald DE, Begel M, Senalik CA, Williamson T (2018) Evaluation of creep performance of structural insulated panels (SIPs): Phase 2. Research Paper FPL-RP-697. U.S. Department of Agriculture, Forest Service, Forest Products Laboratory, Madison, WI. 12 pp.

Mcintosh J, Guthrie C (2010) Structural insulated panels: A sustainable option for house construction in New Zealand. Int. J. Hous. Sci. 34(1):1-13.

Medina MA, King JB, Zhang M (2008) On the heat transfer rate reduction of structural insulated panels (SIPs) outfitted with phase change materials (PCMs). Energy 33(4):667-678.

Morley M 2000. Structural insulated panels: Strength and energy efficiency through structural panel construction. Taunton Press, Newton, CT.

Statistical Analysis System (SAS) Institute (2013) User guide: Statistics (Release 9.4). SAS Institute, Cary, NC.

CHARACTERIZATION AND ANALYSIS OF VERY VOLATILE ORGANIC COMPOUNDS AND ODORS FROM MEDIUM DENSITY FIBERBOARD COATED WITH DIFFERENT LACQUERS USING GAS CHROMATOGRAPHY COUPLED WITH MASS SPECTROMETRY AND OLFACTOMETRY

Weidong Wang
PhD Student
E-mail: weidong_wang1024@163.com

*Jun Shen**
Professor
E-mail: shenjunr@126.com

Wang Xu
Master
E-mail: xuwang@nefu.edu.cn

Ming Liu
Master
E-mail: liuming1997@nefu.edu.cn

Huiyu Wang
Master Student
E-mail: gigikoko@nefu.edu.cn

Yu Chen
PhD Student
Key Laboratory of Bio-Based Material Science and Technology (Ministry of Education)
Northeast Forestry University
Harbin, China
E-mail: chenyu@nefu.edu.cn

Anlei Du
Engineer
Zhaoqing Modern Zhumei Furnishings Co., Ltd.
Guangdong, China
E-mail: dal315@126.com

(Received April 2022)

Abstract. Volatile organic compounds (VOCs) from furniture and interior furnishing materials have been proven to pose adverse health effects. However, very VOCs (VVOCs) and odors were rarely taken into account. To bridge this gap, emissions of VVOCs and odors from medium density fiberboard (MDF) coated with different lacquers were characterized using gas chromatography coupled with mass spectrometry and olfactometry detection. The results demonstrated that the total VVOC at the 28th d ($TVVOC_{28}$) from the control sample was higher than that of the other three lacquered samples. Alcohol VVOCs were the most abundant chemicals from the control MDF, followed by ketones, esters, and ethers, accounting for more than 90%

* Corresponding author

Wood and Fiber Science, 54(3), 2022, pp. 196-211
https://doi.org/10.22382/wfs-2022-19

of the total concentration. Also, they were the major odor-contributing substances with higher odor intensities. Nitrocellulose (NC), polyurethane (PU), and water-based (WB) lacquer paintings had a suppressive effect on the emission of certain VVOCs but promotion of the others. After the lacquer paintings, alcohols and ethers were the major components, accounting for 82.3% ~88.0% of the total VVOC. In addition, odors were affected by these three lacquer paintings. Fruity was the dominant odor impression of MDF, NC, and PU decoration MDF, with an odor rating of 4.4, 7.1, and 4.9, respectively. A multiodor mixture was the major odor impression of WB decoration MDF, with an odor rating around 4.0. The odor may differ from one lacquer to another. Additionally, a newly added fishy-like odor arose in PU lacquer painting. From the data analysis of this study, PU and WB decoration MDF might be suitable for furniture or decorative materials due to their lower pollutants and odor emissions. Based on the comprehensive evaluation indices, the latter may be more preferred and was highly recommended for indoor applications.

Keywords: Medium density fiberboard (MDF), odor; lacquer painting, very volatile organic compounds (VVOCs), emission.

INTRODUCTION

With the rapid development of the economy and urbanization, various kinds of lacquered wood-based panels are widely used in the production of fashionable furniture for their beautiful patters, rich colors, and superior water resistance. People spend a substantial amount of time indoors daily (Klepeis et al 2001; Simon et al 2020) and the presence of volatile air pollutants is an increasingly widespread concern. It is a fact that volatile air pollutants from differently lacquer-covered wood-based panels have become one of the major contributors to indoor air pollution, which can directly affect people's mental emotion and production efficiency (Aatamila et al 2011; Wang et al 2022; Jiang et al 2018; Shao Y et al 2018) and even impair human physical health (Adamova et al 2020; Que et al 2013). By far, previous researches on indoor air pollutants have concentrated on volatile organic compounds (VOCs) that mainly included chemical components and emission levels (He et al 2012; Wang et al 2019b), testing and sampling methods (Kim et al 2010), emission mechanism models (He et al 2019; Wang et al 2021; Xiong et al 2019; Zhang et al 2021), environmental factors (Jiang et al 2017; Wang et al 2018), and health risk assessment (Capikova et al 2019; Tong et al 2019; Wang et al 2019a). These results not only contribute to a better understanding of the dynamic quality of indoor air and its relationship with the health of the residents, but also can be used to guide the choice of furniture materials. In addition, the existence of the unpleasant odors and sensory irritations can lead to complaints by a conspicuous number of inhabitants. Some odors might induce both physiological symptoms and reactions (irritation, dizziness, headache, nausea, hematopoietic, central nervous, and respiratory issues) and mental stress (Schiffman 1998). It is, therefore, worthwhile to monitor and optimize the volatile air pollutants emission level.

To date, little effort has been devoted to the emission of very VOCs (VVOCs) from wood-based panels. The German Committee on Health-related Evaluation Procedure for Volatile Organic Compounds from Building Products (AgBB) has proposed a retention range for VVOCs below C_6 (AgBB 2015), which should be given more attention because of their high volatility, strong toxicity, and carcinogenicity. In addition, the ISO 16000-6 standard designated substances that eluted before n-hexane on a nonpolar gas chromatography column as VVOCs. The VVOCs characteristics from solid wood with different lacquers were reported in another research (Wang et al 2020b). Esters and alcohols were determined to be the main VVOCs. Ethyl acetate from the ester VVOCs was the dominant odor substance that may originate from the solvents of UV coatings. More recently, Schieweck identified the presence of VVOCs in a study. The C_4 and C_5 alkanes were identified as the most abundant substances, and they were considered to be propellants from insulating materials. The findings further underlined that the proper selection of construction materials remained important to achieve an acceptable indoor air quality (Schieweck 2021).

The correlation between volatile components and odors (flavors from substances) can be achieved

by using gas chromatography in combination with different detectors, including olfactometry (GC-O), mass spectrometry (GC-MS) and flame ionization (GC-FID) (Aith Barbara et al 2020). Gas chromatography–olfactometry harmoniously combines the separation capacity of GC with the sensitivity recognition of human olfactory and has proved to be a valuable and reliable tool for investigating the single-substance separation from complex compounds as well as for the detection and identification of the odorous compounds coming from a wide range of materials. So far, with its unique properties, this approach has found its way into a wide range of fields involving perfume (Ngassoum et al 2004) and food aromas (Zhu and Xiao 2018) and is becoming increasingly common in areas related to environment, medicine, and materials. Wang et al found more than 10 odor compounds from particleboards coated with water-based (WB) lacquer, and aromatics and alcohols were determined to be the main odor impression (Wang et al 2019b). Ghadiriasli et al demonstrated the composition of oak's odor through the extract dilution analysis (OEDA) and two-dimensional GC-MS/O. 97 odor substances were identified during the entire odor testing, consisting of terpenes, aldehydes, acids, and lactones, as well as a small portion of phenols (Ghadiriasli et al 2018). Dong et al examined the odor characteristics from PVC-overlaid medium density fiberboard (MDF) using GC-MS/O. A total of 23 odor compounds were detected and the dominant odor characteristics were determined to be aromatic, sour, and fresh scent, coming from toluene, ethylbenzene, phenanthrene, and dibutyl phthalate (Dong et al 2019). Liu et al identified 11 VOCs from wood-based panels that classified as hazardous air pollutants. Aldehydes had some unpleasant odors, with octanal being the main odor contributor to these aldehydes (Liu et al 2020). The work of Jiang et al investigated VOCs emissions from particleboard. A total of 44 VOCs were identified, consisting of alkanes, aromatic hydrocarbons, carbonyl compounds, alcohols, and esters. Aldehydes, particularly hexanal and pentanal, were listed as the main odorants (Jiang et al 2017).

To our knowledge, this is the first more comprehensive and detailed study of the characteristics of VVOCs and odors emitted from veneered MDF coated with different lacquers, typically used for furniture and decorative materials. The aim of this study was to better investigate VVOCs and odors using GC-MS/O, and to further broaden the detection scope of low-molecular-weight compounds, as well as to provide a clearer understanding of the hazardous substances from lacquer-covered wood-based panels. A 15-L environmental chamber with controlled conditions was used for gas sampling, which could realistically simulate indoor human living conditions. The total VVOC at the 28th d ($TVVOC_{28}$) and the chemical components were qualitatively and quantitatively analyzed, and the possible sources of VVOCs were simultaneously clarified. It will serve as a valuable guidance when choosing these lacquered MDF as furniture or decorative materials, and provide a reference for improving the painting process and developing the reduction measures.

MATERIALS AND METHODS

Materials

The MDF was obtained from a furniture manufacturer in Guangzhou, China, and had a formaldehyde (HCHO) emission level of E1 according to the standard EN 13896. The original dimensions were 1200 × 1200 × 18 mm, and eucalyptus was used as the main raw material for MDF production. The density and MC varied from 0.7 to 0.8 g/cm^3 and 8% to 12%, respectively. The hot-pressing temperature was 180-230°C, and the glues used for MDF production were urea–formaldehyde resin. The dimensions of the secondary machined specimen were 400 × 400 × 18 mm, and 0.25 mm thick *Fraxinus mandshurica Rupr* veneer was glued to the specimen surface on a hot press using a 6:4 mass ratio of urea–formaldehyde resin and polyvinyl acetate adhesive. The amount of glue to be used on one side veneer was 150 g/m^2. The hot-pressing temperature, time, and pressure for veneer lamination were 100°C, 3 min, and 1 MPa, respectively. The sample measuring 150 × 75 ×18 mm was prepared in a wooden factory. A self-adhesive aluminum foil was attached to the edges of samples to avoid leakage of gas. The samples were painted

with nitrocellulose lacquer (NC lacquer), polyurethane lacquer (PU lacquer), and WB lacquer. The parameters for these three lacquer paintings were listed as follows: the NC lacquer, Bauhinia paints, transparent undercoat/white matte topcoat, main paint: diluent = 2:1, painted two layers of undercoat (150 g/m^2/session) and two layers of topcoat (150 g/m^2/session), at least 12 h among painting sessions; PU lacquer, Bauhinia paints, transparent undercoat/white topcoat, main paint: diluent: curing agent = 2:1:1, painted two layers of undercoat (150 g/m^2/session) and two layers of topcoat (150 g/m^2/session), at least 12 h among painting sessions; WB lacquer, Xinletian, transparent undercoat/twilight gray topcoat, main paint: diluent (distilled water) = 1:10, painted two layers of undercoat (150 g/m^2/session) and two layers of topcoat (150 g/m^2/session), at least 12 h among painting sessions. Four kinds of MDF were used as testing materials, namely, MDF, NC decoration MDF (NC-MDF), PU decoration MDF (PU-MDF), and WB decoration MDF (WB-MDF). Before the testing, these tested materials were stored indoors for 28 d at a temperature of 20-23°C and an RH of 50% ± 10%.

Methods

Sampling methods. According to GB/T 29899-2013, a 15-L environmental chamber was used for gas sampling, which was independently designed by Northeast Forestry University (Harbin, China). This chamber, consisting of glass materials and silicone hoses, did not release volatile contaminants. The schematic representation of a 15-L environmental chamber is shown in Fig 1. An RH of the chamber was regulated by allowing a portion of the airflow to bubble via distilled water in a glass bottle at a controlled temperature level. An automatic digital temperature and humidity sensor was installed in the air inlet of the chamber to continuously register temperature and humidity. Ultrapure nitrogen gas (99.999% purity, Harbin Liming Gas Co., Harbin, China) was introduced into the chamber as a carrier gas and exchanged with the external environment. The chamber was performed at a temperature of 23°C ± 0.5°C and RH of 50% ± 5% to be as close as possible to a typical indoor environment.

Before loading chamber with measuring sample, the chamber inner surfaces were cleaned until the quantity was acceptable. Blank sampling tube should have sufficiently low concentrations and not contain the target compound. Each measured sample was rapidly placed in the center iron holder of the chamber, with a total exposed area of 0.0225 m^2 and a loading rate of 1.5 m^2/m^3. Ultrapure N_2 was continuously introduced into the chamber at 250 mL/min. The electric fan mounted on the top of the chamber was powered on and held until the testing was completed.

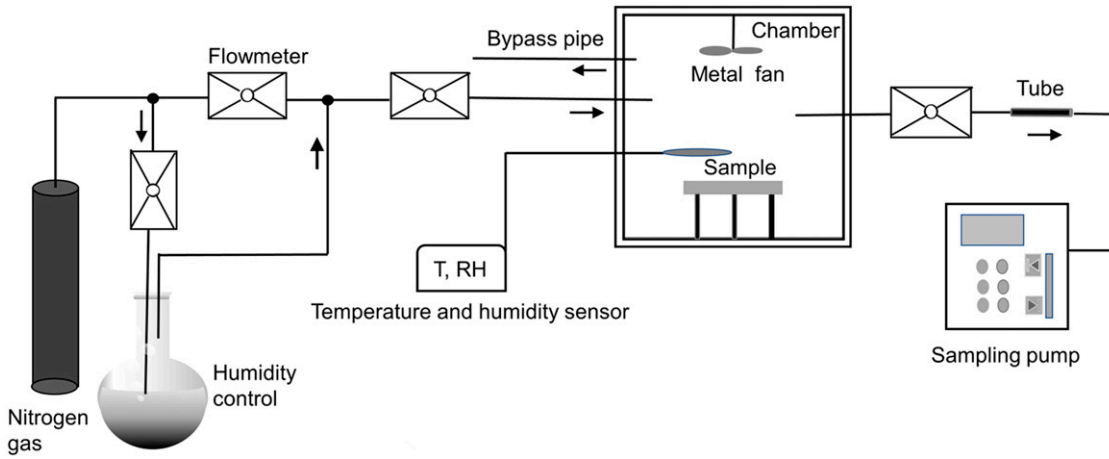

Figure 1. Schematic representation of a 15-L environmental chamber.

Thus, the gases in the chamber could be adequately mixed. The sample cycle time in the chamber was 3.5 h.

The stainless steel tube (produced by Markes International Inc., Llantrisant., UK) containing carbopack C, carbopack B, and carboxen 1000 was used for gas sampling. Before starting sampling, the tubes were pretreated at four temperature intervals (100°C, 200°C, 300°C, and 380°C) with a N_2 rate of 50 ~100 mL/min through a thermal analysis processor (TP-2040; Beijing Beifen Tianpu Instrument Technology Co., Beijing, China). The pretreated time was set to 15 min at each temperature point. The gas sampling flow rate was set at 250 mL/min, and the sampling time was 12 min, 3 L gas was collected into each tube using a miniature vacuum pump (ANJ6513; Chengdu Xinweicheng Technology Co., Chengdu, China). As soon as the sampling was completed, two ends of the tube must be tightly plugged with special brass caps supplied by the adsorption tube manufacturer. The collected gas samples were immediately desorbed for analysis.

Analytical method for GC-MS. The external standard method was used in this experiment. The gas mixture was analyzed using a thermal desorption instrument coupled with gas chromatography–mass spectrometry (TD-GC-MS) and quantified to Chinese National Standard GB/T 29899-2013. The automatic thermal desorption instrument was produced by Markes International. Gases were thermally transferred and refocused on a cryogenic capillary trap. Both cold trap desorption and thermal desorption were performed at a temperature of 300°C. The dry purge and tube desorption held for 5 min and 10 min, respectively. Ultrapure helium gas (99.999% purity) was used as the carrier gas for GC at 1 mL/min.

The DSQ II series quadrupole GC-MS was produced by Thermo Fisher Scientific, and a nonpolar GC column (DB-5MS, 30m length, 0.25 mm inner diameter, 0.25 μm film thickness, Agilent Technologies, State of California, USA) was employed for the gas separation. The temperature program for GC oven was initially started 40°C, and kept for 2 min, then increased to 50°C at 2°C/min and held 50°C for 4 min, and then increased to 150°C at 5°C/min and stayed 150°C for 2 min, and finally increased to 250°C at 10°C/min and maintained 250°C for 8 min. The desorbed gas components were identified based on the retention times and MS detector, and compared with National Institute of Standards and Technology (NIST) and Wiley libraries. The MS detector had a full scan mode and an electron impact energy at 70 eV. The mass-to-charge ratio varied from 40 to 450 amu. The ion source temperature was kept at 230°C. The relative percentage content of each VVOC component was obtained through the area normalization method. Repeated experiments were conducted in triplicate and the mean VVOC concentration was calculated from the duplicated measurements. The $TVVOC_{28}$ was obtained by the concentration summation of odor and nonodor compounds. The total odor intensity at the 28th d (TOI_{28}) was obtained from the summation of the intensities of all odorous substances.

Analytical method for GC-O. The sniffer 9100 olfactory port (Bruchbuhler, Switzerland) was applied in this sniffing experiment. The transmission line temperature was determined to be 150°C so as to prevent condensation of the analytes on the capillary walls. The gas mixture was separated by GC column after thermal desorption and part of it went to the MS for identification and the rest to the sniffer for sniffing operation. The GC effluents were split 1:1. The moist air supplied by a water bottle was continuously added to the glass conical port to reduce damage to nasal mucosa of the odor assessors due to dryness. The schematic representation of gas chromatography–mass spectrometry coupled with olfactory detector is shown in Fig 2. The time-intensity method was used in this experiment. Six-point odor intensity (from 0 to 5) was used to determine the odor grade according to Japanese Standards (Ministry of the Environment Law 1971). The correlation between odor intensity and characterization is shown in Table 1. Based on some certain screenings and training recommendations in accordance with International Organization for Standardization 2017 (ISO 12219-2017-7), five trained and experienced odor assessors

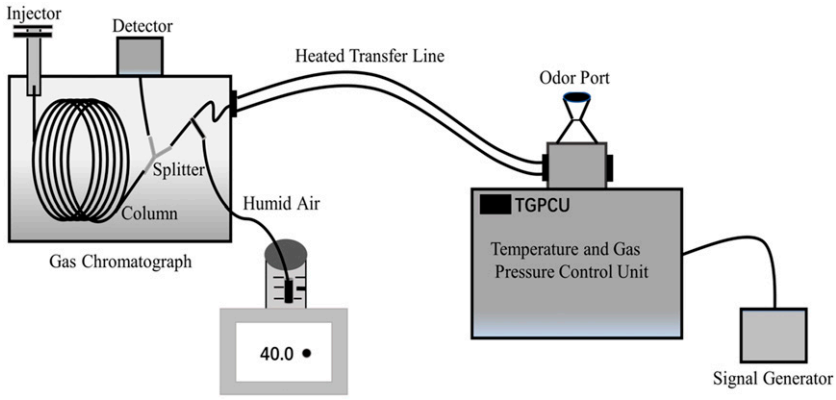

Figure 2. Schematic representation of gas chromatography–mass spectrometry coupled with olfactory detector.

(aged between 20 and 30 yr old, with no smoking history and no olfactory impairment or allergic rhinitis) were selected to form an odor assessment group to evaluate these odors. All assessors were already screened for sensitivity, motivation, ability to concentrate, and ability to remember and identify odor characteristics. Some activities, such as eating or drinking strongly irritating foods and chewing gum, were prohibited for 5 h prior to taking this GC-O testing. In addition, they were not allowed to use heavy cosmetics and perfumes, or strong deodorants during the day of the olfactory assessment. The sniffing results were simultaneously registered, including the retention time, odor type, and intensity grade of the odoriferous stimuli. At least two assessors smelled the same odor at the same retention time, which was used for the sniffing results. The final odor intensity was an average from the same sniffing results.

According to the National Standards Authority of Ireland in EN 13725-2003, the sniffing laboratory with a temperature of 21 ∼23°C and a RH of 40%, was required a good ventilation and no other smell during the entire sniffing operation.

Risk evaluation method. Since some small changes in chemical structure may have a significant effect on biological activity, particularly if toxicity is mediated by binding to receptors, it is very, therefore, necessary to consider certain minimum criteria when using predictive methods for hazard assessment. The lowest concentration of interest (LCI) is an assessment level of pollutants, above which adverse effects are potentially to arise in the indoor environment (Lu et al 2020). Based on LCI guidelines (AgBB 2015), they are required to quantify using their individual calibration factors when the concentration of substances in the test chamber exceeds 5 μg/m^3. For each compound *i*, the R_i is equal to the ratio of C_i to LCI_i, where C_i is the chamber concentration of compound *i*. If R_i is <1, it indicates that there is no effect. When several compounds are detected at concentrations >5 μg/m^3, an additive effect is assumed, and then the risk index *R*-value (the sum of all R_i) will not exceed the value 1. However, because of insufficient studies and experimental data, the EU-LCI values for some chemicals are not directly obtained. In such case, if test data are available for a range of structurally closely related chemicals, it is possible to confidently extrapolate from data-rich compounds to data-poor ones. But even so, some EU-LCI data are still not available. According to health-related evaluation procedure criteria for VOC emissions from building products of AgBB, $TVVOC_{28}$, TOI_{28}, the risk index

Table 1. The correlation between odor intensity and odor characteristic.

Odor intensity	0	1	2	3	4	5
Characterization	None	Very weak	Weak	Moderate	Strong	Very strong

R-value, and the concentrations of nonassessed compounds were used as evaluation indicators. The VVOC components without LCI values are calculated and to avoid the risk of positive evaluation of materials that release substantial amounts of nonassessable substances. The detailed evaluation procedures were referred to Wang's previous study (Wang et al 2020a).

RESULTS AND DISCUSSION

VVOC Emission Characteristics and Source Analysis of MDF Coated with Different Lacquers

Figure 3 shows $TVVOC_{28}$ concentration and TOI_{28} of MDF coated with different lacquers. As shown in Fig 3, the control sample (MDF) had the highest maximum $TVVOC_{28}$ concentration of 426.78 μg/m^3, followed by NC-MDF (223.65 μg/m^3), WB-MDF (205.27 μg/m^3) while the PU-MDF was the lowest (196.05 μg/m^3). The maximum $TVVOC_{28}$ for the control sample were approximately 2-folds higher than the maximum $TVVOC_{28}$ values for the other three lacquered MDF. After the lacquer painting, $TVVOC_{28}$ concentration values displayed a downward trend, decreasing by 47.59%, 51.90%, and 54.06%, respectively. On the whole, $TVVOC_{28}$ concentration values of these three

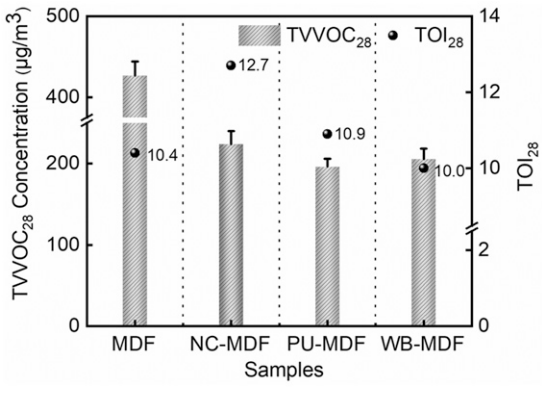

Figure 3. Total very volatile organic compounds at the 28th d ($TVVOC_{28}$) concentration and total odor intensity at the 28th d (TOI_{28}) of medium density fiberboard (MDF) coated with different lacquers.

lacquer-covered MDF in the equilibrium stage tended to be at a stable level with little discrepancy. Certainly, as we expected, the three lacquer paintings provided an inhibiting effect on the $TVVOC_{28}$ emissions, this tendency was generally similar with earlier study (Wang et al 2020a). On the one side, when the control MDF was covered with a lacquer layer, part of the lacquer paintings could penetrate into the pore structure of the wood-based panel causing blockage, resulting in volatile pollutants not being easily evaporated and diffused, whereas on the other side, the cured painting film enclosed most of the contaminants within the panel. It was equivalent to adding a mass transfer barrier layer on the surface of MDF to increase the resistance of VVOCs diffusion, thereby reducing its release rate. However, it was found that the TOI_{28} was irregular when the control MDF was coated with different lacquers. Although the control had the largest $TVVOC_{28}$ concentration, the TOI_{28} was not the most powerful in these different kinds of MDF. It was obvious to see that the NC-MDF has the greatest TOI_{28} value, with an odor rating of 12.7, next were 10.9 for PU-MDF, 10.4 for MDF, and 10.0 for WB-MDF. After the lacquer treatments, the TOI_{28} values for these three lacquered MDF were slightly higher or comparable to that of the control MDF, implying that the odors of these lacquered MDF could not disperse sufficiently within a shorter time and required longer ventilation to dissipate. Generally speaking, the lacquer paintings could dramatically mitigate pollutant emission levels. Taking into account $TVVOC_{28}$ concentrations and TOI_{28} values with the gaseous pollutant level for the four kinds of MDF, the WB-MDF was probably the best, followed by the PU-MDF and the NC-MDF, and the control sample (MDF) may be the worst.

Figure 4 shows the detailed VVOCs composition and their percentage content of MDF with different lacquers. As described in Fig 4, the major VVOCs detected from the control MDF were divided into the following six groups, namely alkanes, alcohols, aldehydes and ketones, esters, ethers, and others, of which concentrations of alkanes and other components were very small amounts, each

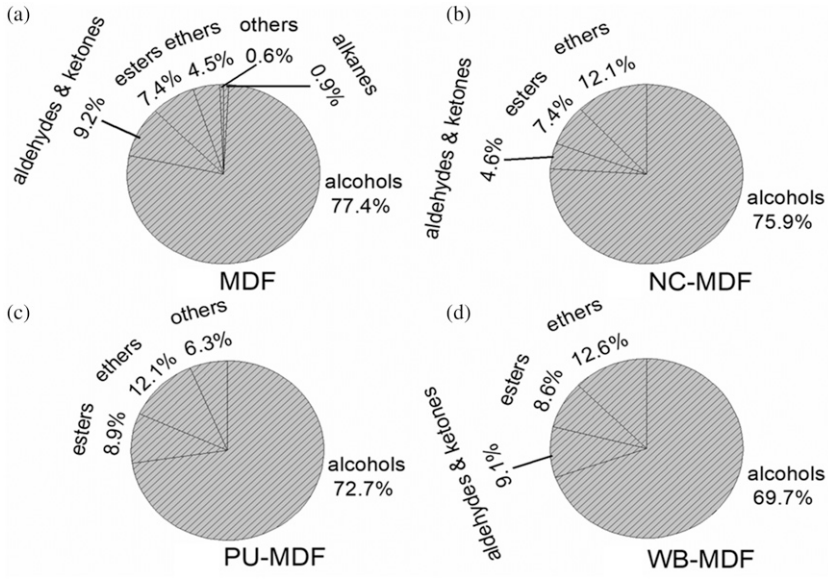

Figure 4. VVOC composition of MDF with different lacquers and their percentage content.

constituting <1% of the $TVVOC_{28}$ concentration. Alcohol VVOCs were the most abundant species for the control MDF, followed by aldehydes and ketones and esters, which together accounted for more than 90% of the total VVOC. Alcohol VVOCs made up >75% of the total emission, with ethanol being the most abundant component and 1-butanol as the second contributor, contributing 54.14% and 23.24% of the total VVOC emissions, respectively. Meanwhile, ketones, esters, and ethers VVOCs were the major chemical species detected in the control MDF. The concentrations of acetone and ethyl acetate were also the large fractions of the total emissions for the control MDF. The formation of alcohols and ketones VVOCs in the control MDF was more complicated and probably originated from the degradation of wood carbohydrates and lipids (Fagerson 1969). Also, these two groups also partially derived from adhesives and other additives. For example, ethanol and acetone were commonly used as solvents for adhesives and the latter was also applied as an important cleaning agent for residual adhesives on the edges after high temperature and pressure. The hydrolysis reactions of adhesives in panels could generate 1-butanol, which was consistent with the previous report (Karlsson et al 1989). In addition, ketones VVOCs were formed by chemical degradation of polyunsaturated fatty acids (Chatonnet and Dubourdieu 1998). Ethyl acetate from esters VVOCs was partially derived from the complex chemical reactions in the cellulose and hemicellulose during the hot pressing, the remainder may be generated from the adhesive solvent. The proportion of ethers VVOCs was only 4.5% of the total VVOC. There were also furan derivatives formed by repeated dehydration and rearrangement of carbohydrates during heating (Cullere et al 2013), and tetrahydrofuran of the ethers was produced by the thermal degradation of lignocellulose during hot pressing of the control MDF (Ning et al 2013). The concentrations of dichloromethane and 1,4-dioxane were very small, only 3.85 $\mu g/m^3$ and 2.75 $\mu g/m^3$ respectively (Table 2). These two substances could often be blended with other solvents to facilitate the dissolution of the resin used in the adhesive. Even in small amounts, attention should be paid to them because of their carcinogenicity. It was noted that the main compositions of VVOCs from these three lacquered MDF were roughly

Table 2. The odor characteristics of MDF coated with different lacquers.

Category	No	Compounds	LCI (μg/m^3)	RI	Formula	Odor	Concentration (μg/m^3), R*i* (C*i*/LCI*i*)			
							MDF	NC-MDF	PU-MDF	WB-MDF
Alkanes	1	dichloromethane	—	<600	CH_2Cl_2	—	3.85/—	x	x	x
Alcohols	2	ethanol	1860	<600	C_2H_6O	alcohol-like	231.08/0.1242	68.02/0.0365	62.91/0.0338	57.94/0.0311
	3	1-butanol	3000	647	$C_4H_{10}O$	alcohol-like, sweet	99.22/0.0330	x	x	x
	4	1,2-propanediol	2500	<600	$C_3H_8O_2$	sweet	x	101.78/0.0407	79.67/0.0318	85.16/0.0340
Esters	5	ethyl acetate	3620	<600	$C_4H_8O_2$	fruity	31.41/0.0086	8.75/0.0024	10.16/0.0028	9.49/0.0026
	6	2-methyl 2-propenoic acid-methyl ester	110	701	$C_5H_8O_2$	pungent	x	7.73/0.0702	7.37/0.0670	8.16/0.0741
Aldehydes	7	acetaldehyde	1200	<600	C_2H_4O	pungent	x	x	x	18.70/0.0155
and	8	3-methyl butyraldehyde	—	686	$C_5H_{10}O$	fruity, apple-like	x	5.56/—	x	x
Ketones	9	acetone	1200	<600	C_3H_6O	pungent	39.22/0.0326	x	x	x
	10	3-methyl-2(5H)-furanone	—	974	$C_5H_6O_2$	—	x	4.80/—	x	x
Ethers	11	tetrahydrofuran	1500	627	C_4H_8O	fruity, ether-like	19.25/0.0128	27.01/0.0180	23.51/0.0156	25.79/0.0171
Others	12	1,4-dioxane	73	700	$C_4H_8O_2$	—	2.75/0.0376	x	x	x
	13	1-aminobutane	—	780	$C_4H_{11}N$	—	x	x	3.61/—	x
	14	N, N-dimethylformamide	15	772	C_3H_7NO	fishy-like	x	x	8.82/0.5880	x

similar to that of the control MDF, but their emission levels varied considerably. Additionally, the emission results for these three lacquered MDF were quite similar and no obvious differences were found in the outlines of the components. Alcohol VVOCs were also the largest chemical group, which accounted for 69.7% ~75.9% of the total VVOC emissions. It could be clearly seen that the lacquer treatments had a remarkable barrier effect on the emitted alkane VVOCs, utterly blocking them and reducing them to zero. As far as alcohols VVOCs, 1-butanol was wholly inhibited and the concentration of ethanol decreased to a great extent after the lacquer treatment, but a relatively high level of 1,2-propanediol was found in these lacquer paintings. Similarly, esters and ethers VVOCs were relatively abundant components and were slightly affected when MDF was coated with different lacquers. In relation to ethers VVOCs, this value raised from 4.5% to 12.1% (NC-MDF), 12.0% (PU-MDF), and 12.6% (WB-MDF), a jump of 7.6%, 7.5%, and 8.1%, respectively. The alcohols, esters and ethers VVOCs may be partially derived from panels themselves and another large part was commonly from the solvents, cosolvents and auxiliary additives used in the production and application of these lacquered paintings. 1,2-propanediol was commonly added to coatings as a film-forming additive and 2-methyl 2-propenoic acid-methyl ester was traditionally used as a synthetic raw material for the lacquer coatings. In addition, aldehyde and ketone VVOCs were also correspondingly decreased, especially for PU-MDF, aldehyde and ketone VVOCs were completely confined internally, reducing the hazard posed by the emission of these low-molecular-weight carbonyl compounds. In general, these lacquer paintings could not only improve properties and esthetic characteristics, but also limited the emission levels of VVOCs. It was worth mentioning that the previously mentioned lacquers inhibited the emission of certain substances and provided complete barrier containment to dichloromethane, 1-butanol, acetone, and 1,4-dioxane but increased that of others. Because of the irritating and unpleasant odor of some of the newly added substances and even their high toxicity, the higher ventilation rates and additional placement time of these lacquered MDF needs to be added appropriately and to make sure of these added VVOCs were distributed as possible.

Characterization of Odor Compounds of MDF Coated with Different Lacquers

To further determine the odor compounds of MDF coated with different lacquers, GC-O olfactory technology was applied in this experiment. The odor compound was registered when any one of four specimens had an odor intensity >1. The detail odor characteristics of MDF coated with different lacquers is summarized in Table 2. As can be seen from this table, a total of 14 VVOCs were successfully detected from these samples. Figure 5 shows the odor–time intensity spectrum of MDF coated with different lacquers. As demonstrated in Fig 5, 10 odor compounds were simultaneously measured based on the olfactory analysis and they were mainly composed of alcohols (3 substances), esters (2 substances), aldehydes and ketones (3 substances), esters (1 substance), and others (1 substance). The vast majority of VVOC odorous substances from these lacquered MDF had a rather short retention time and mostly being detected within 10 min, concentrated between 3 and 8 min. Only 1 VVOC odorous substance was retained for longer than 10 min and that was N, N-dimethylformamide. The overall odor intensity of all odor compounds detected from these four samples was not too high, with the highest odor

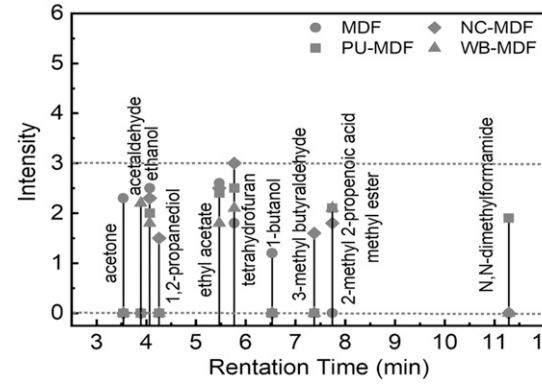

Figure 5. The odor-time intensity spectrum of MDF coated with different lacquers.

intensity being tetrahydrofuran from NC-MDF at 3.0. It was also found that the intensities of ethanol and ethyl acetate reduced to some extent after the lacquer treatments. The two odor compounds (acetone and 1-butanol) were not detected and they were well suppressed after treatment. The tetrahydrofuran was found in both the control MDF and the lacquered MDF, and its intensity was elevated after treatment. Another five odor compounds, namely, 1,2-propanediol; 2-methyl 2-propenoic acid-methyl ester; 3-methyl butyraldehyde; N, N-dimethylformamide; acetaldehyde, were not detected in the control group, and appeared after the lacquer paintings.

As evidenced in Table 2, acetone was reported as pungent odor, similar to the previous finding (O'Neil 2013). Acetaldehyde detected in this study had a pungent odor, similar to the pungent odor reported elsewhere (Hagemeyer 2014), whereas this substance was reported to have a fruity odor (Lewis 2007). Ethanol was perceived as having a pleasant and alcohol-like odor, a similar observation reported in the CAMEO chemicals hazardous materials database. In addition, a fragrant and vinous odor characteristic of ethanol was described by U.S. National Institute for Occupational Safety and Health (NISOH 2010). Similarly, our measured results found 1-butanol was considered to have an odor similar to that of alcohol-like, which agreed with the previous study (Verschueren 2001). In our present testing results, 1,2-propanediol was perceived as slightly sweet. Ethyl acetate was perceived to be a fruity odor, which was consistent with the description of NIOSH (2010), but Sax (1984) also believed this substance had a fragrant odor characteristic (Sax 1984). Our measuring results found that tetrahydrofuran had a fruity odor. Research showed that 3-methyl butyraldehyde had a fruity and apple-like odor characteristic. The 2-methyl 2-propenoic acid-methyl ester was detected with a pungent odor. The N, N-dimethylformamide showed a fishy-like odor, whereas it was also presented a faint and amine-like odor, as reported by NIOSH (2010). The odor compound characteristics are closely related not only to the concentration but also to the medium of the substance. The same substance may have a variety of odor characteristics when the concentration and the medium were changed. Certainly, as seen in Fig 5 and Table 2, ethanol had a considerable concentration but not the highest odor intensity. In contrast, the tetrahydrofuran had a lower concentration but the greatest odor intensity, indicating that the intensity of the same odor compound was influenced by the concentration and that there was no exact correlation between the intensities and their concentrations of different odor compounds.

When mixtures of different odor chemicals were combined together, there were four main ways that influenced the interaction and their relationships could be independence from one another, integration, synergism, or antagonism effect (Cain and Drexler 1974). With integration, the total intensity was the addition of the two odor intensities. With synergism, the total odor intensity was stronger than the addition of the two odor intensities. With antagonism, the total intensity was considered to be less than the addition of the two odor intensities. For an independent effect, the total odor intensity was mainly determined by the odor intensity of a certain odor compound. To better understand the differences before and after the lacquer paintings and to consider the complexity of the interactions of various odor compounds at the same time, the integration effect was used in this odor analysis based on the previous report (Schreiner et al 2017). According to the identification results, the odor characteristics from four samples were classified into the following six categories: alcohol-like, sweet, fruity, pungent, ether-like, and fishy-like. Figure 6 shows the odor radar profile spectra of MDF coated with different lacquers. As depicted in Fig 6(a), fruity was the major odor impression of the control MDF, with an odor rating of 4.4, followed by alcohol-like (3.7), both of which contributed the major determinants to the formation of the overall odor. In addition, pungent and ether-like odors had a relatively positive complement effect to the formation of the overall odor, with an odor rating around 2. Esters, ethers, and alcohols VVOCs were determined as the major odor sources for the control MDF, with the main odor-contributing substances

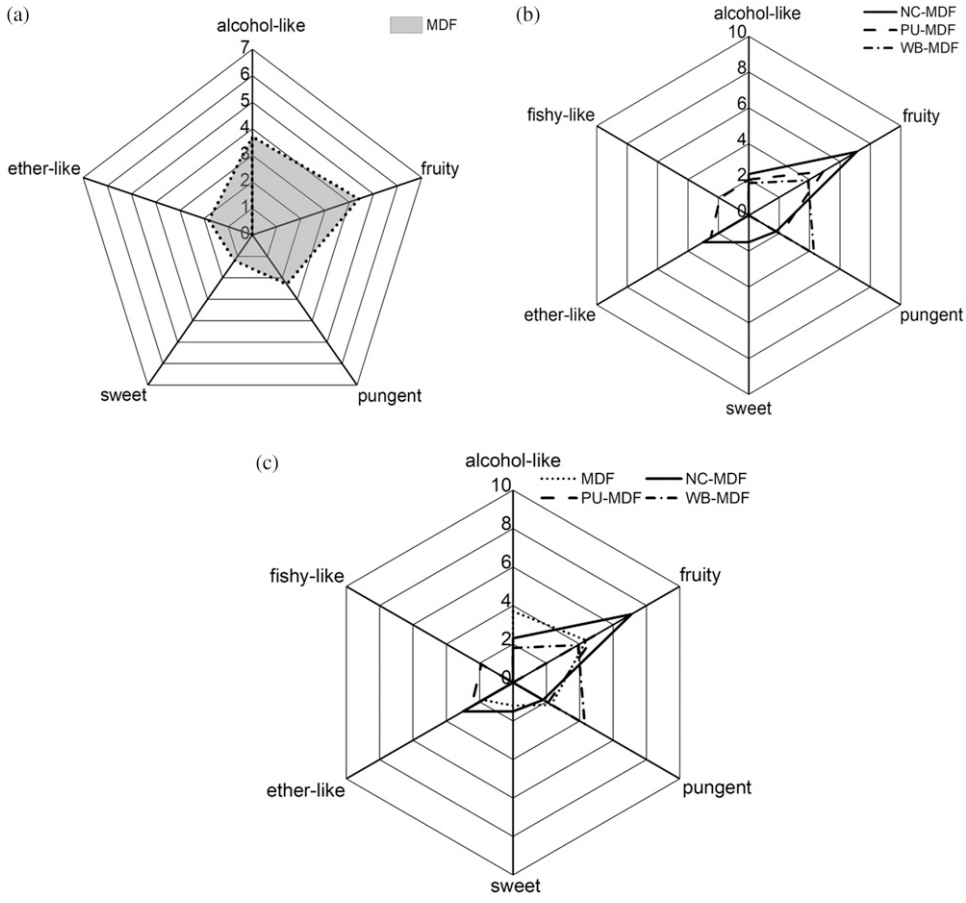

Figure 6. The odor radar profile spectra of MDF coated with different lacquers. (a) MDF; (b) three lacquered MDF; (c) MDF and three kinds of lacquered MDF.

being ethyl acetate, tetrahydrofuran, ethanol and 1-butanol. It could be seen in Fig 6(b) that the fruity was the dominant odor impression of the NC-MDF, with a higher odor rating of 7.1, playing a fundamental and decisive role in the formation of the overall odor, followed by ether-like (3.0), then alcohol-like and pungent, with an odor rating of about 2.0, having an auxiliary modification role to the formation of the overall odor. Esters, ethers, and aldehydes VVOCs were the major odor contributors and the main odor-contributing substances were ethyl acetate, tetrahydrofuran and 3-methyl butyraldehyde. And for the PU-MDF, fruity was also the major odor impression, with an odor rating of 4.9, acting as an active contributor to the formation of the overall odor. Next in order were ether-like (2.5), pungent (2.1), and alcohol-like (2.0), which were the fundamental modifiers to the composition of the overall odor. Esters and ethers VVOCs were the main odor contributors and the main odor-contributing substances were ethyl acetate and tetrahydrofuran. Conversely, the pungent was recognized as a predominant odor impression of the WB-MDF, with an odor rating of 4.3, followed by fruity (3.9) and ether-like (2.1). In general, the WB-MDF was endowed with a multitude of odor blends. Esters, ethers, and aldehydes VVOCs were the major odor providers and the main odor-contributing substances were ethyl acetate,

2-methyl 2-propenoic acid-methyl ester, tetrahydrofuran, and acetaldehyde.

Figure 6(c) shows a comparison of the odor radar before and after the lacquer paintings. As clearly seen from this figure, the odor radar profile after the lacquer painting was generally similar to that of the control group, but with clear differences. Fruity and a multiodor mixture remained the dominant odor impression in these three lacquered MDF. The major odor impression may be changed after the lacquer paintings, but they are basically pleasurable, meaning that most individuals would feel comfortable when they were in such an environment, with the exception of some allergic individuals. It was found that NC, PU, and WB lacquer paintings had a sealing effect on alcohol-like odor, especially for PU, where this odor characteristic completely disappeared after lacquering. And in the meanwhile, another newly added odor characteristic, fishy-like (1.9) occurred in the PU lacquer, which was attributed to the presence of N, N-dimethylformamide. This substance was used on the one hand as a solvent for the synthesis of PU, and on the other hand to dissolve low-solubility pigments. Research results showed that the fruity character of the NC and PU paintings increased in varying degrees, with an increase in intensity of 2.7 and 0.5, respectively. The intensities of more odor characteristics changed to a varying degree after the lacquer treatment. After the lacquer paintings, the odor intensity of pungent decreased slightly in the NC and PU paintings, whereas WB painting increased by 2.0. The sweet intensity remained weak, and was completely inhibited after the PU and WB lacquer paintings, which had little impact on the overall odor profile. The ether-like odor character slightly increased, and their intensities increased from 1.8 to 3.0, 2.5, and 2.1, increased by 1.2, 0.7, and 0.3, respectively, but which had little influence to the overall odor profile.

Risk Evaluation of MDF Coated with Different Lacquers

Figures 3 and 7 show all the risk assessment results of MDF coated with different lacquers.

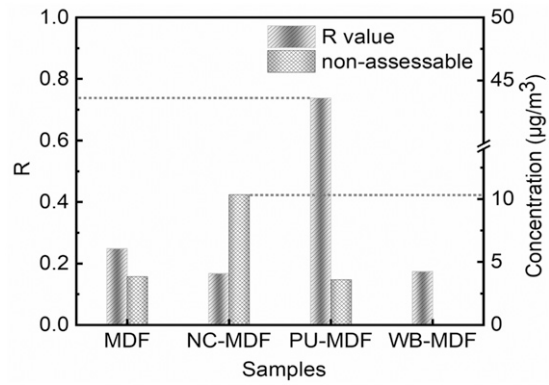

Figure 7. The risk assessment of MDF coated with different lacquers.

As seen in Fig 7, PU-MDF had the largest risk index *R*-value of 0.7390, followed by MDF (0.2488), WB-MDF (0.1744) while NC-MDF (0.1678) was the lowest. After the lacquer paintings, the *R*-value became weaker, with the exception of PU-MDF. The *R*-value of PU-MDF was approximately 3-folds higher than that of the control group, which was directly correlated with the lower EU-LCI value of N, N-dimethylformamide. The concentration of nonassessable substances of the NC-MDF was higher than that of the others, which should be given more attention. As previously mentioned, it could be concluded that the lacquer paintings did block the emission of VVOCs, but at the same time increased the odorous characteristics. Although the *R*-value and odor intensity of the control MDF were not very strong, the $TVVOC_{28}$ were the highest. In terms of VVOCs contaminant emissions and its evaluation levels, it was not recommended to use the MDF directly as furniture or other decorative materials for interior application whenever possible. Certainly, the MDF covered with various kinds of decorative materials or lacquer paintings is highly recommended as furniture materials or other decorative materials, which may be a great option for reducing pollutant emissions. If the MDF is truly needed, additional placement time can be added as appropriate. Even more importantly, manufacturers are expected to address the issue of pollutants and odor emissions at the source of wood-based panel production and they

can seek greener, more environmentally friendly solvents to substitute the usage of alcohols, ketones, and ester solvents and use modified glues and low-odorous wood raw materials, thus, manufacturing environmentally friendly panels. Though the lacquer paintings reduced the pollutant emissions, the odors emitted may exceed those of the control group for a shorter limited time and thus also required more attention. Among these three lacquered MDF, NC-MDF had not only the largest $TVVOC_{28}$ concentration but also the maximum odor intensity value. As far as its environmental characteristics are concerned, it is not advocated for use as furniture or other decorative materials within a limited period of time after painting. It is, therefore, highly recommended to keep NC-MDF in a well-ventilated location for a considerable period of time before using it. If it is necessary to use NC-MDF indoors for a short time after lacquering, the high ventilation rates are one of the options for addressing indoor pollutant and odor problems. Although taking both energy consumption and air quality aspects sufficiently into account demands, an optimum air exchange rate might be confirmed, above which is economically viable. The PU-MDF and WB-MDF might be a better choice as furniture or other decorative materials due to their lower pollutants and odor emissions. When the risk index *R*-value and nonassessable compounds were simultaneously under consideration, the evaluation results may be changed. When emissions of materials were considered comprehensively, WB-MDF might be more preferable and was suggested for indoor applications based on the lower evaluation indices of $TVVOC_{28}$, TOI_{28}, *R*-value, and concentrations of nonassessment compounds. Certainly, VVOCs are only one type of volatile pollutants and do not represent the full information about these materials. When occupants choose these lacquer-covered materials for indoor applications, the emissions of VOCs, SVOCs, and carbonyl compounds should also be taken into account.

CONCLUSIONS

In this study, a 15-L environmental chamber, combined with multisorbent adsorption tubes, was used for gas sampling. Emissions of VVOCs and odors from MDF coated with different lacquers were investigated by gas chromatography coupled with mass spectrometry and olfactory detection. The results indicated that the lacquer paintings had an impact on VVOCs and odor emissions. The $TVVOC_{28}$ from the control MDF was higher than that of the other three lacquered samples. After painting, $TVVOC_{28}$ was decreased by 47.59%, 51.90%, and 54.06%, respectively. The most abundant VVOCs components from the control sample were alcohols, followed by ketones, esters, and ethers, accounting for more than 90% of the total. Also, they were the major odor-contributing substances with higher odor intensity values. After the lacquer paintings, alcohols and ethers VVOCs were the major chemicals, which accounted for 82.3% ~88.0% of the total VVOC. It was shown that these three lacquers had a suppressive effect on the emission of certain VVOCs but increased that of the others. In addition, odors were affected by these three lacquer paintings. The TOI_{28} for these three lacquered MDF were slightly higher or comparable to the control MDF. Fruity and a multiodor mixture were the dominant odor impression of these kinds of lacquered MDF. The three lacquers had a strong inhibition of the alcohol-like and sweet, but increased the ether-like. A newly added fishy-like arose in PU lacquer painting. The PU-MDF and WB-MDF might be a better choice as furniture or other decorative materials due to their lower pollutants and odor emissions. Based on the comprehensive evaluation indices of the $TVVOC_{28}$, TOI_{28}, *R*-value, and concentrations of nonassessment compounds, the WB-MDF may be more preferred and the WB paints is highly encouraged to use indoor to reduce indoor air pollution problems if possible.

ACKNOWLEDGMENTS

This study was supported by the Central Financial Services Demonstration Project for the Promotion of Forestry Science and Technology (Hei [2021] TG 18) and the National Natural Science Foundation of China (31971582). All authors gratefully acknowledge the technical

support provided by the Key Laboratory of Bio-based Materials Science and Technology (Ministry of Education).

REFERENCES

Aatamila M, Verkasalo PK, Korhonen MJ, Suominen AL, Hirvonen M-R, Viluksela MK, Nevalainen A (2011) Odour annoyance and physical symptoms among residents living near waste treatment centres. Environ Res 111(1):164-170.

Adamova T, Hradecky J, Panek M (2020) Volatile organic compounds (VOCs) from wood and wood-based panels: Methods for evaluation, potential health risks, and mitigation. Polymers (Basel) 12(10):2289.

AgBB (2015) Health-related evaluation procedure for volatile organic compounds emissions from building products. Committee for health-related evaluation of building products.

Aith Barbara J, Primieri Nicolli K, Souza-Silva EA, Biasoto ACT, Welke JE, Zini CA (2020) Volatile profile and aroma potential of tropical Syrah wines elaborated in different maturation and maceration times using comprehensive two-dimensional gas chromatography and olfactometry. Food Chem 308:125552.

Cain WS, Drexler M (1974) Scope and evaluation of odor counteraction and masking. Ann N Y Acad Sci 237(1): 427-439.

Capikova A, Tesarova D, Hlavaty J, Ekielski A, Mishra PK (2019) Estimation of volatile organic compounds (VOCs) and human health risk assessment of simulated indoor environment consisting of upholstered furniture made of commercially available foams. Adv Polym Technol 2019:5727536.

Chatonnet P, Dubourdieu D (1998) Identification of substances responsible for the "sawdust" aroma in oak wood. J Sci Food Agric 76(2):179-188.

Cullere L, Fernandez de Simon B, Cadahia E, Ferreira V, Hernandez-Orte P, Cacho J (2013) Characterization by gas chromatography–olfactometry of the most odor-active compounds in extracts prepared from acacia, chestnut, cherry, ash and oak woods. LWT—Food. Sci Tech (Paris) 53(1):240-248.

Dong H, Jiang L, Shen J, Zhao Z, Wang Q, Shen X (2019) Identification and analysis of odor-active substances from PVC-overlaid MDF. Environ Sci Pollut R 26(20):20769-20779.

Fagerson IS (1969) Thermal degradation of carbohydrates: A review. J Agric Food Chem 17(4):747-750.

Ghadiriasli R, Wagenstaller M, Buettner A (2018) Identification of odorous compounds in oak wood using odor extract dilution analysis and two-dimensional gas chromatography–mass spectrometry/olfactometry. Anal Bioanal Chem 410(25):6595-6607.

Hagemeyer HJ (2014) Acetaldehyde. Kirk–Othmer encyclopedia of chemical technology (1999-2015). John Wiley & Sons, New York, NY.

He Z, Xiong J, Kumagai K, Chen W (2019) An improved mechanism-based model for predicting the long-term formaldehyde emissions from composite wood products with exposed edges and seams. Environ Int 132: 105086.

He Z, Zhang Y, Wei W (2012) Formaldehyde and VOC emissions at different manufacturing stages of wood-based panels. Build Environ 47:197-204.

International Organization for Standardization (2017) ISO 12219-7: Interior air of road vehicles—Part 7: Odour determination in interior air of road vehicles and test chamber air of trim components by olfactory measurements. International Organization for Standardization, Geneva, Switzerland.

Jiang C, Li D, Zhang P, Li J, Wang J, Yu J (2017) Formaldehyde and volatile organic compound (VOC) emissions from particleboard: Identification of odorous compounds and effects of heat treatment. Build Environ 117:118-126.

Jiang L, Shen J, Li H, Wang Q, Shen X (2018) Effects of volatile organic compounds released by different decorative particleboards on indoor air quality. Bioresources 13(4):7595–7605.

Karlsson S, Banhidi ZG, Albertsson AC (1989) Gas chromatographic detection of volatile amines found in indoor air due to putrefactive degradation of casein-containing building materials. Mater Struct 22(3):163-169.

Kim S, Choi Y-K, Park KW, Kim JT (2010) Test methods and reduction of organic pollutant compound emissions from wood-based building and furniture materials. Biores Technol 101(16):6562-6568.

Klepeis NE, Nelson WC, Ott WR, Robinson JP, Tsang AM, Switzer P, Behar JV, Hern SC, Engelmann WH (2001) The national human activity pattern survey (NHAPS): A resource for assessing exposure to environmental pollutants. J Expo Sci Environ Epidemiol 11(3):231-252.

Lewis RJS (2007) Hawley's condensed chemical dictionary, 15th edition. John Wiley & Sons, Inc., New York, NY.

Liu Y, Zhu X, Qin X, Wang W, Hu Y, Yuan D (2020) Identification and characterization of odorous volatile organic compounds emitted from wood-based panels. Environ Monit Assess 192(6):348.

Lu Z, Wang Q, Sun G, Wu L (2020) Research on the harmfulness of different veneer particleboards based on multiple VOC co-existence evaluation method. For Eng 36(2):49-54, 80.

Ministry of the Environment Law (1971) No. 91 of 1971: Offensive odor control law. Government of Japan, Tokyo, Japan.

National Institute for Occupational Safety & Health (NIOSH) (2010) NIOSH pocket guide to chemical hazards. DHHS (NIOSH) Publication No. 168. Department of Health & Human Services, Centers for Disease Control & Prevention.

Ning S, Liu Q, Ma L, Wang T, Zhang Q, Li Y (2013) Degradation of cellulose into furan derivatives in hot compressed steam. *in* International Conference on Biorefinery towards Bioenergy.

Ngassoum MB, Ousmaila H, Ngamo LT, Maponmetsem PM, Jirovetz L, Buchbauer G (2004) Aroma compounds of essential oils of two varieties of the spice plant *Ocimum canum* sims from northern Cameroon. J Food Compos Anal 17(2):197-204.

O'Neil MJ (2013) The Merck index-an encyclopedia of chemicals, drugs, and biologicals. Royal Society of Chemistry, Cambridge, MA.

Que ZL, Wang FB, Li JZ, Furuno T (2013) Assessment on emission of volatile organic compounds and formaldehyde from building materials. Compos, Part B Eng 49:36-42.

Sax NI (1984) Dangerous properties of industrial materials, 6th edition. Van Nostrand Reinhold, New York, NY.

Schieweck A (2021) Very volatile organic compounds (VVOC) as emissions from wooden materials and in indoor air of new prefabricated wooden houses. Build Environ 190:107537.

Schiffman SS (1998) Livestock odors: Implications for human health and well-being. J Anim Sci 76(5):1343-1355.

Schreiner L, Loos HM, Buettner A (2017) Identification of odorants in wood of *Calocedrus decurrens (torr.) florin* by aroma extract dilution analysis and two-dimensional gas chromatography–mass spectrometry/olfactometry. Anal Bioanal Chem 409(15):3719-3729.

Shao Y, Shen J, Shen X, Qin J (2018) Effect of panel area-volume ratio on TVOC released from decorative particleboards. Wood Fiber Sci 50(2):1-11.

Simon V, Uitterhaegen E, Robillard A, Ballas S, Veronese T, Vilarem G, Merah O, Talou T, Evon P (2020) VOC and carbonyl compound emissions of a fiberboard resulting from a coriander biorefinery: Comparison with two commercial wood-based building materials. Environ Sci Pollut R 27(14):16121-16133.

Tong R, Zhang L, Xiaoyi Y, Liu J, Zhou P, Li J (2019) Emission characteristics and probabilistic health risk of volatile organic compounds from solvents in wooden furniture manufacturing. J Clean Prod 208:1096-1108.

Verschueren K (2001) Handbook of environmental data on organic chemicals. Volumes 1-2, 4th edition. John Wiley & Sons, New York, NY.

Xiong J, Chen F, Sun L, Yu X, Zhao J, Hu Y, Wang Y (2019) Characterization of VOC emissions from composite wood furniture: Parameter determination and simplified model. Build Environ 161:106237.

Wang Q, Shen J, Du J, Cao T, Xiwei S (2018) Characterization of odorants in particleboard coated with nitrocellulose lacquer under different environment conditions. Forest Prod J 68(3):272-280.

Wang Q, Chen J, Cao T, Du J, Dong H, Shen X (2019a) Emission characteristics and health risks of volatile organic compounds and odor from PVC-overlaid particleboard. BioResources 14(2):4385-4402.

Wang Q, Shen J, Shao Y, Dong H, Li Z, Shen X (2019b) Volatile organic compounds and odor emissions from veneered particleboards coated with water-based lacquer detected by gas chromatography–mass spectrometry/olfactometry. Eur J Wood Wood Prod 77(5):771-781.

Wang Q, Zeng B, Shen J, Wang H (2020a) Effect of lacquer decoration on VOCs and odor release from *P. neurantha (hemsl.) gamble.* Sci Rep-UK 10(1):9565.

Wang Q, Shen J, Zeng B, Wang H (2020b) Identification and analysis of odor-active compounds from *Choerospondias axillaris* (Roxb.) Burtt et Hill with different moisture content levels and lacquer treatments. Sci Rep-UK 10(1):14856.

Wang W, Shen X, Zhang S, Lv R, Liu M, Xu W, Chen Y, Wang H (2022) Research on very volatile compounds and odors from veneered medium density fiberboard coated with water-based lacquers. Molecules 27(11):3626.

Wang Y, Wang H, Tan Y, Liu J, Wang K, Ji W, Sun L, Yu X, Zhao J, Xu B, Xiong J (2021) Measurement of the key parameters of VOC emissions from wooden furniture, and the impact of temperature. Atmos Environ 259:118510.

Zhang R, Wang H, Tan Y, Zhang M, Zhang X, Wang K, Ji W, Sun L, Yu X, Zhao J, Xu B, Xiong J (2021) Using a machine learning approach to predict the emission characteristics of VOCs from furniture. Build Environ 196:107786.

Zhu J, Xiao Z (2018) Characterization of the major odor-active compounds in dry jujube cultivars by application of gas chromatography–olfactometry and odor activity value. J Agric Food Chem 66(29):7722-7734.

REVIEWED COMMENTARY: FACTORY-GROWN WOOD, THE FUTURE OF FORESTRY?

Eric Hansen†*

Professor and Department Head
Department of Wood Science and Engineering
Oregon State University
Corvallis, OR
E-mail: eric.hansen@oregonstate.edu

Ashley Beckwith

Mechanical Engineering
MA Institute of Technology
Boston, MA
E-mail: ashbeck@alum.mit.edu

Cady Lancaster†

Assistant Professor, Senior Research
Wood Science and Engineering
Oregon State University
Corvallis, OR
E-mail: cady.lancaster@oregonstate.edu

Scott Leavengood†

Professor and Director
Oregon Wood Innovation Center
and
Wood Science and Engineering
Oregon State University
Corvallis, OR
E-mail: scott.leavengood@oregonstate.edu

(Received December 2021)

Abstract. Recent developments in factory-grown foods suggest that factory-grown wood (FGW) may be on the horizon. In fact, recent work at Massachusetts Institute of Technology introduces tunable plant-based materials, an early indicator of what may evolve into a new source of raw material for forest sector companies, and others. Industry and academia would be wise to monitor developments in this field as they may present significant opportunities and/or adjustments for both. We explore the state-of-the-art in this budding area of science and contemplate implications of successfully growing wood or other lignocellulosic materials in factories. Given a changing climate and focus on carbon emissions, the pressure to drastically reduce CO_2 production will continue climb. Could reduction of their footprint via FGW be an important part of this equation for forest sector companies, going beyond the need to "make every tree count"? In other words, might FGW present an environmental and climate protection breakthrough? Or might it simply trade forest-based environmental impacts for others? What other consequences does FGW promise for companies? And what might it mean for wood science programs, critical suppliers of research and development and skilled employees for the industry? We explore each of these questions and contemplate potential actions and outcomes.

Keywords: Factory-grown wood, disruptive technologies, forest sector, plant-based materials.

* Corresponding author
† SWST member

INTRODUCTION

In the development of disruptive technologies, science fiction has been the dreamscape in which modern conveniences were born—whether predicted or manifested into the minds of contemporary innovators. As early as 1911, Hugo Gernsback predicted video calling, allowing Alice 212B423 to call Ralph 124C 41+ for aid from 4000 miles away (Gernsback 1925). In 2017, Hugo and Nebula Award winning N. K. Jemisin brought us Syl Anagist, a technologically advanced civilization in which buildings are "walls of patterned cellulose," and bygone, inorganic brick and concrete structures superannuated, almost feared for their lack of self-healing properties (Jemisin 2017). Paradigm shifts in human thinking on natural resource consumption, backed by recent scientific advancements, encourages exploration of the burgeoning field of biotechnology once relegated to the feedstock of science fiction.

Recent work on cultured plant materials (Beckwith et al 2021) triggered a forestry futurist to speculate about a distant reality in which wood is produced in factories rather than grown in forests (Bengston 2021). Recent developments in the related world of cellular agriculture for food production indicate that this vision may not be so far removed. Factory-grown meat is receiving significant injections of capital (Fassler 2021) as proponents claim a windfall in animal welfare (eg elimination of feedlots/chicken houses) and positive climate impacts (eg less deforestation, lower methane emissions) and a segment of the market is ready to pay for such products (Kantor and Kantor 2021). Despite skepticism by some (Fassler 2021), factory-grown meat operations are allegedly scaling up to grow meat products which could soon be purchased in the local grocery store (eg Future Meat 2022). Cost-effective scale-up of cultured food indicates possibilities for the emergence of other cultured commodities, like wood products. The ongoing push to promote a forest-based bioeconomy is poised to increase the demand for wood-based goods (Ceccherini et al 2020). Meanwhile, companies face demands to reduce their footprint and "make every tree count." Lab- or factory-grown wood (FGW), produced by using cells to grow wood products and materials without growing whole trees, could provide an answer—by reducing reliance on trees as a source of forest products and enabling growth of only what is needed, where it's needed, when it's needed.

The following perspective piece first characterizes the state-of-the art with respect to FGW and lab-grown cellulosics. Based on current development status, the provided discussion speculates on the implications that a FGW industry could ultimately have on the forest sector, examining issues around new products, environmental impacts, and business/marketing practices. Final thoughts consider how such a transition could affect the academy, particularly wood science programs.

LAB-GROWN CELLULOSICS

For the purposes of this discussion, FGW is considered to be a cellulosic material that has been selectively grown in a controlled environment (eg laboratory, factory) using biological processes and exhibiting chemical, microstructural, and mechanical similarities to natural wood. The following text explores the state-of-the art of FGW technologies in addition to adjacent advancements in FGW Alternatives (FGWAs) that can be used as replacements for natural wood in some applications and may possess some but not all of the chemical, microstructural, and mechanical properties of natural wood.

Factory-Grown Wood (FGW)

The promise of FGW is only just emerging and recent work provides a first window into how the nascent technology may develop (Beckwith et al 2021). Making strategic use of plant cell culture, tissue-like plant materials (with properties akin to natural wood) can be selectively grown in defined shapes to produce materials that do not require the cultivation and processing of whole plants. Historically, cultured plant cells have not been widely considered as a means of materials production, although plant cell culture has been in practice for over a century (Hussain et al 2012) and now constitutes a sizable and growing industry (Srivas and Sumant 2021). Commonly, plant cell culture is

used as an intermediate process step in bolstering plant populations. This culture technique, referred to as micropropagation, can enhance desirable traits in a population through clonal replication, and expand populations of species that are slow to reproduce, endangered, or otherwise, difficult to propagate (Isikawa 1984). More recently, plant cells have been employed as "green factories" to pump out secondary metabolites with applications in food, cosmetic, and pharmaceutical industries (Ochoa-Villarreal et al 2016). Molecular farming techniques are particularly useful in cases where the natural biological source is endangered or produces the desired compound in low quantities and the molecule is too complex to be generated through chemical synthesis (eg Paclitaxel, an anticancer drug initially unsustainably sourced from the Yew tree [Sanchez-Muñoz et al 2019]). Protalix Biotherapeutics, Dow Agrosciences, Phyton Biotech, and Greenovation Biopharmaceuticals are just a handful of players exploring the plant culture pharmaceutical space. Protalix was the first company to achieve FDA approval for a plant cell-expressed biotherapeutic and has demonstrated systems for large-scale cultivation of plant cells and their by-products (Tekoah et al 2015). Given the potential of plant cell cultures to facilitate the concentrated production of desirable plant products in accessible formats and with improved yields, using culture systems to generate improved materials seems a logical progression of the existing plant culture industry. Work by Beckwith et al presents the first published demonstration of grown-to-order plant materials using techniques that allow for control over chemical, microstructural, and mechanical properties, as well as material form (Beckwith et al 2021, 2022). Because of the limited existing knowledge in materials production by way of plant cell culture, we consider this nascent approach as a jumping off point for the following discussions.

Current progress toward FGW production leverages established techniques for generating, maintaining and scaling plant cell cultures (Mustafa et al 2011), directing cell development (Fukuda and Komamine 1980; Möller et al 2003; Turner et al 2007), and bioprinting (Seidel et al 2017; Vancauwenberghe et al 2017; Emmermacher et al 2020; Park et al 2020). By the reported methods, plant cells grown within a structured, nutrient-rich culture environment are directed to develop specific cellular identities and attributes, enabling grown materials to exhibit xylem-like characteristics (Beckwith et al 2021). By modifying the culture environment of growing cells, cultivated materials exhibit great dexterity in their emergent chemical, microstructural, and mechanical characteristics (Beckwith et al 2022). Not only do these customizable plant materials have the potential to one day mimic natural wood materials in mechanical, structural, and chemical respects, but tunability afforded by the culture methods could open the door to an entirely new family of plant-based materials (eg with specialized microstructures and spatially controlled properties) or optimized materials and wood constituents with improved accessibility to reduce processing requirements (eg lignin-free wood, or easy-to-isolate tree-derived biopolymers such as cellulose or lignin). The available proof-of-concept demonstrations have been completed in nonwoody plant species to date, but the developed methods are translatable across species and the fundamental biological principles (eg controllable differentiation into vascular cell types) have already been independently established for cultures of woody species (Möller et al 2003).

Realistically, producing a lab-grown wood product that mimics all characteristics of natural wood, will require years of foundational research. In pursuit of such a wood substitute, future efforts will need to be made in: the translation of developed techniques to woody species, genetic engineering to enhance the uniformity and synchronicity of cellular developments, and improvements to the understanding of cell-scaffold interactions so that improved growth control and competitive material properties can be achieved. In the nearer term, however, developments in plant cell culture could deliver alternatives to wood in select applications. For example, consider applications where wood structure and form are noncritical and intense processing is required to isolate desired end products (eg cellulose for pulp). Given such opportunities

for feedstock improvement and the growing wave of support for cellular agriculture, FGW and its precursors are technologies to watch.

In practice, successful FGW generation could effectively untether forest products from forest resources. Inputs and infrastructure for an FGW operation would, therefore, look quite different to traditional practice. Although specifics will vary with species, culture format, and desired output, certain inputs will be common to all plant culture operations. To facilitate growth, plant cell cultures (not unlike whole plants) must be supplied with water, oxygen, macroelements, microelements, vitamins, and carbon (Mustafa et al 2011). A carbon source may take the form of carbon dioxide or soluble polymers such as sucrose. The selected carbon source will have implications on the achievable formats of culture and density of production, which can be achieved. For cultures making use of photosynthesis, eg ensuring adequate light penetration is essential to sustained growth, but becomes increasingly difficult to ensure at high cell densities as optical density increases (Yoon et al 2015). On the other hand, for sucrose-supplied cultures, higher density growth may be possible, but environmental implications of the sucrose supply will need to be factored into the ultimate impact equation. In addition to these consumable inputs, supporting technology is required to: ensure sterility of the growth environment, maintain environmental conditions conducive to growth, ensure adequate gas exchange, and replenish nutrients while removing unwanted metabolites (Allan et al 2019). The supporting technology, often taking the form of a bioreactor, essentially replaces higher level functions that occur naturally in whole plants. On a case-by-case basis, it will be necessary to assess whether the benefits attained thanks to selectivity and tunability of cultured plant material growth are sufficient to overcome any inefficiencies that result from this increased role of technology in production.

A critical element of FGW success and market penetration will be process scalability. How to effectively scale modern culture technologies to displace a meaningful portion of the natural wood market (or any high-volume market, eg meat [Humbird 2021]) remains an open question. Existing demonstrations of plant culture at large scales (Tekoah et al 2015; Ochoa-Villarreal et al 2016; Eibl et al 2018), while promising, are still miniscule relative to the volume of many global wood product streams. Thus, advancements in scalable culture technology will be integral to the widespread permeation of FGW and related products. Specific challenges of scaling cultures today include maintaining an aseptic growth environment and homogeneous growth conditions throughout, as system (eg bioreactor) size increases (Humbird 2021). Accomplishing these criteria while minimizing required energy and media waste will be necessary to achieve an environmental and economic edge. Beneficially, the numerous culture formats allowable in culture of plant cells (eg suspension, callus, dispersed gel cultures, and beyond) create opportunities for solutions beyond the standard liquid bioreactor.

Factory-Grown Wood Alternatives (FGWAs)

Wood by-products and wood-derivatives could represent an intermediate checkpoint en route to a plant culture-based FGW. These types of FGWAs, which could serve to replace natural wood in a limited range of applications, may even find origins outside of the plant kingdom. In some circumstances, FGWAs may provide opportunities to improve on wood as a feedstock for certain applications. Bacterial cellulose technologies provide one such example.

Today, the cellulose pulp used to produce paper, textiles, food and drug additives, and specialty cellulose products (eg filters, acetates, and esters) is predominantly obtained from natural wood (Li et al 2018) in a multistage pulping process. Complex, energy-intensive pulping is necessitated by the structure and chemistry of natural wood. However, by modifying the structure and chemistry of the cellulosic feedstock (eg by reducing lignin content), the need for intensive processing could be substantially reduced. Consider one such example: bacterial cellulose. Bacterial cellulose is

a high-purity, extracellular product of certain bacterial cell cultures that is naturally lignin-free.

Like plant cell cultures, bacterial cultures are sustained on a nutrient-rich broth. In these conditions, some types of bacteria (eg Gluconacetobacter xylinus) can directly produce extracellular nano-sized cellulose fibers (known as bacterial cellulose) at purities, which reduce needed downstream processing (Betlej et al 2020). Bacterial cellulose is chemically similar to plant cellulose (Blanco Parte et al 2020) but differs in crystallinity and molecular weight (Betlej et al 2020). Nonetheless, bacterial cellulose can serve as a replacement for wood-sourced cellulose in some applications. Bacterial cellulose has already been demonstrated as a partial substitute for wood-derived pulp in paper production and even improved paper strength (Skočaj 2019; Betlej et al 2020; Kalyoncu and Peşman 2020). Culture-derived cellulose has also been used in the production of textiles (Gao et al 2011; Babaeipour et al 2021) and combining bacterial cellulose with other structural agents can even yield materials with the approximate look and strength of natural wood (Symmetry Wood n.d.). The value of FGWAs is 2-fold, they serve to provide a new supply of a traditionally tree-sourced product, but also encourage the development of culture technologies with improved scalability and resource efficiency. With respect to plant cell cultures specifically, a promising entry point for FGWAs is high-value by-products or metabolites (eg Paclitaxel from the Yew tree; Tekoah et al 2015). As successes in these early applications drive improvements in bioreactor design and fundamental biological knowledge, lower-price point materials, such as high-purity pulp, may also become an accessible target.

Products constituting FGWAs, including the given example of bacterial cellulose and beyond, again provide opportunities to separate forest resources from forest products. If done successfully, this transition could represent an impactful shift. In a factory setting, the tight control allowed over production density and product growth could enable huge increases in production volume per unit land area. Industrial production could also mean reduced environmental sensitivity—with production free from variation in climatic conditions, natural disasters, pests, and disease affecting natural plant populations. In addition, because of their environmental apathy, FG products could be produced anywhere in a democratized fashion. As a result, cultivation could be made more efficient and more robust by colocation of facilities and consumers.

These opportunities for improvement over standard practice are presented with cautious optimism. As in the case with FGWs, an overhauling of supply chains and process flows make estimating comparative impacts of the old and new difficult until the science behind FGW and FGWAs progresses further. In all cases, careful analysis is required to understand under what conditions and for which applications the culture systems can provide sufficient benefit over traditional practice.

In summary, research progress toward FGW is underway. Although achieving parity with natural wood will require continued scientific development, production of wood by-products and derivatives presents a near-term steppingstone, which could support ongoing progress toward a true wood replacement. A new production process will make use of a supply chain distinct from traditional forestry activities and rely on different supporting technologies. The specifics of process inputs and technologies will vary with product output and the impacts of these specifics will need to be uniquely evaluated. A key challenge is ensuring an FGWA can improve upon environmental and or social aspects of current practice while presenting a scalable solution delivering at approximately competitive costs.

WHAT'S THE FUTURE?

Growing wood commercially in a lab is likely decades into the future and there is little empirical work on this promising technology. The sections that follow are best described as "educated speculation," by design and necessity. We use words such as "might" and "could" to communicate that future developments are highly uncertain, yet critical for wood scientist to contemplate. Recent developments in lab-grown plant materials are a

signal for anyone interested in forests, forestry, and wood products to consider implications of this development, including: 1) what products might result; 2) how might existing industry be impacted; and 3) what might it mean for the academy?

What Products?

In general, FGW has the potential to eliminate many of the inefficiencies in production and preparation of tree products. The current model of utilizing cone-shaped, long-lived plants as raw materials is inherently inefficient. Recovery rates have increased drastically over past decades, but geometry dictates a certain percentage of material that will not meet final product (eg lumber or veneer) requirements. And while modern primary processing facilities convert 99% or more of a delivered log to sellable products, as much as 50% of the end products are lower value by-products such as chips, shavings, bark mulch, or energy (Simmons et al 2021). And, there is considerable biomass left on the forest floor that never makes it to a mill.

There are clear trade-offs in considering potential products that may result from FGW. One might argue that the best opportunities will be situations for truly engineered, high-value products, with high unit costs, significant processing requirements (and significant losses in yield each time it is processed), inadequate performance, limited supply, or significant environmental impact. Components for musical instruments (eg material for fretboards for guitars) would seem to meet all of these categories. On the other hand, pioneering a new technology like FGW by targeting wood for musical instruments might be analogous to striving to be an Olympic sprinter before learning to crawl. Therefore, we propose three examples for FGW that span the range of complexity (that being a relative term here), volume, and value.

Cellulose fibers. Near-term opportunities for FGWA may include specialty products such as those produced from cellulose nanomaterials (CNMs). CNMs are candidates for solving global environmental issues (Mokhena and John 2020) and the market is estimated to consume 35 million metric tons annually when key features of the technology are realized (Shatkin et al 2014). Currently, CNMs are mechanically separated from plant and animal tissues using mechanical filtration followed by chemical or biological treatments, which results in unaligned fibers. The most significant component to CNM macroscale functionality is controlling fiber alignment (Li et al 2021). Another limiting feature in making nanocellulose materials sustainable is developing isolation strategies for high-grade cellulose of specific morphology. FGWA could provide access to high volumes of high-purity cellulose material, in specific alignments, thereby allowing for applications in environmental remediation, energy storage/conversion, packaging, biomedical, sensors, textiles and filters, etc. (Mokhena and John 2020; Wang et al 2020).

Cellulose fibers from wood have been used for well over a century to produce textile fibers as well as paper. For example, in the viscose process, pulp is dissolved into a liquid and then regenerated to form the fabric rayon. The first patent on this process dates to 1893 (Wilkes 2000) and alternative processes have been developed over the years to lessen the environmental impacts of the viscose process. For example, Spinnova, a Finnish firm, promotes its product as ". . . the most sustainable natural fibre in the world" (Spinnova 2021). In simple terms, the process involves mechanically refining pulp to break it down, chemical purification, and then solubilization of cellulose, followed by spinning into longer fibers (Pineda 2020). In this situation, FGWAs might easily substitute for wood-based cellulose.

The development of specialized FGWA for "smart materials" (eg self-healing) is currently a niche market with noteworthy growth potential. Caro-Astorga et al (2021) have already developed a patternable engineered living material based on bacterial cellulose that is self-repairing through regeneration of cellulose in response to damage. In the biomedical field, CNMs are incorporated with hydrogels to improve mechanical properties. Shao et al (2017) demonstrated the healing efficiency of wood-pulp derived cellulose nanocrystal

hydrogels networks during cyclic tensile and compressive loading–unloading tests and cleavage. Cellulose nanosheets have been used in the development of compliant, self-adhesive, and flexible skin strain sensors (Lu et al 2020).

And working up the scale to consider larger aggregations of fibers, the wood composites sector converts high-volumes of relatively low-quality materials (eg chips, flakes, and sawdust) into useful products through proper design/engineering and just the right adhesives. Tradition and the genuine utility of many composite products may mean their continuation regardless of raw material. Might it be possible for FGW to be grown as networks of fibers and preformed into direct substitutes for the common end products of particleboard, MDF, and hardboard, ie panels, countertops, cladding, molding, cabinet components, etc.?

Custom architectural components. Natural wood is anisotropic, ie its properties differ depending on the orientation of the anatomical elements (tracheid, fibers, vessels, etc.). Anisotropy in large part dictates the shape of lumber, and this in turn has dictated the form/structure of historic buildings—think lots of rectangles. These days, digital and parametric design, 3D printing, and CNC processing are slowly changing these constraints, allowing creations like the Metropol Parasol in Spain. Consider the possibilities that FGW might enable for architectural components engineered and grown to specific shapes and with precise and consistent structural properties. Long, straight pieces no longer need be a necessity. Nor would designers need to be limited by the variation inherent to different wood species as well as lumber or panel grades.

Tone woods. And now finally, working up the value chain, we may consider tone woods: high-value timber, often from endangered or protected species, frequently poached and unsustainably harvested for their color and acoustic properties (Sheppard 2012; Department of Justice, US Attorney's Office 2015; Gibson and Warren 2016). Therefore, components for musical instruments might seem a good place to start. This end use appears to "tick all the boxes" related to value, limited supply of the current resource, inefficient conversion practices, environmental challenges, etc. However, given the complexity, and well-ingrained traditions of using specific species, even from specific regions, for instruments (Brown 1978; Rymer 2004; Wegst et al 2007), this market is likely in the distant future.

The science that emerges as fiber-based and architectural products are developed could enable growing materials with specific physical, mechanical, and even acoustical properties for musical instruments. Using adulterated wood is not an uncommon practice—Stradivari himself did not rely solely on the properties of maple and ebony, but incorporated borax, zinc, copper, and alum (Su et al 2021). Su et al (2021) have already posited that engineered wood can reintroduce the cellulose rearrangement and hemicellulose fragmentation created by famed Cremonese violin makers of the 1700s. Modern analytical techniques have allowed scientists to identify the properties of prized musical instruments—can these properties be replicated via FGW?

Impacts on Forest Sector Companies

A growing field of research emphasizes "corporate foresight," the ability of firms to perceive possible futures and better prepare their strategies and operations for those eventualities (eg Rohrbeck and Kum 2018). Corporate foresight informed perceptions of the future can complement innovation management, helping to identify the "right" innovation pathways to pursue. Improved innovation management and corporate foresight may be essential ingredients for successful transition of forest sector companies to the circular bioeconomy (Hansen et al 2021), and navigate changes tied to development of FGW. While the largest global forest sector companies may be nurturing corporate foresight capabilities, there is little evidence suggesting that it is common practice (Näyhä 2020). In fact, forest sector companies are often criticized for lacking the innovativeness and forward-thinking necessary to effectively navigate evolving market needs (Hansen 2010; Näyhä 2020). Moving from natural wood to FGW would

be more than evolutionary, impacting many aspects of company operations, from strategic decisions to tactical communication. Supply issues would shift significantly with a different set of risks and constraints and there would likely be special considerations for those parts of the industry that currently rely on by-products from primary producers.

Impacts will differ based on whether a company chooses to passively accept a new type of supply or, instead, proactively engages with development of the technology. In the context of bioeconomy transition, considerable emphasis has been given to the need for forest sector companies to collaborate with nonsector firms to develop next-generation products such as wood-based chemicals and textiles (Guerrero and Hansen 2021). In this case, the most innovative firms might collaborate with bioscience companies to develop FGW technology and become suppliers not only of natural wood, but the intellectual property of producing FGW. This brings us to the idea of FGW as a disruptive technology, displacing established products, as plastics did glass among other things, or as a sustaining technology that improves existing product performance.

One must consider the idea of "forest sector company" in the light of this disruptive technology. In its infancy, producing morphologically or chemically specific cellulose and lignin, FGW could generate a novel industry—especially if traditional forest sector companies do not track and participate with interdisciplinary research in bioscience and materials engineering as discussed previously. Could there be an era in which "forest" materials are no longer linked to natural forests?

Environmental performance. In comparison with natural wood, factory-grown materials promise a number of advantages. Forest-free, environmentally protected growth of materials could allow for more robust supply chains and resilience against climate change, pests, diseases, and natural disasters. FGW could enable the localization of production to potentially reduce transport-related emissions. Furthermore, direct growth of plant materials enables control over both material properties and form. As a result, materials could be optimized to reduce processing and increase yields of high-value products in downstream activities. But, despite the potential of FGW to address limitations in existing forest-product industries, these advantages must be weighed against new impacts introduced by a more demanding production process and an accompanying raw material supply. Optimized FGW may reduce energy required in harvest, hauling, and downstream processing, but the growth of the material itself will naturally demand electrical energy, infrastructure, and raw material inputs that forests do not. Thus, to fully understand and address environmental impacts, responsible FGW production will need to consider everything from host grid cleanliness and carbon sourcing to lab-consumable usage and waste management. On the other hand, if FGW is proven to be environmentally advantageous in some applications, the broader implications of devaluing forest resources must also be considered as an unintended consequence. If standing timber is of lesser value, forestlands may experience increased conversion to other uses (Hannah et al 2011). Comprehensive assessments are, therefore, needed to evaluate the magnitude and value of these and other tradeoffs and to determine under which conditions and for which applications FGW can provide net environmental benefits.

Although an understanding of the ultimate environmental impact equation is in the future, early indications are that FGW may be a meaningful opportunity for forest sector firms. Forest sector companies have seen pressure for environmental performance improvements from society and environmental nongovernmental organizations for decades. The issues have been many and global, and have ranged from dioxin in pulping operations to harvesting old growth. Simply put, most members of the general public have a negative gut reaction to trees being cut and often for good reason: illegal logging is the third largest international crime and largest natural resource crime (May 2017) and accounts for an estimated 30% of all logging activities (Nellemann 2012). Based

on the pressure from the public and various interest groups, the forest sector has made real changes in both philosophy and operations. Reduced emissions, certified forests, and corporate sustainability reports are examples. The current state of the global environment does not suggest a reprieve for forest sector companies. Instead, all indicators are that redoubled efforts will be necessary to maintain a social license to operate.

Current momentum around a forest-based bioeconomy may dramatically increase demand for wood fiber. Early signs of this are occurring in Europe where there has been a spike in total forest harvest as well as unit harvest sizes (Ceccherini et al 2020). This development leads to concerns over adverse effects on biodiversity, soil erosion, and water regulation. Of course, this is all framed within the context of such global societal challenges as climate change, increasing population, and the declaration by the United Nations of 2020-2030 as a decade of restoration, suggesting the focus on companies and their forest footprint (acres managed) are only likely to increase.

Because of the threat of global warming and climate change, the carbon impacts of forest sector operations are especially relevant. Quantification of these impacts and their true role in nature-based solutions are not without controversy (eg Hudiburg et al 2019; Seddon et al 2021), but, ultimately, the sector will be seeking to further improve its carbon story. Decarbonization, the movement toward net-zero carbon emissions, through growth of renewable fiber and design and use of long-lived products is an inherent advantage for the sector. The decarbonization potential of wood products is increasingly tied to waste reduction, repairability, repurposability, refurbishability, reuse, and recycling. Significant design and technology developments are needed to facilitate the "re's" abovementioned and FGW may play a meaningful role through improved design-for-purpose.

Fiber geolocation shifts. For most of history, production of natural wood products has had a strong connection to the physical location of forests. Although wood has been traded internationally for centuries, it is only in the recent decades of globalization that a major shift in production has happened, such as China becoming a global center for furniture production despite its relative lack of forests. The sector has long been effective at adapting to new supply realities, to the point that new product development has largely been tied to supply characteristics rather than customer demands (Bull and Ferguson 2006). In the mid-1990s in Oregon, ponderosa pine was in short supply due to severe harvest reductions on Federal land. Secondary manufacturers throughout the state were experimenting with radiata pine from New Zealand, and none were happy with the new raw material. However, fast forward several years and those same operations had adapted effectively to the peculiarities of radiata pine. Similarly, Western US softwood sawmills have quickly adapted to shrinking log diameters by retooling operations.

Relying on natural wood for supply comes with a specific set of risks. Forests, be they natural, planted, or industrial, plantations are susceptible to disease, insects, wildfire, hurricanes, and, overall, climate change. For example, the British Columbia beetle epidemic drastically reduced harvests in that region and ultimately contributed to Canadian companies investing in the US South. West Coast US companies have also made investment shifts to the US South, partially to maintain supply continuity. Factory operations change the nature of logistics and transportation, likely simplifying chain of custody. Systemic challenges in identifying and monitoring suppliers in complex value-webs, are leading companies, across sectors, toward vertical integration (Murcia et al 2021). However, vertical integration may seldom be an economically viable approach in a globalized economy and it maintains many negative social externalities (Panwar 2020).

Instead of a connection to forests, FGW is more likely connected to the dynamics of industrial clusters where competitive advantage derives from the colocation of competing firms that drives increasing productivity, innovation, and stimulates formation of new businesses (Porter 1998). The concentration of similarly oriented firms attracts

suppliers, service providers, specialized workers, etc. Just as Silicon Valley fosters high-tech start-ups and operations, FGW might be especially well-suited to a particular location, where water is cheap and accessible and the electricity grid is particularly clean. Alternatively, clustering could hold for research and development aspects of FGW, but actual production could easily be well-suited to small-scale, distributed production for local markets. One can envision franchise factories (growing operations) operated by entrepreneurs, potentially colocated with customers, essentially eliminating channels of distribution.

Competitive advantage. Sustained competitive advantage is achieved when a company possesses resources that are rare, valuable, nonsubstitutable, and inimitable (Barney 1991). This advantage is held over rivals in the marketplace and can be based on tangible and/or intangible resources. The traditional approach to competition in the sector, commodity production with a concentration on price (Näyhä 2020), is becoming, and will become even rarer in the future. Developing a sustained competitive advantage associated with FGW likely fits into two broad scenarios; 1) a company holds exclusive rights to a source of FGW: or 2) a company possesses the intellectual property associated with producing FGW. Either scenario requires collaboration outside of the sector or actively investing in small startups with promising technology (where FGW will likely find its genesis). Intellectual property and accumulated knowledge from these collaborations can be rare, valuable, nonsubstitutable, and inimitable resources. Ultimately, it is a question of whether forest sector company leaders can envision and implement collaboration with, eg bioscience companies to develop future feedstock. The alternative is to sit back, wait, and buy FGW as it becomes available on the open market. This would unlikely provide meaningful contribution to sustained competitive advantage.

Marketing strategy. Fundamentally, marketing strategy consists of choices about the type of product offered, the customer targeted, the location of that customer, and competencies or capabilities that allow the company to effectively compete. Generally, forest sector firms are moving from a focus on commodity products to special and custom-made products (Hansen and Juslin 2018). FGW could contribute to this evolution, where the raw material or a final product can be grown to stringent customer specifications. FGW could open a new set of positive environmental claims that could be used to target customers/regions with a high environmental ethic. Concerns over origin and supply chain infiltration of illegal products could cease to be relevant. The level of supply chain control possible through FGW would facilitate business models mirroring the farm-to-market and Know Your Fisherman approaches. Customization and effective targeting open a host of new branding opportunities. Of course, some of these opportunities could come at the expense of natural-grown wood and could cause confusion in the marketplace regarding what is "good" wood and whether "bad" wood is still better than nonrenewable materials. Overall, FGW could facilitate increased sophistication of marketing strategies and tactics undertaken by the sector.

Implications for the Academy

Decarbonization of the global economy creates many opportunities for wood and wood-like materials as industries look to substitute fossil-based raw materials with renewables. What does this mean for wood scientists? We believe that the field will become ever more interdisciplinary, attracting biologist, chemists, engineers, and others, exploring developments such as FGW in applications across many sectors of the economy. Accordingly, wood scientists must embrace these opportunities through, eg leadership of transdisciplinary teams to drive innovation and commercialization of wood-based products. Societal interest in mass timber buildings has injected significant resources into many wood science programs. FGW presents a similar opportunity for growth and renewal.

As the science changes, curricula must follow. Although much of currently taught foundational wood science knowledge would remain, a new knowledge base around the nature and possibilities

of alternative supply would be necessary. Dendrology and forest management courses typical of today's curricula might become plant physiology, cellular biology, and biological systems engineering tomorrow. These developments could ultimately benefit wood-based undergraduate programs through enhanced student interest and enrollment. Today, there is a shortage of highly-skilled employees for traditional forest sector firms. The diversification of industries utilizing wood-based products will enhance demand for specialized employees and wood science graduates will find themselves employed by companies throughout the economy. Often referred to as a "discovery" major, wood-based degree programs must capitalize on the buzz associated with futuristic technologies and the promise of high-tech jobs. A whole new student demographic, one that is highly STEM-focused and destined for laboratory and research and development work should be a target for wood science programs.

SUMMARY

It is reasonable to expect that FGW is on the distant horizon. New techniques for producing traditionally tree-sourced materials such as wood and biopolymers (ie cellulose, lignin) promise optimized plant products with grown-to-order properties and structures. The forest-free production of these materials can facilitate democratization of production and build in resilience to climate change, pests, and natural disasters. Tunability and selective production of desired plant tissues could reduce upstream and downstream processing with plant tissues optimally designed to meet application needs. On the other hand, real-world implications of these new technologies have yet to be fully understood or characterized. The timeline and manifestation of the technology can only be speculated at this time, but implications are highly relevant to forest sector companies and wood science programs; active consideration of emerging innovations in forest technology enable both industry and academia to adapt and remain relevant. This thought-experiment is motivated by nascent scientific advances, the aspirations of industry, and demands of modern society. Just as today's modern conveniences were yesterday's Sci-Fi, today's Sci-Fi will be tomorrow's conveniences. FGW, self-healing architecture, climate change resilient enterprises, and net zero emissions connect the precipice of innovation-led futurology to the pinnacle of science fiction.

ACKNOWLEDGMENTS

The authors would like to thank Rajat Panwar, Associate Professor, Oregon State University, who helped in the initial conceptual development of this manuscript as well as contributed meaningfully to its content. In addition, we would like to thank the following people for their feedback and ideas: Andreja Kutnar, Director, InnoRenew Centre of Excellence, Slovenia; Ernesto Wagner, Managing Director, V-W Ltd, Chile; Duncan Mayes, Founder and Principal, Lignutech Oy, Finland; and Steve Killgore, CEO, Timber Products Company, USA.

REFERENCES

Allan SJ, De Bank PA, Ellis MJ (2019) Bioprocess design considerations for cultured meat production with a focus on the expansion bioreactor. Front Sustain Food Syst 3:44.

Babaeipour V, Hamid M, Chegeni A, Imani M, Bahrami A (2021) Study of structural characteristics of regenerated bacterial and plant cellulose. Polym Sci Ser A 63: 412-419.

Barney J (1991) Firm resources and sustained competitive advantage. J Manage 17(1):99-120.

Beckwith AL, Borenstein JT, Velásquez-García LF (2021) Tunable plant-based materials via in vitro cell culture using a Zinnia elegans model. J Clean Prod 288: 125571.

Beckwith AL, Borenstein JT, Velásquez-García LF (2022) Physical, mechanical, and microstructural characterization of novel, 3D-printable, tunable, lab-grown plant materials generated from Zinnia elegans cell cultures. Mater Today (in press).

Bengston DN (2021) Lab-grown wood: A potential game changer for forestry and forest products. The Forestry Source. 26(3):10-17.

Betlej I, Salerno-Kochan R, Krajewski KJ, Zawadzki J, Boruszewski P (2020) The influence of culture medium components on the physical and mechanical properties of cellulose synthesized by kombucha microorganisms. BioResources 15(2):3125-3135.

Blanco Parte FG, Santoso SP, Chou CC, Verma V, Wang HT, Ismadji S, Cheng KC (2020) Current progress on

the production, modification, and applications of bacterial cellulose. Crit Rev Biotechnol 40(3):397-414.

Brown W (1978). Timbers of the world: South America, Vol. 2. United Kingdom: TRADA Technology Ltd.

Bull L, Ferguson I (2006) Factors influencing the success of wood product innovations in Australia and New Zealand. For Policy Econ 8(7):742-750.

Caro-Astorga J, Walker KT, Herrera N, Lee KY, Ellis T (2021) Bacterial cellulose spheroids as building blocks for 3D and patterned living materials and for regeneration. Nat Commun 12(1):1-9.

Ceccherini G, Duveiller G, Grassi G, Lemoine G, Avitabile V, Pilli R, Cescatti A (2020) Abrupt increase in harvested forest area over Europe after 2015. Nature 583(7814):72-77.

Department of Justice, US Attorney's Office (2015 November 16) Mill owner pleads guilty to violating the lacey act with purchases and sales of figured maple from national forest [Press Release]. https://www.justice.gov/usao-wdwa/pr/mill-owner-pleads-guilty-violating-lacey-act-purchases-and-sales-figured-maple-national (accessed 15 January 2022).

Eibl R, Meier P, Stutz I, Schildberger D, Hühn T, Eibl D (2018) Plant cell culture technology in the cosmetics and food industries: Current state and future trends. Appl Microbiol Biotechnol 102(20):8661-8675.

Emmermacher J, Spura D, Cziommer J, Kilian D, Wollborn T, Fritsching U, Steingroewer J, Walther T, Gelinsky M, Lode A (2020) Engineering considerations on extrusion-based bioprinting: Interactions of material behavior, mechanical forces and cells in the printing needle. Biofabrication 12(2):025022.

Fassler J (2021 September 22) Lab-grown meat is supposed to be inevitable. The science tells a different story. The Counter. https://thecounter.org/lab-grown-cultivated-meat-cost-at-scale/ (11 February 2022).

Fukuda H, Komamine A (1980) Establishment of an experimental system for the study of tracheary element differentiation from single cells isolated from the Mesophyll of Zinnia elegans. Plant Physiol 65(1):57-60.

Future Meat (2022) Bringing cultivated meat to the table. https://www.future-meat.com/ (11 February 2022).

Gao Q, Shen X, Lu X (2011) Regenerated bacterial cellulose fibers prepared by the NMMO·H_2O process. Carbohydr Polym 83:1253-1256.

Gernsback H (1925) Ralph 124C 41+: A romance of the year 2660. New York: Public Domain.

Gibson C, Warren A (2016) Resource-sensitive global production networks: Reconfigured geographies of timber and acoustic guitar manufacturing. Econ Geogr 91: 430-454.

Guerrero J, Hansen E (2021) Cross-sector collaboration in Oregon's forest sector: Insights from owners and CEOs. Int Wood Prod J 12(2):135-143.

Hannah L, Costello C, Guo C, Ries L, Kolstad C, Panitz D, Snider N (2011) The impact of climate change on California timberlands. Clim Change 109(1):429-443.

Hansen E (2010) The role of innovation in the forest products industry. J Forestry 108(7):348-353.

Hansen E, Juslin H (2018) Strategic marketing in the global forest industries (3rd digital ed.). Oregon State University Creative Commons. https://open.oregonstate.education/strategicmarketing (accessed 15 January 2022).

Hansen E, Kangas J, Hujala T (2021) Synthesis towards Future-Fittest for mature forest sector multinationals. Can J For Res 51(999):1-8.

Hudiburg TW, Law BE, Moomaw WR, Harmon ME, Stenzel JE (2019) Meeting GHG reduction targets requires accounting for all forest sector emissions. Environ Res Lett 14(9):095005.

Humbird D (2021) Scale-up economics for cultured meat. Biotechnol Bioeng 118:3239-3250.

Hussain A, Ahmed I, Nazir H, Ullah I (2012) Plant tissue culture: Current status and opportunities. *in* A Leva, ed. Recent advances in plant in vitro culture. London, UK: InTechOpen.

Isikawa H (1984) In vitro culture of forest tree calluses and organs. Jpn Agric Res Q 18:11.

Jemisin NK (2017) The stone sky: The broken earth series, Book 3. Orbit, New York, NY.

Kalyoncu EE, Peşman E (2020) Bacterial cellulose as reinforcement in paper made from recycled office waste pulp. BioResources 15(4):8496.

Kantor J, Kantor BN (2021) Public attitudes and willingness to pay for cultured meat: A cross-sectional study. Front Sustain Food Syst 5:26.

Li H, Legere S, He Z, Zhang H, Li J, Yang B, Zhang S, Zhang L, Zheng L, Ni Y (2018) Methods to increase the reactivity of dissolving pulp in the viscose rayon production process: A review. Cellulose 25:3733-3753.

Li K, Clarkson CM, Wang L, Liu Y, Lamm M, Pang Z, Zhou Y, Qian J, Tajvidi M, Gardner DJ, Tekinalp H, Hu L, Li T, Ragauskas AJ, Youngblood JP, Ozcan S (2021) Alignment of cellulose nanofibers: Harnessing nanoscale properties to macroscale benefits. ACS Nano 15(3):3646-3673.

Lu F, Wang Y, Wang C, Kuga S, Huang Y, Wu M (2020) Two-dimensional nanocellulose-enhanced high-strength, self-adhesive, and strain-sensitive poly(acrylic acid) hydrogels fabricated by a radical-induced strategy for a skin sensor. ACS Sustain Chem Eng 8(8):3427-3436.

May C (2017). Transnational crime and the developing world. Global Financial Integrity, Washington, D.C.

Mokhena TC, John MJ (2020) Cellulose nanomaterials: New generation materials for solving global issues. Cellulose 27:1149-1194.

Möller R, McDonald AG, Walter C, Harris PJ (2003) Cell differentiation, secondary cell-wall formation and transformation of callus tissue of *Pinus radiata* D. Don. Planta 217(5):736-747.

Murcia MJ, Panwar R, Tarzijan J (2021) Socially responsible firms outsource less. Bus Soc 60(6):1507-1545.

Mustafa NR, de Winter W, van Iren F, Verpoorte R (2011) Initiation, growth and cryopreservation of plant cell suspension cultures. Nat Protoc 6(6):715-742.

Nellemann C, INTERPOL Environmental Crime Programme, eds. (2012) Green carbon, black trade: Illegal logging, tax fraud and laundering in the World's Tropical Forests. A Rapid Response Assessment. Norway: United Nations Environment Programme, GRID-Arendal. https://wedocs.unep.org/handle/20.500.11822/8030.

Näyhä A (2020) Finnish forest-based companies in transition to the circular bioeconomy-drivers, organizational resources and innovations. For Policy Econ 110:101936.

Ochoa-Villarreal M, Howat S, Hong S, Jang MO, Jin YW, Lee EK, Loake GJ (2016) Plant cell culture strategies for the production of natural products. BMB Rep 49:149-158.

Panwar R (2020) It's time to develop local production and supply networks. Calif Manage Rev 28.

Park SM, Kim HW, Park HJ (2020) Callus-based 3D printing for food exemplified with carrot tissues and its potential for innovative food production. J Food Eng 271:109781.

Pineda RN (2020) Biocomposite with continuous spun cellulose fibers. Master's thesis, Materials Engineering, Luleå University of Technology, Department of Engineering Sciences and Mathematics, Luleå, Sweden. 69 pp.

Porter ME (1998) Clusters and the new economics of competition. Harvard Bus Rev 76(6):77-90.

Rohrbeck R, Kum ME (2018) Corporate foresight and its impact on firm performance: A longitudinal analysis. Technol Forecast Soc Change 129:105-116.

Rymer R (2004) Saving the music tree. Smithsonian 35(1): 52-63.

Sanchez-Muñoz R, Moyano E, Khojasteh A, Bonfill M, Cusido RM, Palazon J (2019) Genomic methylation in plant cell cultures: A barrier to the development of commercial long-term biofactories. Eng Life Sci 19(12): 872-879.

Seddon N, Smith A, Smith P, Key I, Chausson A, Girardin C, House J, Srivastava S, Turner B (2021) Getting the message right on nature-based solutions to climate change. Glob Change Biol 27(8):1518-1546.

Seidel J, Ahlfeld T, Adolph M, Kümmritz S, Steingroewer J, Krujatz F, Bley T, Gelinsky M, Lode A (2017) Green bioprinting: Extrusion-based fabrication of plant cell-laden biopolymer hydrogel scaffolds. Biofabrication 9: 045011.

Shao C, Wang M, Chang H, Xu F, Yang J (2017) A self-healing cellulose nanocrystal-poly(ethylene glycol) nanocomposite hydrogel via diels–alder click reaction. ACS Sustain Chem Eng 5(7):6167-6174.

Shatkin JA, Wegner TH, Bilek EM, Cowie J (2014) Market projections of cellulose nanomaterial-enabled products—Part 1: Applications. Tappi J 13(5):9-16.

Sheppard K (2012 August 7). Gibson guitars and feds settle in illegal wood case. Mother Jones. https://www.motherjones.com/politics/2012/08/gibson-and-feds-settle-illegal-wood-case/ (accessed 15 January 2022).

Simmons EA, Marcille KC, Lettman GJ, Morgan TA, Smith DC, Rymniak LA, Christensen GA (2021) Oregon's forest products industry and timber harvest 2017 with trends through 2018 (General Technical Report-PNW-GTR-997). USDA Pacific Northwest Research Station.

Skočaj M (2019) Bacterial nanocellulose in papermaking. Cellulose 26:6477-6488.

Spinnova (2021) https://spinnova.com (6 December 2021).

Srivas A, Sumant O (2021) Plant tissue culture market: Global opportunity analysis and industry forecast, 2021-2030. Allied Market Research. https://www.alliedmarketresearch.com/plant-tissue-culture-market-A14265 (22 December 2021).

Su CK, Chen SY, Chung JH, Li GC, Brandmair B, Huthwelker T, Fulton JL, Borca CN, Huang SJ, Nagyvary J, Tseng HH, Chang CH, Chung DT, Vescovi R, Tsai YS, Cai W, Lu BJ, Xu JW, Hsu CS, Wu JJ, Li HZ, Jheng YK, Lo SF, Chen HM, Hsieh YT, Chung PW, Chen CS, Sun YC, Chan JCC, Tai HC (2021) Materials engineering of violin soundboards by Stradivari and Guarneri. Angew Chem Int Ed 60(35):19144-19154.

Symmetry Wood (n.d.) Symmetry wood. http://symmetrywood.com/#rec304830222 (5 October 2021).

Tekoah Y, Shulman A, Kizhner T, Ruderfer I, Fux L, Nataf Y, Bartfeld D, Ariel T, Gingis-Velitski S, Hanania U, Shaaltiel Y (2015) Large-scale production of pharmaceutical proteins in plant cell culture-the protalix experience. Plant Biotechnol J 13(8):1199-1208.

Turner S, Gallois P, Brown D (2007) Tracheary element differentiation. Annu Rev Plant Biol 58:407-433.

Vancauwenberghe V, Baiye Mfortaw Mbong V, Vanstreels E, Verboven P, Lammertyn J, Nicolai B (2017) 3D printing of plant tissue for innovative food manufacturing: Encapsulation of alive plant cells into pectin based bio-ink. J Food Eng 263:454-464.

Wang D, Lee SH, Kim J, Park CB (2020) "Waste to Wealth": Lignin as a renewable building block for energy harvesting/storage and environmental remediation. ChemSusChem 13:2807.

Wegst U, Oberhoff S, Walker M, Ashby M (2007) Materials for violin bows. Int J Mater Res 98:1230-1237.

Wilkes AG (2000) Chapter 3: The viscose process. 331 pp *in* C. Woodings ed. Regenerated cellulose fibres. The textile institute. Woodhead Publishing Limited, Cambridge, UK.

Yoon JH, Shin J-H, Park JH, Park TH (2015) Effect of light intensity on the correlation between cell mass concentration and optical density in high density culture of a filamentous microorganism. Korean J Chem Eng 32(9):1842-1846.

EDITORIAL AND PUBLICATION POLICY

Wood and Fiber Science as the official publication of the Society of Wood Science and Technology publishes papers with both professional and technical content. Original papers of professional concern, or based on research of international interest dealing with the science, processing, and manufacture of wood and composite products of wood or wood fiber origin will be considered.

All manuscripts are to be written in US English, the text should be proofread by a native speaker of English prior to submission. Any manuscript submitted must be unpublished work not being offered for publication elsewhere.

Papers will be reviewed by referees selected by the editor and will be published in approximately the order in which the final version is received. Research papers will be judged on the basis of their contribution of original data, rigor of analysis, and interpretations of results; in the case of reviews, on their relevancy and completeness.

As of January 1, 2022, Wood and Fiber Science will be an online only, Open Access journal. There will be no print copies. Color photos/graphics will be offered at no additional cost to authors. The Open Access fee will be $1800/article for SWST members and $2000/article for nonmembers. The previous five years of articles are still copyright protected (accept those that are identified as Open Access) and can be accessed through member subscriptions. Once a previous article has reached its 5th anniversary date since publication, it becomes Open Access.

Technical Notes

Authors are invited to submit Technical Notes to the Journal. A Technical Note is a concise description of a new research finding, development, procedure, or device. The length should be **no more than two printed pages** in WFS, which would be five pages or less of double-spaced text (TNR12) with normal margins on 8.5 x 11 paper, including space for figures and tables. In order to meet the limitation on space, figures and tables should be minimized, as should be the introduction, literature review and references. The Journal will attempt to expedite the review and publication process. As with research papers, Technical Notes must be original and go through a similar double-blind, peer review process.

On-line Access to *Wood and Fiber Science* Back Issues

SWST is providing readers with a means of searching all articles in *Wood and Fiber Science* from 1968 to present Articles from 1968 to 2017 are available to anyone, but in order to see 2017 to 2021 articles you must have an SWST membership or subscription. SWST members and subscribers have full search capability and can download PDF versions of the papers If you do not have a membership or subscription, you will not be able to view the full-text pdf.

Visit the SWST website at http://www.swst.org and go to Wood & Fiber Science Online. Click on either SWST Member Publication access (SWST members) or Subscriber Publication access (Institution Access). All must login with their email and password on the HYPERLINK "http://www.swst.org" www.swst.org site, or use their ip authentication if they have a site license.

As an added benefit to our current subscribers, you can now access the electronic version of every printed article along with exciting enhancements that include:

- IP authentication for institutions (only with site license)
- Enhanced search capabilities
- Email alerting of new issues
- Custom links to your favorite titles

(ISSN 0735-6161)
CODEN WOOFAJ

WOOD AND FIBER SCIENCE

JOURNAL OF THE SOCIETY OF WOOD SCIENCE AND TECHNOLOGY

VOLUME 54 JULY 2022 NUMBER 3

CONTENTS

Articles

Reviewed Commentary